Doctoral Dissertation

Academic Year 2013

Biochemical Simulation and Metabolomic Analysis for the Improvement of Red Blood Cell Storage

Graduate School of Media and Governance

Keio University

Taiko Nishino

Abstract

In this dissertation, we displayed the metabolic dynamics of long-term stored erythrocytes by using the mathematical simulation and metabolomic analysis towards optimization of blood storage method in order to prolong the expiration date. It is quite difficult to maintain the constant levels of ATP and 2,3-BPG in red cells during storage period with commonly-used preservative methods, although these are strongly associated with red cell viability and oxygen delivery after transfusion. The depletion of metabolite is caused by an intricate regulatory network of biochemical reactions. Mathematical modeling and metabolomic analysis are powerful tools for integrating and understanding such complex and dynamic systems.

Firstly, we developed the metabolic model of cold-stored red cells preserved with conventional storage solutions, based on the published stead-state model at 37℃. *In silico* analysis of our model indicated that the depletion of ATP and 2,3-BPG is largely dependent on the inactivation of upper glycolytic enzymes, which may serve as possible targets for improving blood storage methods. We also performed quantitative metabolomics experiments, which provided a comprehensive view of the metabolic dynamics in the cold-stored erythrocyte.

Secondly, using the model, we reproduced metabolic dynamics of cold erythrocytes stored in a novel storage solution, Phosphate Adenine Glucose Guanosine Gluconate Mannitol, which can maintain both ATP and 2,3-BPG for 5 weeks. The prediction clarified the metabolic mechanism of high efficiency production of ATP and 2,3-BPG in the context of metabolic benefits and possible side effects.

These works showed that *in silico* analysis of the human erythrocyte combined

with metabolomics experiments can reveal its detailed dynamics under cold storage condition, and can propose novel strategies for prolonged cold-preservation. This also suggested that quantitative predictions based on computational simulations and metabolomic measurements can provide new insights into cellular behavior as a result of complicated interactions between a large number of compounds.

Keywords: Erythrocyte metabolism, Blood storage, Mathematical model, Metabolomic analysis, Systems biology

論文題目

血液保存手法の改良に向けた赤血球代謝シミュレーションとメタボロミクス解析

論文要旨

本研究では、数値シミュレーションとメタボロミクス解析により、血液保存下における代謝動態の特性を明らかにし、良好な状態での血液の長期保存方法を考察する。赤血球中の ATP と 2,3-ビスホスホグリセリン酸（2,3-BPG）は、輸血後の細胞生存率と酸素運搬能に直接関与することが知られているが、これらの代謝物質を効率良く維持できる赤血球の保存方法はいまだ確立されていない。また、これらの代謝物質が血液保存時に減少する本質的なメカニズムは解明されてこなかった。細胞シミュレーションとメタボロミクス解析は、複雑な生化学反応ネットワークの動的な変動により生じるこれらの代謝物質濃度の減少を包括的かつ根本的に理解する上で、非常に有効な手段である。

まず、従来の血液保存法により保存された赤血球の代謝を模した数理モデルを構築し、メタボロミクス実験によるモデルの検証を行った。また、当モデルを用いた予測によって、血液保存下で観測される ATP と 2,3-BPG の減少が解糖系上流の酵素反応（ヘキソキナーゼ、ホスホフルクトキナーゼ）の活性低下によることを明らかにした。今回予測したこれらの酵素反応段階は、血液保存法

開発のターゲットになりうる。さらに、メタボロミクス解析によって血液保存下における赤血球内代謝物質の網羅的な測定を世界で初めて行った。

次に、構築した保存赤血球モデルを用いて、ATP と 2,3-BPG の減少を緩和する新規保存液（PAGGGM 液）による赤血球保存の状態を再現した。さらに、*in vitro* 実験では困難な代謝動態の観測と解析をシミュレーション実験により行った。予測結果から、保存液に含まれるアデニンおよびグアノシンによる協調効果が保存初期におけるペントースリン酸回路と解糖系上流の活性化を促進し、保存期間を通じた ATP および 2,3-BPG の効率良い維持に貢献していることを解明した。

本研究の成果は、メタボロミクス解析による精緻なモデリングに基づいた *in silico* 実験による血液保存法最適化の道筋を示した。このことは、数理シミュレーションと網羅的測定技術を融合した本研究のストラテジーが、多数の要素の複雑な相互作用からなる生命機能を理解し予測する上で、非常に有効であることを示している。

キーワード:
赤血球代謝、血液保存、細胞シミュレーション、メタボロミクス解析、システム生物学

Table of Contents

List of Figures

List of Tables

Chapter 1

Introduction

1.1 Background

Over the last century, the reductionist approach, which regards a system as nothing but the sum of its parts, has been prevailing in biology. This approach has been useful to identify cellular components in molecular level, and, in part, their functions. Tremendous progress in molecular biology and biochemistry has made it possible for us to get a large amount of information related to cellular systems, so-called omics data sets, such as genome sequences, protein-protein interactions and transcriptional profiles. However, it is difficult to reconstitute the knowledge of cellular systems based on the interrelation between each component in order to understand their biological functions.

Systems biology is a new perspective on biology in the beginning of this century, which focuses on complex interactions within biological systems, rather than a part of cellular components [1,2,3]. Systems biology is expected to serve as a new framework that can investigate cellular functions by means of measurements, analyses, and integrations of the huge and complicated data. Moreover, development of high-throughput technologies that can generate omics data also accelerates the progress in systems biology.

In systems biology, the biological knowledge about a target system is often reconstructed into a mathematical model for the analysis of its nonlinear behavior. This knowledge translation provides a holistic perspective for the target system that allows us

to investigate biological nature. In fact, detailed mathematical models are useful to analyze complex regulations in functional organs, tissues, and cells [4].

The integrated framework in systems biology, such as a generation of multi-omics data in a high-throughput manner, an integration of these data sets with mathematical models, and an analysis and computation of the models, has been applied for the human metabolic network. In 2007, the first reconstruction of the global human metabolic network was presented [5]. Following this study, predictions of tissue specific metabolic behavior and disease metabolic states have been performed [6,7,8].

In recent years, the focus has shifted to the medical application, such as investigating biomarkers and drug targets [9,10], and improvement of blood storage [11].

1.1.1 Blood storage: A history and problem

Even today artificial blood substitutes are not in common use yet, and blood transfusion is a key element of modern medical care. The aim of blood transfusion is to provide viable and functional blood components for patients. In particular, red blood cells (RBCs) transfusion supports fatal medicine, high-risk obstetric care and all forms of surgery. To meet these broad needs and demands, blood/RBC storage systems have been developed over a century.

The three basic requirements for RBC storage are: (1) to keep their viability during reasonable time in circulation after transfusion, (2) to keep their plasticity within blood vessels, and (3) to keep their ability to transport oxygen. Firstly, post-transfusion viability of RBC is positively correlated with intracellular ATP concentration [12]. Dern *et al*. reported that ATP is essential for stored RBC survival in circulation [13]. Secondly,

the drastic ATP decrease can lead to the loss of erythrocyte plasticity and membrane stability [14], but nevertheless it is difficult to directly observe the post-transfusion erythrocyte plasticity. Lastly, the loss of 2,3-bisphosphoglycerate (2,3-BPG) results in changes in hemoglobin oxygen affinity, which leads to the loss of oxygen delivery to tissues [15,16]. For these reasons, efforts to improve RBC storage methods have almost entirely focused on optimizing intracellular ATP and 2,3-BPG levels under storage conditions from the early time of blood preservation research.

Table 1.1 Properties of the whole blood storage solutions.

Solution	Composition	Effective life	Recovery rate	References
ACD	citrate, sodium citrate, glucose	21 days	75%	[17,18]
CPD	citrate, sodium citrate, glucose, sodium phosphate	21 days	79%	[18,19]
CPDA-1	citrate, sodium citrate, glucose, sodium phosphate, adenine	35 days	72%	[20,21]
CPDA-2	citrate, sodium citrate, glucose, sodium phosphate, adenine	42 days	83.6%	[21,22]

Table 1.2 Properties of the additive solutions for red cell concentrates.

Solution	Composition	Effective life	Recovery rate	References
SAGM	glucose, adenine, mannitol, saline	42 days	78-84%	[23,24]
AS-1	glucose, adenine, mannitol, saline	42 days	72%	[25,26,27]
AS-3	glucose, adenine, mannitol, saline	42 days	78-84%	[24,25]
MAP	citrate, sodium citrate, glucose, sodium phosphate, adenine, mannitol, saline	42 days	82%	[28,29]
PAGGSM	glucose, sodium phosphate, adenine, mannitol, saline, guanosine	49 days	74%	[30]

Table 1.1 shows that composition, shelf life and 24 hours post-transfusion recovery rate of the typical whole blood storage solutions for the last half century. The first modern whole blood storage solution, Acid Citrate Dextrose (ACD), was born in the 1940's [17]. ACD allowed for 21 days of blood/RBC storage with 75 % of 24 hours post-transfusion recovery [18]. Citrate Phosphate Dextrose (CPD) was also designed for the whole blood storage [19]. CPD, which was made of ACD and phosphate, was less acidic than ACD and maintained 2,3-BPG better than in ACD. However, RBCs stored with these solutions rapidly decrease intracellular ATP and 2,3-BPG and lost their membrane plasticity and oxygen affinity [31]. In the 1960's, Nakao *et al*. found that ATP is directly associated with RBC viability before/after transfusion and the addition of adenine (ADE) can improve the synthesis of ATP in RBC [12]. Based on these findings, CPD with ADE (CPDA-1, CPDA-2) solutions, which prolonged the storage period of blood to 35 days, were developed [20,21].

Along with the advent of blood component transfusion in the 1970's-80's, the demands of additive solutions for red cell concentrates were increased. Red cell concentrates are prepared with a hematocrit level of less than 80%. The major additive solutions and their information are shown in Table 1.2. Saline Adenine Glucose Mannitol (SAGM), Additive Solution-1 (AS-1) AS-3, and Phosphate Adenine Guanosine Glucose Saline Mannitol (PAGGSM) have been developed and generally used in the United States and European countries, and Mannitol Adenine Phosphate (MAP) is a commonly-used additive solution in Japan. These solutions show the same tendency in RBC storage. One major benefit of the additive system is an increase in the level of ATP that can enhance red cell viability and extend the shelf-life of the red cells to 42 days. This facilitates better inventory control of blood as well as widely use in

pre-deposit autologous donations. At the same time, however, current additive solutions do not maintain a constant level of 2,3-BPG after less than 2 weeks of storage. Although it is known that stored RBCs restore their 2,3-BPG to be normal level within 24 hours transfusion [32], there is the agreement that blood with nearly normal oxygen affinity should be used for massive transfusions, infants, older patients, and patients with cardiovascular and pulmonary disease. Recently, Korte and his colleague have reported a blood storage experiment with the novel alkaline solution named Phosphate Adenine Glucose Guanosine Gluconate Mannitol (PAGGGM), which maintained both ATP and 2,3-BPG during 35 days of storage. Nevertheless, PAGGGM is not put into practical use yet and the underlying mechanism why both ATP and 2,3-BPG are maintained has not been investigated [33].

As mentioned above, ideally, blood storage solutions should ensure not only the maximum viability for the longest storage period, but also the optimal oxygen delivery. However, with commonly-used liquid blood storage methods, optimal conditions for either ATP or 2,3-BPG usually have an opposite effect on the other. Moreover, the previous blood storage methods have been developed through time consuming “trial and error” approach, but not based on the biochemical mechanism underlying the depletion of 2,3-BPG and ATP during cold blood storage. In order to overcome these problems and find out the optimal preservative by the shortest way, it is important to elucidate the whole-cell metabolic dynamics of RBC during storage.

1.1.2 Mathematical modeling of the erythrocyte metabolism

A human erythrocyte is a good subject for mathematical modeling and simulation studies in various fields, such as biochemistry, physiology and biomechanics,

because of its simple cell structure and functions. They lack a cell nucleus and most organelles in the process of cell maturation to accommodate maximum space for hemoglobin, which serves as an efficiency oxygen transport mechanism [34]. Despite the simplicity, erythrocytes are the principal means of oxygen delivery from a lung to body tissues via blood flow through the circulatory system.

A number of models of RBC metabolism have been developed with various levels of abstractions since the early 1980's [35,36,37,38,39,40,41]. A single RBC can be assumed to be a closed system, and its metabolism seemed to be robust in physiological conditions. Because of this simplicity and robustness, as well as the abundance of information and knowledge concerning biochemical properties of metabolic enzymes, the RBC metabolic network has been a suitable subject for mathematical modeling and system level analysis. In spite of the long history of computational study in erythrocyte metabolism, for the incompleteness in the reaction network, the existing erythrocyte models are rarely applied to clinical situations and the investigation of other physiological functions of the erythrocyte.

E-Cell project was started in 1997 at Keio University with the purpose of development of whole cell scale mathematical models [42]. The project has provided a unique simulation platform named E-Cell System/E-Cell Simulation Environment, which allows for multi-timescale/multi-algorithm simulations and modeling in the fully object-oriented manner for a cell simulation model. As a part of the project, we developed the RBC metabolism model using E-Cell System. The E-Cell RBC model includes not only the major metabolic reactions, membrane transport systems or ion binding reactions in human erythrocyte, but also allosteric transitions in hemoglobin in response to the partial pressure of oxygen and consequent change in affinity of

metabolites and enzymes to different hemoglobin states [43]. The model has provided valuable insights into the molecular physiology of erythrocyte, for example, the pathology associated with hereditary glucose 6-phosphate dehydrogenase (G6PD) deficiency [44,45], and RBC response to hypoxia condition [46]. Thus, the model serves as a useful platform for the integration of the erythrocyte metabolic dynamics, which is utilized to facilitate the understanding and interpretation of the complicated kinetics in the erythrocyte metabolism at the whole-cell level.

1.1.3 Metabolomics analysis of erythrocyte

Recent advances in measurement technologies enable comprehensive and quantitative monitoring of cellular components in a high-throughput manner. Omics analysis is expected to collect, integrate and analyze the abundance of cellular properties to decipher the biological nature of living organisms. Metabolomics is one of the fields of omics study concerned with the comprehensive detection and the quantitative measurements of metabolites in various biological systems. It can provide an overview of the metabolic status and global biochemical events associated with a cellular or physiological system. Metabolomic analyses have been performed with a variety of analytical platforms such as nuclear magnetic resonance (NMR) spectroscopy and mass spectrometry (MS) with gas chromatography (GC) or liquid chromatography (LC) based separation method [47]. Capillary electrophoresis mass spectrometry (CE-MS) is one of the novel metabolomics techniques, which allows the simultaneous and quantitative measurement of charged metabolites with high mass resolution [48]. In particular, capillary electrophoresis time-of-flight mass spectrometry (CE-TOFMS), which is mainly used as an instrument of metabolomic analysis in this thesis, provides

higher mass resolution and mass accuracy than conventional CE-MS.

Human erythrocyte metabolomics has become popular in recent years. Sana *et al*. reported that a total of 2730 features were detected across multiple pHs by LC-MS analysis of the erythrocyte metabolites [49]. This type of comprehensive and non-targeted metabolomic analysis of human erythrocyte has rapidly increased for the past few years, and has been used to address the biochemical pathology of human RBCs, which include some different genotypes or phenotypes, such as the sickle cell disease [50] and malaria infection [51]. On the other hand, quantitative and targeted metabolomic analysis of RBCs has performed over the past 30 years [46,52,53,54,55,56]. Kuchel and his co-workers measured time-series of multiple metabolites by $^{13}C/^{31}P$ NMR spectroscopy to compare with a computer simulation that covered about 10 species of metabolites included in non-oxidative hexose monophosphate shunt in the human erythrocyte [53,54,57]. Kinoshita *et al*. monitored the time-related alteration of glycolytic intermediates in RBCs under hypoxia, and clarified the pivotal role for protein-metabolite interactions in the temporal metabolic response to hypoxia [46]. In this way, quantitative and targeted metabolomic analysis is a powerful tool to confirm the accuracy of dynamic metabolic simulation, as well as to reveal the behavior of whole-cell metabolic dynamics *in vivo*.

1.2 Contributions

The primary objective of this study was to investigate the metabolic dynamics of preserved erythrocytes during the long-term storage through the systems biology approaches combining metabolic simulation and metabolomics analysis. The main

contribution of this thesis is to show the path toward an optimization of blood storage protocol based on the systematic experiments of both *in silico* and *in vivo,* which are performed with the detailed kinetic model and the quantitative metabolomics technique in a high-throughput manner.

Firstly, we constructed a large-scale precise kinetic model of cold-stored RBCs for predicting whole-cell metabolic dynamics, which is difficult to be observed by *in vitro* experiments. Metabolomic data taken from CE-TOFMS analysis was used to validate the *in silico* model. Secondly, using the model, the metabolic dynamics associated with the depletion of ATP and 2,3-BPG was displayed. In particular, the model allowed for the observation of long-term effect of additive solutions on the metabolic dynamics in every possible condition. These works indicate the possibility of the mathematical model of large-scale metabolism in human erythrocytes to predict the metabolic status in cold-stored erythrocytes and the usability of the model to suggest the novel methods for cold-preservation of erythrocytes.

1.3 Organization of this dissertation

In Chapter 2, we will discuss the first metabolic modeling and the metabolomic analysis of RBCs preserved in conventional additive solution. Firstly, we developed the kinetic model of RBCs stored in MAP solution at 4°C for 49 days, by extending a previously published large-scale erythrocyte model. The accuracy of the new model was validated by CE-TOFMS measurements of metabolic intermediates. From the *in silico* analysis, we predicted that the inactivation of upper glycolytic enzymatic activities, such as hexokinase (HK) and phosphofructokinase (PFK), would lead to the decline of

ATP and 2,3-BPG levels during RBC storage.

In Chapter 3, we will discuss the metabolic dynamics and the effect of additive agents during red cell preservation in the context of metabolic benefits and possible side effects. Firstly, using the stored RBC model, we reproduced the metabolic dynamics of red cells stored with ADE and guanosine (GUO) as preservative additives. From the simulation analyses of metabolic fates of the additives, the dynamic retention mechanism of ATP and 2,3-BPG by ADE and GUO were illustrated. ADE is used as a source of adenylate pool, which maintains constant ATP level, but induces 2,3-BPG reduction. On the other hand, GUO can boost the upper glycolysis that results in the efficient production of 2,3-BPG without reducing the supply of ATP.

Lastly, in Chapter 4, summary of the dissertation and future direction will be discussed.

Chapter 2

In silico modeling and metabolomic analysis of erythrocytes stored in cold-MAP solution

In Chapter 2, we provided a mathematical model and time-related metabolomics data of RBCs, and analyzed the mechanisms of the depletion of essential metabolites during long-term blood storage. Until this work was published, no studies had discussed the underlying mechanism of the metabolic impairment in stored RBCs. Throughout this chapter, we showed that the detailed kinetic model and comprehensive view of metabolic status obtained from metabolomics are helpful for us to investigate metabolic dynamics of stored RBCs.

2.1 Introduction

As mentioned in Chapter 1, to improve the prolonged storage of RBCs and RBC function, solution additives and storage conditions have been targeted to maintain ATP and 2,3-BPG levels because these metabolites are directly associated with cell survival and oxygen delivery. All currently used blood storage solutions have an expiration date of 42 days, but none of them can simultaneously maintain ATP and 2,3-BPG levels throughout the entire storage time [16,58,59,60]. In Japan, the MAP solution is used as a clinical blood storage solution. Although cold MAP-stored RBCs (RC-MAP) can maintain ATP levels at ~ 50% of those in the fresh RBCs over 42 days

of storage, 2,3-BPG is depleted after only two weeks [28].

Changes in the levels of metabolic indicators such as ATP and 2,3-BPG result from underlying complex metabolic networks, and biochemical metabolic events are also regulated by various physical or chemical factors, such as pH and temperature. Mathematical modeling and metabolomic analysis are the powerful tools for integrating and analyzing such complex, dynamic, and large systems in systems biology.

We provide here a mathematical model for predicting metabolic behaviors in RC-MAP. This model was developed by using Genetic Algorithm (GA) parameter estimation based on a previously published simulation model for normal circulating RBCs. Our model successfully reproduced the reported time-courses of ATP and 2,3-BPG during long-term storage in commercially used RC-MAP. Our model also indicated several factors that could be used to maintain the levels of these two metabolic indicators, ATP and 2,3-BPG. These factors are possible targets for the refinement of storage solutions and/or conditions. Moreover, we investigated the time-course of alterations in various metabolic intermediates in RBCs stored in cold-MAP for 49 days, using the metabolomic analysis with CE-TOFMS [48,61]. The metabolome measurement showed that most glycolytic intermediates sharply increased in the first week, but rapidly decreased during long storage. However, pyruvate (PYR) and lactate (LAC) were significantly accumulated through the storage period. Though there may be differences in the experimental conditions between our metabolomic analysis under laboratory conditions and the reported data from commercially used stored blood (which was used for parameter estimation), our model predictions of the intermediate concentrations after 49 days of storage agreed well with the metabolome data. Our model also predicted the large accumulation of hypoxanthine (HX) and sedoheptulose

7-phosphate (S7P).

2.2 Materials and Methods

2.2.1 Construction of the metabolic model of MAP-stored erythrocytes

We used a published model of human erythrocyte metabolism constructed in E-Cell System Version 3 (E-Cell 3) as the basis of our cold MAP-stored RBC model [46]. The basal model consists of the major metabolic pathways of human erythrocytes, such as glycolysis, pentose phosphate pathway, adenine nucleotide (purine) metabolism, some membrane transport systems of intermediates, ion leak processes, ATP-dependent Na^+/K^+ pump, and binding reactions between hemoglobin and metabolites. Rate equations of enzymes were derived for each of the enzyme-catalyzed reactions using King-Altman method except for some reactions in purine metabolism and purine transport, which were described in Michaelis-Menten or first-order kinetics. Some enzymatic reactions in glycolysis, such as HK, PFK, glyceraldehyde phosphate dehydrogenase (GAPDH), pyruvate kinase (PK), lactate dehydrogenase (LDH), and 2,3-BPG shunt reactions (2,3-BPG shunt) including 2,3-BPG mutase (DPGM) and 2,3-BPG phosphatase (DPGase), are represented as pH-dependent kinetics. The transition of hemoglobin between the oxygenated state (R-state) and deoxygenated state (T-state), and the consequent changes in the levels of intermediates through the difference between affinities to metabolites in the two hemoglobin states are also implemented in the basal model. Furthermore, this model involves the consideration of the most abundant RBC membrane protein, band3, which mediates interactions with

hemoglobins and glycolytic enzymes, including PFK, aldolase, and GAPDH. We modified the basal model, which predicts the behavior of circulating erythrocytes at body temperature, to predict the metabolic behavior in RC-MAP.

Components of blood storage solutions must maintain erythrocytes in a good condition during long-term storage. The MAP solution is comprised of 7.21 g/L of glucose and 0.14 g/L of ADE as metabolic substrates of glycolysis and the synthetic pathway of ATP, 0.2 g/L of citrate and 1.5 g/L of sodium citrate for preventing blood coagulation, 0.94 g/L of sodium phosphate as a source of phosphate, and 14.57 g/L of mannitol and 4.97 g/L of sodium chloride as osmoregulatory substrates that prevent erythrocytes hemolysis. The hematocrit level was set to be 60%, which is equal to that in commercially used RC-MAP. We set the extracellular environment in the model mimicking the MAP solution as 40.02 mM of glucose, 1.04 mM of ADE, 106.37 mM of sodium ion, and 6.03 mM of inorganic phosphate. The osmotic pressure was assumed to be unchanged and erythrocyte aggregation was assumed not to occur during cold-MAP storage.

We also modeled the pH-degradation profile, tense-relaxed state transition of hemoglobin, and inactivation of enzymes induced by additives in the MAP solution or by the low storage temperature at 4°C. The intracellular pH of RC-MAP is lower than that of normal erythrocytes due to the large concentration of citrate. In addition, the pH value gradually decreases due to the LAC accumulation [62]. As the storage time dependent pH variation of the model, we used the published time-course data of intracellular pH in commercially available cold-RC-MAP [28]. The initial pH value was set to be 6.95, and the decrease in intracellular pH during storage over 49 days was linear, with the first-order coefficient of 8.66×10^{-8} s^{-1}.

Hemoglobin is more stable in the R- than the T-state at low temperatures [63]. This transition of hemoglobin largely modulates erythrocyte metabolism [46,64]. In our model, we designated all hemoglobin as in the R-state during cold storage.

At 4°C, all chemical reactions, including enzymatic reactions, chemical binding reactions, and active transport processes, should be significantly inactivated. In particular, Na^+/K^+ pumps are highly sensitive to lowered temperature [65]. Purine metabolism enzyme activities, including those of adenosine deaminase, adenosine monophosphate phosphohydrolase (AMPase), inosine monophosphatase, and adenosine monophosphate deaminase (AMPDA) [66,67,68,69,70], but not adenosine kinase (AK) or hypoxanthine-guanine phosphoryl transferase (HGPRT), are optimized or activated at relatively low pH like storage conditions [71,72]. Taking these facts into consideration, we divided the enzyme activities in the model into three groups: activity of Na^+/K^+ pump, activities of eight purine metabolism enzymes, and all remaining enzymatic or binding activities. All of the enzymatic reactions included in the model are listed in Table 2.1, and the schematic representation of the model of RC-MAP is shown in Figure 2.1.

Table 2.1 Enzymatic reactions included in the model. [a]

Enzyme / Process	Abbreviation	Substrates [d]		Products [e]	Effectors [f]
Hexokinase	HK	GLC + MgATP	→	G6P + MgADP	2,3-BPG, GDP, GSH, pH
Phosphoglucoisomerase	PGI	G6P	↔	F6P	
Phosphofructokinase	PFK	F6P + MgATP	→	F1,6-BP + MgADP	ATP, Mg, 2,3-BPG, AMP, Pi, GDP, pH
Aldolase	ALD	F1,6-BP	↔	DHAP + GA3P	2,3-BPG, Mg2,3-BPG
Triose phosphate isomerase	TPI	DHAP	↔	GA3P	
Glyceraldehyde phosphate dehydrogenase	GAPDH	GA3P + Pi + NAD	↔	1,3-BPG + NADH	pH
2,3-bisphosphoglycerate shunt	DPGM	1,3-BPG	→	2,3-BPG	pH
2,3-bisphosphoglycerate shunt	DPGase	2,3-BPG	→	3PG + Pi	pH
Phosphoglycerate kinase	PGK	1,3-BPG + MgADP	↔	3PG + Pi	
Phosphoglyceromutase	PGM	3PG	↔	2PG	
Enolase	EN	2PG	↔	PEP	Mg
Pyruvate kinase	PK	PEP + MgADP	↔	PYR + MgATP	ATP, F1,6-BP, GDP, pH
Lactate dehydrogenase	LDH	PYR + NADH	→	LAC + NAD	pH
Lactate dehydrogenase (NADPH)	LDHP	PYR + NADPH	→	LAC + NADP	
Glucose 6-phosphate dehydrogenase	G6PDH	G6P + NADP	→	GL6P + NAPDH	MgATP, 2,3-BPG
6-phosphogluconolactonase	6PGLase	GL6P	→	GO6P	
6-phosphogluconate dehydrogenase	6PGODH	GO6P + NADP	↔	RU5P + NADPH + CO2	
Transaldolase	TA	S7P + GA3P	→	E4P + F6P	
Transketolase1	TK1	X5P + R5P	→	GA3P + S7P	
Transketolase2	TK2	X5P + E4P	→	GA3P + F6P	
Ribose 5-phosphate isomerase	R5PI	RU5P	→	R5P	
Xylulose 5-phosphate isomerase	X5PI	RU5P	→	X5P	
Gamma-glutamyl cysteine synthetase	L_GCS	MgATP + glutamate + cysteine	↔	MgATP + L_GC + Pi	GSH
Glutathione synthetase	GSH_S	L_GC + glycine + MgATP	↔	GSH + MgATP + Pi	
Glutathione reductase	GSSGR	GSSG + NADPH	→	GSH + MgADP + Pi	
Adenosine kinase	AK	ADO + MgATP	→	MgADP + AMP	
Hypoxanthine-guanine phosphoryl transferase	HGPRT	PRPP + HX	→	IMP + 2Pi	
Adenosine deaminase [b]	ADA	ADO + MgATP	↔	INO	
Adenine phosphoribosyl transferase [b]	ADPRT	ADE + PRPP	→	AMP + 2Pi	
Adenosine monophosphate deaminase [b]	AMPDA	AMP	→	IMP	
Adenosine monophosphate phosphohydrolase [b]	AMPase	AMP	↔	ADO + Pi	
Inosine monophosphatase [b]	IMPase	IMP	↔	INO + Pi	
Purine nucleoside phophorylase [b]	PNPase	INO + Pi	→	HX + R1P	
Phosphoribomutase [b]	PRM	R1P	→	R5P	
Phosphoribosyl pyrophosphate synthetase [b]	PRPPsyn	R5P + MgATP	→	PRPP + AMP + Mg	
Adenylate kinase	APK	ADP + MgADP	→	AMP + MgATP	
Adenosine triphosphate phosphohydrolase	ATPase	MgATP	→	MgADP + Pi	
Glutathione turnover	OX	2GSH	→	GSSG	
Non-glycolytic NADH consumption process	OXNADH	NADH	→	NAD	
Adenine transport process	ADEtr	ADE	→	ADEe	
Adenosine transport process	ADOtr	ADO	→	ADOe	
Hypoxanthine transport process	HXtr	HX	→	HXe	ADEe
Inosine transport process	INOtr	INO	→	INOe	
Lactate transport process	LACtr	LAC	→	LACe	
Pyruvate transport process	PYRtr	PYR	→	PYRe	
Inorganic phosphate transport process	Pitr	Pi	→	Pie	
Glutathione transport process	GSSG transport	GSSG + MgATP	→	GSSGe + MgADP + Pi	
Leak of potassium	K_Leak	Ke	↔	Ki	
Leak of sodium	Na_Leak	Nae	→	Nai	
Sodium/potassium pump [c]	Na^+/K^+ pump	3Nai + 2Ke + MgATP	→	3Nae + 2Ki + MgADP + Pi	

[a] From [46]

[b,c]The enzyme activities in the model were divided into 3 groups: activities of 8 enzymes in purine metabolism (b, *highlighted in red*), the activity of the Na^+/K^+ pump (c, *highlighted in blue*), and the remaining other enzymatic or binding activities.

[d,e,f]Abbreviations used in this table are as follows: GLC, glucose; G6P, glucose 6-phosphate; F6P, fructose 6-phosphate; F1,6-BP, fructose 1,6-bisphosphate; DHAP, dihydroxyacetone phosphate; GA3P, glyceraldehyde 3-phosphate; 1,3-BPG, 1,3-bisphosphoglycerate; 2,3-BPG, 2,3-bisphosphoglycerate, 3PG, 3-phosphoglycerate; 2PG, 2-phosphoglycerate; PEP, phosphoenolpyruvate; PYR, pyruvate; LAC, lactate; GL6P, gluconolactone 6-phosphate; GO6P, gluconate 6-phosphate; RU5P, ribulose 5-phosphate; X5P, xylulose 5-phosphate; E4P, erythrose 4-phosphate; S7P, sedoheptulose 7-phosphate; R5P, ribose 5-phosphate; PRPP, 5-phosphoribosyl

-1-phosphate; ADE, adenine; IMP, inosine monophosphate; R1P, ribose 1-phosphate; INO, inosine; ADO, adenosine; HX, hypoxanthine; AMP, adenosine monophosphate; ADP, adenosine diphosphate; ATP, adenosine triphosphate; NADP, nicotinamide adenine dinucleotide phosphate; NADPH, nicotinamide adenine dinucleotide phosphate (reduced); NAD, nicotinamide adenine dinucleotide; NADH, nicotinamide adenine dinucleotide (reduced); Ki, potassium ion; Nai, sodium ion; Pi, inorganic phosphate; L_GC, L-glutamyl cysteine; GSH, glutathione (reduced); GSSG, glutathione (oxidized).

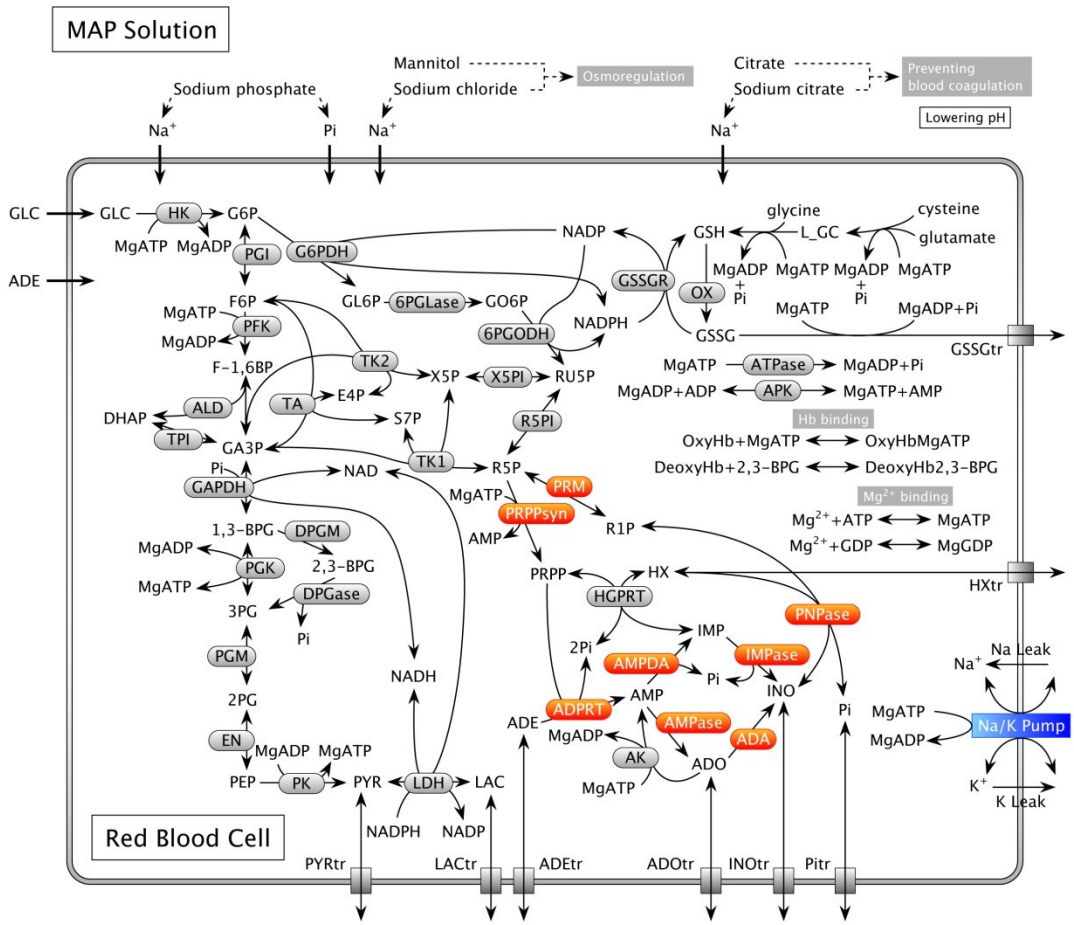

Figure 2.1 Schematic representation of the RC-MAP model.

Three groups of reaction activities as adjustable parameters for estimation using GA are indicated by the color of the background of each enzyme: *red*, purine metabolism enzymes; *blue*, Na^+/K^+ pump; and *gray*, all other enzymatic or binding reactions. Abbreviations of the enzymes and metabolites are given in Table 2.1. The kinetic equations used in this model are published in the literature [46].

2.2.2 Parameter estimation using GA

In the model, the aforementioned three groups of reaction activities were treated as adjustable parameters to reconstruct the reported metabolic behaviors in RC-MAP. We used the real-coded GA implemented in E-Cell 3 [73] to estimate values of these parameters, which were fitted with the time-courses of ATP and 2,3-BPG in the commercially available RC-MAP measured every seven days for 49 days. These time-course measurements included eight data points to evaluate simulation model fitness.

In GA analysis, the upper and lower bounds of the three adjustable enzymatic activities were 100% and 0.1% of the original activities, respectively. The population size of a generation was 300 and the parameter selection was terminated at 4,000 generations. The distance between the experimental data and predicted value was calculated as follows:

$$\mathrm{EV} = \frac{1}{n}\sum_{i=1}^{n}\left(\frac{[\mathrm{ATP}_{\mathrm{exp}}]_i - [\mathrm{ATP}_{\mathrm{pred}}]_i}{[\mathrm{ATP}_{\mathrm{exp}}]_i}\right)^2 + \frac{1}{n}\sum_{i=1}^{n}\left(\frac{[\mathrm{2,3\text{-}BPG}_{\mathrm{exp}}]_i - [\mathrm{2,3\text{-}BPG}_{\mathrm{pred}}]_i}{[\mathrm{2,3\text{-}BPG}_{\mathrm{exp}}]_i}\right)^2 \quad (2.1)$$

where EV is the error rate between the predicted and experimental data, n is the number of data points, $\mathrm{ATP}_{\mathrm{exp}}$ and $\mathrm{2,3\text{-}BPG}_{\mathrm{exp}}$ represent the reference experimental data, and $\mathrm{ATP}_{\mathrm{pred}}$ and $\mathrm{2,3\text{-}BPG}_{\mathrm{pred}}$ are the predicted values by the model. Each parameter was normalized by its initial concentration at day 0.

2.2.3 Blood collection and preservation

Blood was collected from healthy volunteers into vacuum blood collection tubes containing 3.2% sodium citrate. Each volunteer donated ~ 15 mL of blood.

Sample blood was centrifuged at 4670 ×*g* for 6 min, and buffy coat free blood was stored in MAP solution (4.97 g of sodium chloride, 0.14 g of ADE, 7.21 g of glucose, 14.57 g of mannitol, 0.2 g of citrate, 1.5 g of sodium citrate, and 0.94 g of sodium phosphate dissolved in 1 L of Milli-Q water). The final hematocrit of our RC-MAP was 60%. This protocol was almost same as that used for Nisseki RCC-LR, which is commercially used RC-MAP in Japan. Finally, the solution was divided into 5-mL plastic tubes and sealed. These tubes were stored at 4°C for 49 days and subjected to CE-TOFMS analysis.

2.2.4 Preparation of erythrocytes for CE-TOFMS analysis

To isolate erythrocytes, stored blood was centrifuged at 800 ×*g* and 4°C for 10 min, and the cells were washed three times with Tris buffer (Tris/HCl, 10 mM; NaCl, 150 mM; and glucose, 5 mM; pH 7.4). Next, 0.2 mL of the sample erythrocyte pellets were treated with 1.8 mL of cold methanol containing 20 μM methionine sulfone and D-camphor-10-sulfonic acid (CSA) as internal standards. 2 mL of chloroform and 0.8 mL Milli-Q water were added, and the mixture was thoroughly mixed, centrifuged at 3,500 rpm for 5 min at 4°C, and the upper aqueous layer was filtered through a centrifugal filter (Millipore, 5-kDa cut-off filter) to remove proteins. The filtrate was centrifugally concentrated and dissolved in 50 μL Milli-Q water containing reference compounds (200 μM each of 3-aminopyrrolidine and trimesate) immediately prior to CE-TOFMS analysis.

2.2.5 Instrumentation

All CE-TOFMS experiments were performed using an Agilent CE Capillary Electrophoresis System equipped with a G3250 AA LC/MSD TOF system, 1100 isocratic HPLC pump, G1603A CE-MS adapter kit, and G1607A CE-electrospray ionization (ESI)-MS sprayer kit (Agilent Technologies, Waldbronn, Germany). System control and data acquisition were performed using Agilent G2201AA ChemStation software for CE and Analyst QS for Agilent TOFMS.

2.2.6 CE-TOFMS conditions for cationic metabolite analysis

Separations were carried out in a fused-silica capillary (50 μm inner diameter × 100 cm total length) filled with 1 M formic acid as the reference electrolyte [74]. A sample solution was injected at 50 mbar for 3 s, and a positive voltage of 30 kV was applied. The capillary temperature was maintained at 20°C, and the sample tray was cooled below 5°C.

Methanol/water (50% v/v) containing 0.1 μM hexakis (2,2-difluoroethoxy) phosphazene was delivered as the sheath liquid at 10 μL/min. The ESI-TOFMS was operated in the positive ion mode and the capillary voltage was set at 4 kV. A flow rate of heated dry nitrogen gas (heater temperature 300°C) was set at 10 psig. In TOFMS, the fragmenter, skimmer, and octapole radio frequency voltage (Oct RFV) were set at 75 V, 50 V, and 125 V, respectively. Automatic recalibration of each acquired spectrum was performed using two standard reference masses, protonated methanol dimer ^{13}C isotope (*m/z* 66.063199) and protonated hexakis (2,2-difluoroethoxy) phosphazene (*m/z* 622.028963), which provided the lock mass for exact mass measurements. Exact mass

data were acquired at the rate of 1.5 cycles s^{-1} over a 50-1000 *m/z* range.

2.2.7 CE-TOFMS conditions for anionic metabolite analysis

A cationic-polymer-coated SMILE (+) capillary (Nacalai Tesque, Kyoto, Japan) was used as the separation capillary. A 50 mM ammonium acetate solution (pH 8.5) was used as the reference electrolyte [75]. Sample solution was injected at 50 mbar pressure for 30 s and a negative voltage of -30 kV was applied. Ammonium acetate (5 mM) in 50% methanol/water (50% v/v) containing 0.1 μM hexakis (2,2-difluoroethoxy) phosphazene was delivered as the sheath liquid at 10 μL/min. The ESI-TOFMS was conducted in the negative ion mode, and the capillary voltage was set at -3.5 kV. In TOFMS, the fragmenter voltage, skimmer voltage, and Oct RFV were set at 100 V, 50 V, and 200 V, respectively. Automatic recalibration was performed using two standard reference masses: deprotonated acetate dimer ^{13}C isotope (*m/z* 120.038410) and deprotonated hexakis (2,2-difluorothoxy) phosphazene acetate adduct (*m/z* 680.035541). All other conditions were identical to those used in the cationic metabolite analysis.

2.2.8 CE-TOFMS conditions for nucleotide and coenzyme analysis

Separations were performed in a fused-silica capillary with 50 μm inner diameter × 100 cm total length. The electrolyte for the CE separation was 50 mM ammonium acetate (pH 7.5). Prior to the first use, a new capillary was pretreated with preconditioning buffer (25 mM ammonium acetate-75 mM sodium phosphate solution, pH 7.5) for 20 min. Before each injection, the capillary was equilibrated by flushing with preconditioning buffer for 10 min and subsequently with the running electrolyte for

6 min, which was replenished every run using a buffer replenishment system equipped with the Agilent CE [76]. Sample solution (~ 30 nL) was injected at 50 mbar for 30 s, and +30 kV of voltage and 50 mbar of pressure were applied to the inlet capillary during the run. The capillary temperature was kept at 20°C and the sample tray was cooled below 5°C. Methanol/water (50% v/v) containing 0.1 μM hexakis (2,2-difluoroethoxy) phosphazene was delivered as the sheath liquid at 10 μL/min. The ESI-TOFMS was operated in the negative ion mode, and the capillary voltage was set at 3.5 kV. The flow of heated dry nitrogen gas (heater temperature 300°C) was switched off during the preconditioning step, and a pressure of 10 psig was applied 0.5 min after sample injection. In TOFMS, the fragmenter voltage, skimmer voltage, and Oct RFV were set at 125 V, 75 V, and 200 V, respectively. Automatic recalibration was performed using two standard reference masses: deprotonated acetate dimer (*m/z* 119.034984) and deprotonated hexakis (2,2-difluorothoxy) phosphazene acetate adduct (*m/z* 680.035541). Other conditions were identical to those used in the cationic metabolite analysis.

2.2.9 CE-TOFMS data processing

The obtained raw data was integrated by in-house software via the following steps: noise-filtering, baseline-correction, migration time alignment, peak detection, and integration of each peak area from 0.02 *m/z* width sliced electropherograms. Subsequently, the accurate *m/z* for each peak was calculated with Gaussian curve fitting on the *m/z* domain peak. All metabolites were identified by matching the *m/z* values and migration times with the standard compounds.

2.3 Results

2.3.1 Parameter estimation for fitting the RC-MAP data

To construct a model that can accurately predict the metabolism of RC-MAP stored at 4°C, we modified the original RBC model by specifying extracellular component properties, some physical changes such as pH degradation and the R-state stabilization of hemoglobin. Because the reaction activities in cold-stored RC-MAP could not be obtained from the literature, we divided the reaction activities into three groups of reaction properties and used GA to estimate these activities. These estimated activities served as adjustable parameters that were fitted to previously published time-course data of ATP and 2,3-BPG in commercially available RC-MAP at 4°C for 49 days [28].

In the GA estimations, the distance EV converged to 0.0815 at the termination of parameter selection. The three adjustable parameters were estimated as follows: Na^+/K^+ pump activity was 0.6%, purine metabolism activities were 24%, and all other reaction activities were 3.5% of each activity in the basal model. In the experimental data, 2,3-BPG was depleted at two weeks after blood collection. The ATP concentration was slightly increased in the first week, and then it gradually decreased (Figure 2.2A). The calculated variations of 2,3-BPG and ATP of the estimated model successfully traced the observed curves: 2,3-BPG was also depleted during the second week of storage, and the ATP concentration increased at first and then modestly decreased, reaching 30% of the initial concentration at 49 days of storage (Figure 2.2B). Furthermore, intracellular ADE is reportedly depleted at three weeks of storage [28], which was similarly found in our estimated model (data not shown).

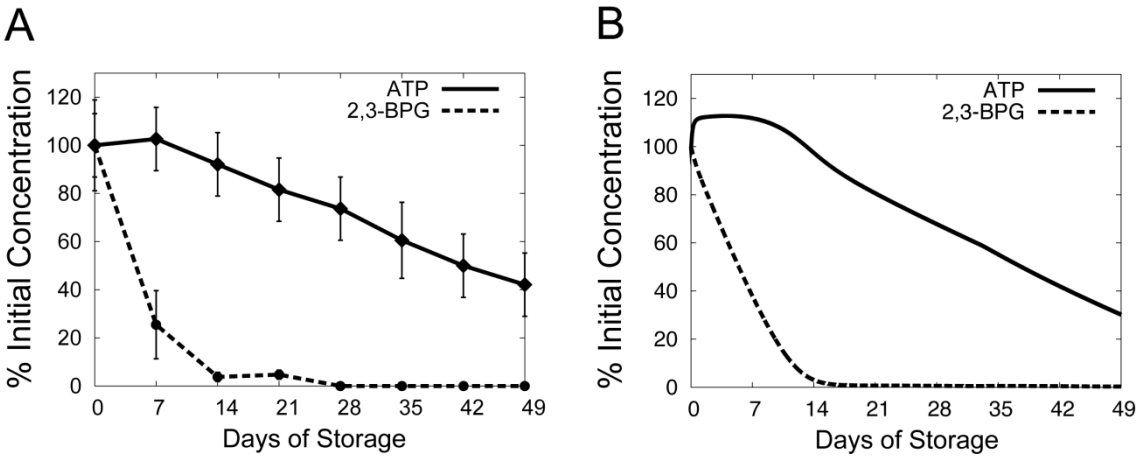

Figure 2.2 Time-related changes in ATP and 2,3-BPG levels in erythrocytes stored in MAP at 4°C for 49 days.

The time-course of ATP (*solid black*) and 2,3-BPG (*broken black*) in cold RC-MAP for 49 days in (A) previously reported data [28] and (B) the prediction of the estimated model derived by GA. Experimental values are shown as the mean ± S.D. of 19 separate experiments. Values are represented as the percentages of the initial concentrations.

2.3.2 Effects of parameters on the concentrations of ATP and 2,3-BPG

We performed parameter analysis to characterize the condition of the commercially available RC-MAP, including the three adjustable parameters used in GA analysis, the initial intracellular pH, and the form of hemoglobin. The initial pH value was varied from 6.5 to 7.25 (Figure 2.3A). The purine metabolism enzyme activities were varied from 2.5% to 50% (Figure 2.3B), the activity of Na^+/K^+ pump was varied from 0.25% to 2.5% (Figure 2.3C), and the other reaction activities were varied from 0.5% to 5% (Figure 2.3D) of their respective basal levels in the original RBC model. The hemoglobin status was set as only R-state, equal mix of R-state and T-state, and only T-state (Figure 2.3E).

When the initial pH value was high, the 2,3-BPG concentration was maintained during 49 days of simulation. In contrast, ATP was maintained by a lower rather than a higher pH (Figure 2.3A). Low activities of the purine enzymes effectively maintained the ATP level (Figure 2.3B). ADE, a known substrate of *de novo* ATP synthesis, was also maintained in the model when purine enzyme activities were kept low (data not shown). In contrast, the behavior of 2,3-BPG was not affected by changing the purine metabolism enzyme activities (Figure 2.3B). The Na^+/K^+ pump activity had the largest effect on ATP level. When its activity was set to a high level (2.5% of the basal level), ATP depletion was significantly accelerated and almost exhausted at five weeks (Figure 2.3C). Furthermore, when the other reaction activities were set to 0.5% of their basal levels, the decline in 2,3-BPG levels was halted; 2,3-BPG levels were maintained at 22% of their initial concentration after 49 days of storage (Figure 2.3D). However, the

effect of the other reaction activities on ATP levels was surprisingly small (Figure 2.3D).

The behavior of ATP and 2,3-BPG was notably affected by the hemoglobin transition status in the simulated condition. When all intracellular hemoglobins existed as the R-state, ATP remained at 30% of its initial level after 49 days of storage, and 2,3-BPG was depleted at 14 days. However, when all the intracellular hemoglobin was set to the T-state, ATP decreased abruptly after day 14 and remained at only 7.7% at 49 days of storage, whereas 2,3-BPG was maintained at its initial level for the whole 49 days. When R- and T-states of hemoglobin existed in equal quantities, ATP remained at 27% of the initial level at 49 days, which was similar to its level in the R-state-only model, while 2,3-BPG maintained its initial value during 49 days of storage, as in the T-state-only model (Figure 2.3E).

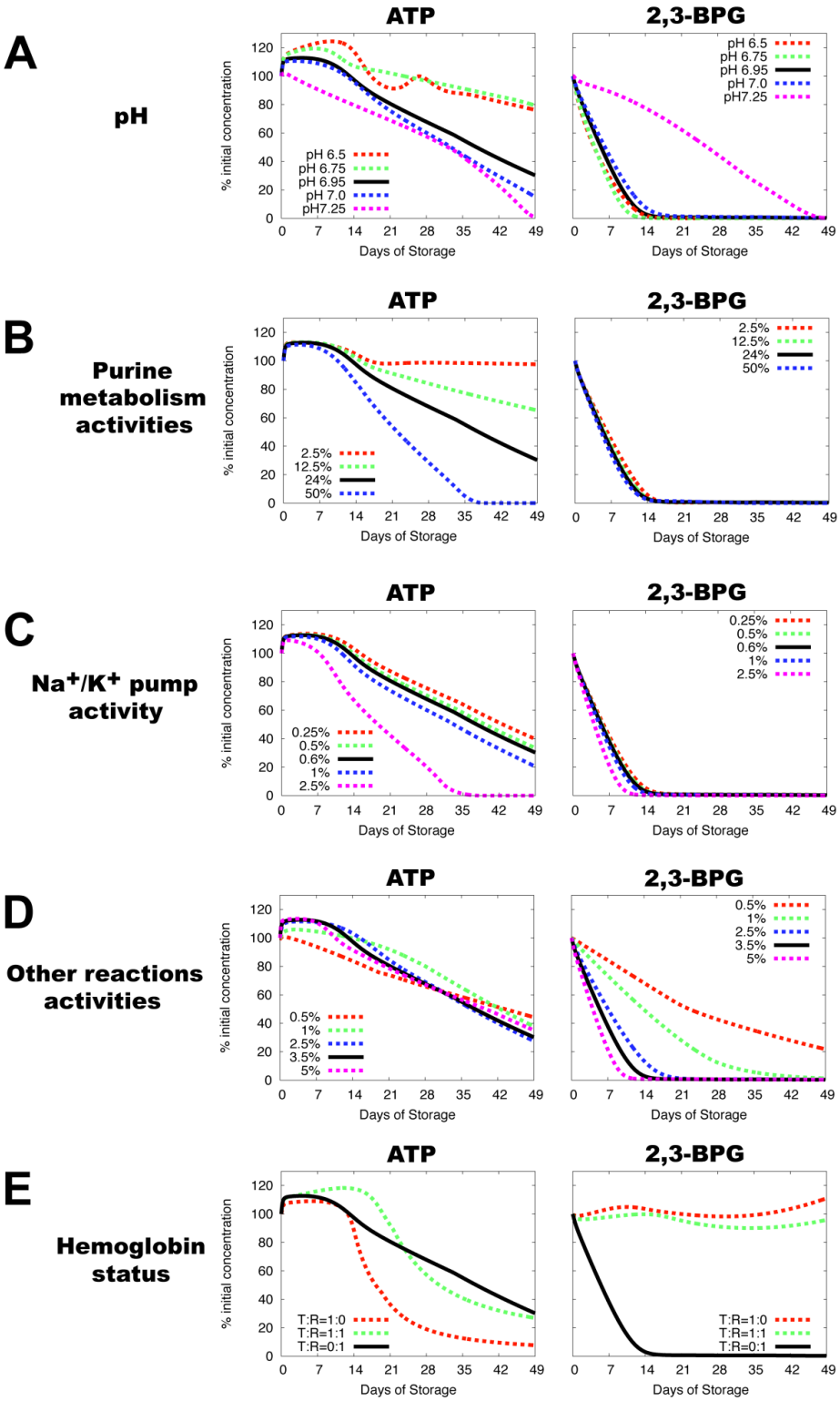

Figure 2.3 Simulation results of parameter analysis of the estimated model on the time-courses of ATP and 2,3-BPG during cold-MAP storage.

Parameters of the estimated model, which were modified from the original RBC model,

were varied. Panels indicate the time-course of ATP (left) or 2,3-BPG (right) under various intracellular pHs (A), purine metabolism enzyme activities (B), Na^+/K^+ pump activities (C), other reaction activities (D), and hemoglobin statuses (E). A, Initial pH was changed to 6.5 (*broken red*), 6.75 (*broken green*), 6.95 (*black, value of the estimated model*), 7.0 (*broken blue*), or 7.25 (*broken pink*). B, Purine metabolism enzyme activities were changed to 2.5% (*broken red*), 12.5% (*broken green*), 24% (*black, value of the estimated model*), or 50% (*broken blue*) of the level in the basal model. C, Activity of the Na^+/K^+ pump was changed to 0.25% (*broken red*), 0.5% (*broken green*), 0.6% (*black, value of the estimated model*), 1% (*broken blue*), or 2.5% (*broken pink*) of the level in the basal model. D, All other reaction activities were changed to 0.5% (*broken red*), 1% (*broken green*), 2.5% (*broken blue*), 3.5% (*black, value of the estimated model*), or 5% (*broken pink*) of the level in the basal model. E, Hemoglobin allosteric status was changed to only R-state (*black, state of the estimated model*), mixture of equal quantities of R-state and T-state (*broken green*), or only T-state (*broken red*).

2.3.3 Sensitivity analysis to identify the key independent enzymes enable to maintain ATP and 2,3-BPG levels

We also performed a sensitivity analysis of the independent enzyme activities in the estimated model, to predict their effects on the ATP and 2,3-BPG concentrations after storage for 28 or 49 days. We calculated the ratio between the concentrations in the estimated model and those in the case where each enzymatic activity was independently increased or decreased by 10% (Table 2.2). Four enzymes, HK, PFK, 2,3-BPG shunt, and AMPase, were predicted to be significant modulators of metabolic alterations during the long storage of RC-MAP, as indicated by ATP and 2,3-BPG levels.

Slight inactivation of 2,3-BPG shunt, which contains all elementary reactions related to 2,3-BPG or 1,3-bisphosphoglycerate (1,3-BPG) synthesis, conserved both ATP and 2,3-BPG levels. When 2,3-BPG shunt was decreased by 10% of that in the estimated model, ATP and 2,3-BPG were significantly increased by 34% and 73%, respectively, at day 49. A decrease in the activity of AMPase, a purine metabolism enzyme, effectively maintained ATP during cold storage. When the activity of AMPase was decreased by 10% of that in the estimated model, ATP was increased by 14% and 2,3-BPG by 13% after 49 days of storage. The activation of HK and PFK effectively maintained both ATP and 2,3-BPG concentrations. When HK activity was increased by 10% of that in the estimated model, the final concentrations of ATP and 2,3-BPG were increased by 30% and 88%, respectively, of those predicted by the estimated model after 49 days of storage. Similarly, slight activation of PFK increased ATP and 2,3-BPG levels by 14% and 30%, respectively, after 49 days. Interestingly, the prediction that activation of HK and PFK was able to maintain ATP and 2,3-BPG levels appears to

conflict with the parameter analysis shown in Figure 2.3D, which showed that smaller reaction activities were more efficient at this maintenance.

Table 2.2 Sensitivity analysis of the estimated model.

Enzyme	Enzymatic activities increased by 10%				Enzymatic activities decreased by 10%			
	28days		49days		28days		49days	
	ATP(%)	2,3-BPG(%)	ATP(%)	2,3-BPG(%)	ATP(%)	2,3-BPG(%)	ATP(%)	2,3-BPG(%)
HK	112 (↑)	157 (↑↑)	130 (↑↑)	188 (↑↑)	87 (↓)	60 (↓↓)	65 (↓↓)	34 (↓↓)
PGI	100	100	100	100	100	100	100	100
PFK	105	121 (↑↑)	114 (↑)	130 (↑↑)	94	81 (↓)	84 (↓)	71 (↓↓)
ALD	100	100	100	100	100	100	100	100
TPI	100	100	100	100	100	100	100	100
GAPDH	100	99	98	97	100	101	102	103
2,3-BPG shunt	89 (↓)	75 (↓↓)	69 (↓↓)	48 (↓↓)	112	135 (↑↑)	134 (↑↑)	173 (↑↑)
PGK	100	100	100	100	100	100	100	100
PGM	100	100	100	100	100	100	100	100
EN	101	99	102	102	99	101	98	98
PK	104	94	112 (↑)	106	96	106	86 (↓)	91
LDH	100	100	100	100	100	100	100	100
LDH2	101	99	102	102	99	101	97	98
G6PDH	100	100	100	100	100	100	100	100
6PGODH	100	100	100	100	100	100	100	100
6PGLase	100	100	100	100	100	100	100	100
GSSGR	100	100	100	99	100	100	100	101
L_GCS	100	98	98	96	100	102	102	104
OX	99	96	94	88 (↓)	101	104	105	111 (↑)
GSH_S	100	100	100	100	100	100	100	100
R5PI	100	100	100	100	100	100	100	100
X5PI	100	100	100	100	100	100	100	100
TK1	100	102	102	104	100	98	98	96
TK2	100	100	100	101	100	100	100	99
TA	101	103	104	108	99	96	95	89 (↓)
PRPPsyn	99	95	93	87 (↓)	101	106	108	114 (↑)
PRM	100	100	100	100	100	100	100	100
PNPase	100	100	100	100	100	100	100	100
AK	101	98	102	101	99	102	97	99
ADA	100	102	98	99	101	98	103	101
AMPDA	100	100	100	100	100	100	100	100
ADPRT	100	99	100	100	100	101	100	101
AMPase	96	102	86 (↓)	86 (↓)	104	98	114 (↑)	113 (↑)
HGPRT	100	101	100	100	100	99	100	100
IMPase	100	100	100	100	100	100	100	100
APK	100	100	100	100	100	100	100	100

The sensitivity analysis allows calculation of the effects of changing independent enzyme activities in the estimated model on ATP and 2,3-BPG levels after 28 or 49 days of storage. Each data point is the percentage of the result of the estimated model at the same storage time point. Up and down arrows in parentheses indicate that the levels were maintained or reduced up to 10% (*single arrow*) and 20% (*double arrows*) of the estimated model. Abbreviations of the enzymes are given in Table 2.1

2.3.4 Comprehensive measurements of intermediate concentrations and model predictions

We performed a metabolome analysis in which multiple intermediates in RC-MAP were measured by CE-TOFMS at days 0, 1, 3, 7, 14, 28, and 49 after blood collection. The results of these measurements and estimated model predictions fitting the reported data of ATP and 2,3-BPG in packed and commercially used RC-MAP are shown in Figure 2.4 and in Table 2.3. Figure 2.4 shows the time-dependent alterations in glycolytic intermediates and Table 2.3 shows the metabolite levels, including glycolytic intermediates, ATP, 2,3-BPG, and any markedly accumulated metabolites after 28 or 49 days of storage.

The measured concentrations of fructose 1,6-bisphosphate (F1,6-BP), dihydroxyacetone phosphate (DHAP), 3-phosphoglycerate (3PG), and phosphoenolpyruvate (PEP) were initially increased and started to decrease significantly within seven days (Figure 2.4). F1,6-BP and DHAP were particularly prone to decrease under blood preservation: F1,6-BP was at 18 ± 6% of its initial level at day 28 and depleted at day 49, while DHAP was almost depleted at day 28 (Table 2.3). The total amounts of glucose 6-phosphate (G6P) and fructose 6-phosphate (F6P) were also decreased at 28 and 49 days after storage. In contrast, PYR and LAC, which are downstream of glycolysis, were significantly accumulated throughout the storage period (Figure 2.4A, Table 2.3).

For the glycolytic intermediate concentration predictions with the estimated model, G6P, F6P, F1,6-BP, DHAP, 3PG, and PEP were qualitatively decreased, while LAC and PYR were significantly increased at 49 days of storage (Figure 2.4B, Table

2.3). This accumulation of LAC and PYR are caused by permeability of these metabolites across erythrocyte membrane and by irreversibility of PK. While the initial concentration peaks of F1,6-BP, DHAP, 3PG, and PEP also appeared in the model prediction, those of F1,6-BP and DHAP were much smaller and occurred earlier than the metabolome experiments (Figure 2.4). The initial peaks of 3PG and PEP were increased in width compared to F1,6-BP and DHAP in both CE-TOFMS measurements and our predictions. While PYR accumulation occurred after 14 days of storage in the experiments, the model predicted that PYR should accumulate early and decrease after 14 days (Figure 2.4).

Table 2.3 CE-TOFMS measurements and model predictions of metabolic intermediates in cold-MAP erythrocytes after 28 days and 49 days of storage.

Metabolite	Percentage of initial concentration (%)			
	28days		49days	
	CE-TOFMS	Model prediction	CE-TOFMS	Model prediction
G6P+F6P	67 ± 8	94	27 ± 12	55
F-1,6BP	18 ± 6	35	0 ± 0	18
DHAP	0 ± 0	21	0 ± 0	14
3PG	78 ± 18	52	41[a]	41
PEP	51 ± 26	55	94 ± 8	46
PYR	1940 ± 260	1310	2660 ± 430	1110
LAC	2770 ± 260	1910	3310 ± 170	2810
HX	18800 ± 4000	25100	64400 ± 22300	48600
S7P	580 ± 50	590	340 ± 90	520
Total ATP	–	68	–	30
Total 2,3-BPG	–	1	–	0
Free form of ATP	36 ± 6	30	6 ± 1	9
Free form of 2,3-BPG	0 ± 0	0	0 ± 0	0

Data represent the mean ± S.D. of five separate experiments. [a] Data represent one experiment.

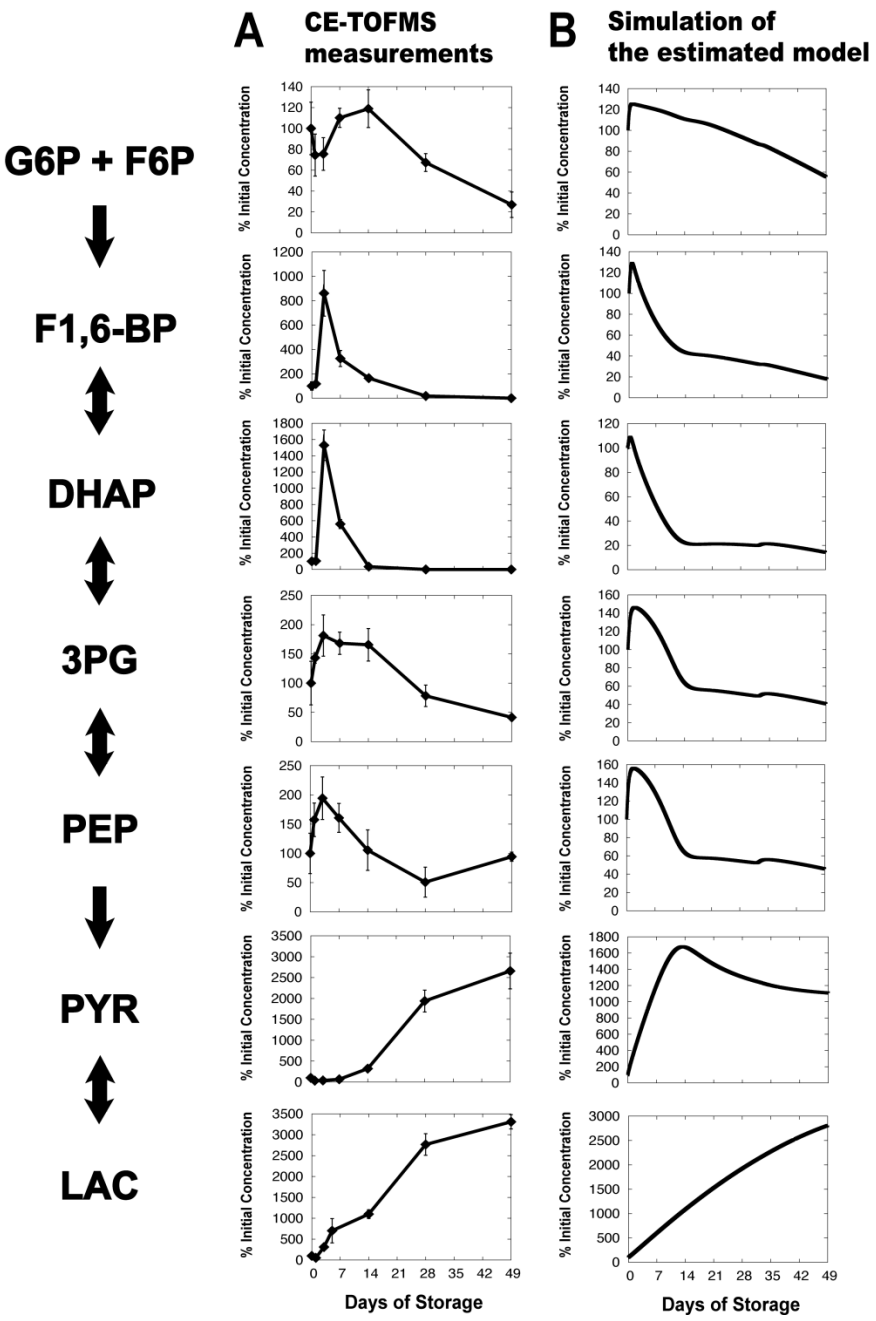

Figure 2.4 Measured and predicted time-courses of glycolytic intermediates in cold-stored MAP-RBC.

A, CE-TOFMS measurements of time-course data of glycolysis in erythrocytes suspended in cold-MAP for 49 days under laboratory conditions. Data represent the mean ± S.D. of five separate experiments. B, Predicted time-courses of glycolytic intermediates from the estimated model fitted to the reported data of ATP and 2,3-BPG in packed and commercially used RC-MAP. 'G6P + F6P' means the sum of the concentrations of G6P and F6P. Values are the percentage of the initial concentration of each metabolite at day 0.

HX, which is one of the purine metabolism intermediates, was remarkably accumulated in RC-MAP at 4°C. HX levels were increased up to 188-fold of their initial level in CE-TOFMS measurements and up to 251-fold in the simulation of the estimated model after 28 days of storage (Table 2.3). HX accumulation dramatically increased as the storage period increased: at 49 days, HX was increased to 644-fold in the measurements and 486-fold in the simulation. Another markedly accumulated metabolite during storage was S7P, a known pentose phosphate pathway intermediate. The level of S7P at 28 days was 5.8-fold of its initial concentration in the metabolome experiment and 5.9-fold of its initial concentration in the simulation, whereas after 49 days this level decreased to 3.4-fold and 5.2-fold of the initial levels observed in CE-TOFMS analysis and the simulation, respectively (Table 2.3). In CE-TOFMS experiments, 2,3-BPG was almost depleted by 28 days, consistent with our model predictions. The measured ATP level decreased to 36% of its initial level at 28 days, and, unlike the previously reported data of commercially used RC-MAP, the level was nearly depleted (6%) at 49 days (Table 2.3). ATP and 2,3-BPG are absorbed by hemoglobins, and some portions of ATP and 2,3-BPG are lost during deproteinization in the metabolome experiment procedure [46]. In addition, these Mg^{2+}-binding metabolites were undetectable by CE-TOFMS analysis. For the sake of comparison, the calculated values of the free forms of ATP and 2,3-BPG are shown in Table 2.3. Consequently, the predicted results of the levels of the free forms of ATP and 2,3-BPG in the estimated model at days 28 and 49 were similar to the measurements.

2.4 Discussion

To refine blood storage solutions, various additives and storage conditions have been experimentally tested. However, none of these trials has achieved the simultaneous maintenance of ATP and 2,3-BPG levels during long storage over 49 days [16,58,59,60]. To systemically identify an effective way to preserve these metabolites, we developed a model that reproduces the metabolic behavior in RC-MAP stored at 4°C based on a detailed erythrocyte metabolic model.

We performed the parameter estimation with GA analysis to fit our model to the reported time-course experimental data of ATP and 2,3-BPG in commercially used RC-MAP. We also carried out a comprehensive parameter search to identify the range of the three adjustable parameters estimated by the GA analysis, which is not shown in this thesis. Briefly, 24^3 patterns of combinations of the three adjustable parameters were simulated by evaluating the fitness to the above experimental data of RC-MAP using the same fitness function as that used in the GA analysis. The comprehensive parameter search provided the ranges of the adjustable parameters in the top 0.1% of fitness in all combinations where their evaluated values (distance EV) were below 0.1, which were confined to certain areas. From the GA analysis and the comprehensive parameter search, Na^+/K^+ pump activity was predicted to be 0.6% (GA) and 0-0.9% (comprehensive search), purine metabolism enzymes activities to be 24% (GA) and 20-30% (comprehensive search), and the other reactions activities to be 3.5% (GA) and 3-6% (comprehensive search) of the basal model values, respectively.

We also confirmed the validity of using these predicted parameters by the following aspects. The Na^+/K^+ pump activity was predicted to be smaller than the

general enzyme activities. Our estimated values are in good agreement with the reported data that Na^+/K^+ pump activity decreases to 0.2-0.8% of the normal level at body temperature when the temperature is decreased to 5°C in most mammalian erythrocytes [65]. The purine metabolism enzymes appeared to be more active than other general enzyme activities. This result agrees with reports that many purine metabolism enzymes have a relatively low optimal pH, which may lead to increases in their activities under lower pH conditions, such as in a stored environment [66,67,68,69,70]. The other reaction activities were predicted to be within the previously reported range, where general enzyme activities at ~ 4°C are suppressed to 1-5% of those at the normal body temperature [77,78]. These results verify that the reactions included in the basal model should be placed into at least three such groups to predict the metabolic conditions of RC-MAP. Moreover, the results also suggest that the reliable prediction of the time-courses in ATP and 2,3-BPG levels in RC-MAP can be obtained only in limited ranges of each adjustable parameter, which can be well explained by physiological properties.

The results from varying the initial pH in our estimated model suggest that high pH is required to maintain 2,3-BPG levels during storage, but is not effective at maintaining ATP levels. This is supported by a previous report indicating that 2,3-BPG is increased but ATP is decreased in erythrocytes stored in an alkaline additive solution at pH 8.7 [79]. Though pH has been studied as a target for developing novel blood storage solutions [15,33,79,80], it is difficult to overcome the trade-off between maintaining 2,3-BPG or ATP levels.

Parameter analysis also indicated that the transition of hemoglobin to the T-state could be more effective than transition to the R-state at maintaining 2,3-BPG

levels. The 100-fold greater affinity of T-state hemoglobin to 2,3-BPG relative to that of R-state hemoglobin may save the free form of 2,3-BPG from excess consumption through metabolic reactions. One method for stabilizing hemoglobin to the T-state is treating RBCs with nitric oxide (NO) [81]. However, the practical use of NO remains difficult because of the irreversibility of the transition of gas-treated hemoglobin.

Parameter analysis for the reaction activities of the three adjustable parameters predicted that lower activities can effectively maintain ATP and 2,3-BPG levels. A seemingly contradictory phenomena was observed in the sensitivity analysis of independent enzymatic activities, which showed that the activation of HK or PFK may maintain both ATP and 2,3-BPG levels, whereas these levels were maintained when the reaction activities were collectively decreased in the parameter analysis. As the catalytic activity of PFK is inhibited by citrate [82], the replacement of citrate in storage solutions to another possible component will effectively keep PFK activity high and consequently maintain ATP and 2,3-BPG levels during blood storage. The pH increase achieved by omitting citrate from the blood storage solution may upregulate the catalytic activity of HK [83,84]. This approach may possibly help preserve the blood, although it does require careful consideration of the balance between the pH-dependent opposite effects on ATP and 2,3-BPG and the direct effects of pH on HK and PFK.

The complex behavior of metabolic indicators results from the dynamics of large-scale metabolic networks with various regulations. With the recent development of a metabolomic analysis using CE-TOFMS, we can now obtain a comprehensive view of metabolism and analyze the detailed dynamics of metabolism behind the complex networks [61,85,86]. We performed the metabolomic analysis of RC-MAP stored for 49 days using CE-TOFMS. In CE-TOFMS measurements, PYR, LAC, HX and S7P were

significantly increased, and all glycolytic intermediates except for PYR and LAC were markedly decreased after 49 days. Though there are differences in the conditions between our experimental and commercially used packed RC-MAP, these measured alterations of intermediates were qualitatively reproduced in an estimated model that was fitted to the reported data of RC-MAP. Actually, the use of random sets of the three adjustable parameters with the estimated model failed to predict these final accumulations or decreases in the intermediate concentrations (Figure 2.5). However, the dynamics of intermediates, such as the extraordinary large increases in F1,6-BP and DHAP in the first week or initial stagnation of PYR, could not be predicted by the estimated model.

Still, it remains possible to bridge these gaps between the lab-conditioned measurements and predictions through further refinement of the estimated model. Slight lowering of the initial pH in the estimated model changes the dynamics of the intermediates; remarkable initial peaks and later complete depletion of F1,6-BP and DHAP in the CE-TOFMS measurements appear following a reduction in the initial pH (Figure 2.6). In addition, the initial stagnation of PYR may be due to PK inactivation, although the reason is unknown. The later rapid accumulation of PYR would explained by the activation of PK through the accumulation of adenosine monophosphate (AMP), an activator of PK, which is shown in the measurements, whereas this effect of AMP on PK is not described in the model. An analysis of the comprehensive metabolomics data enables more precise prediction and observation of underlying aspects that cannot be established by metabolic indicators alone.

In conclusion, we provided the mathematical model of the metabolic status of cold-stored RC-MAP, which was qualitatively validated by CE-TOFMS experiments.

Systemic analysis of our model indicated its possible use for identifying targets for refining storage solutions or preservation methods.

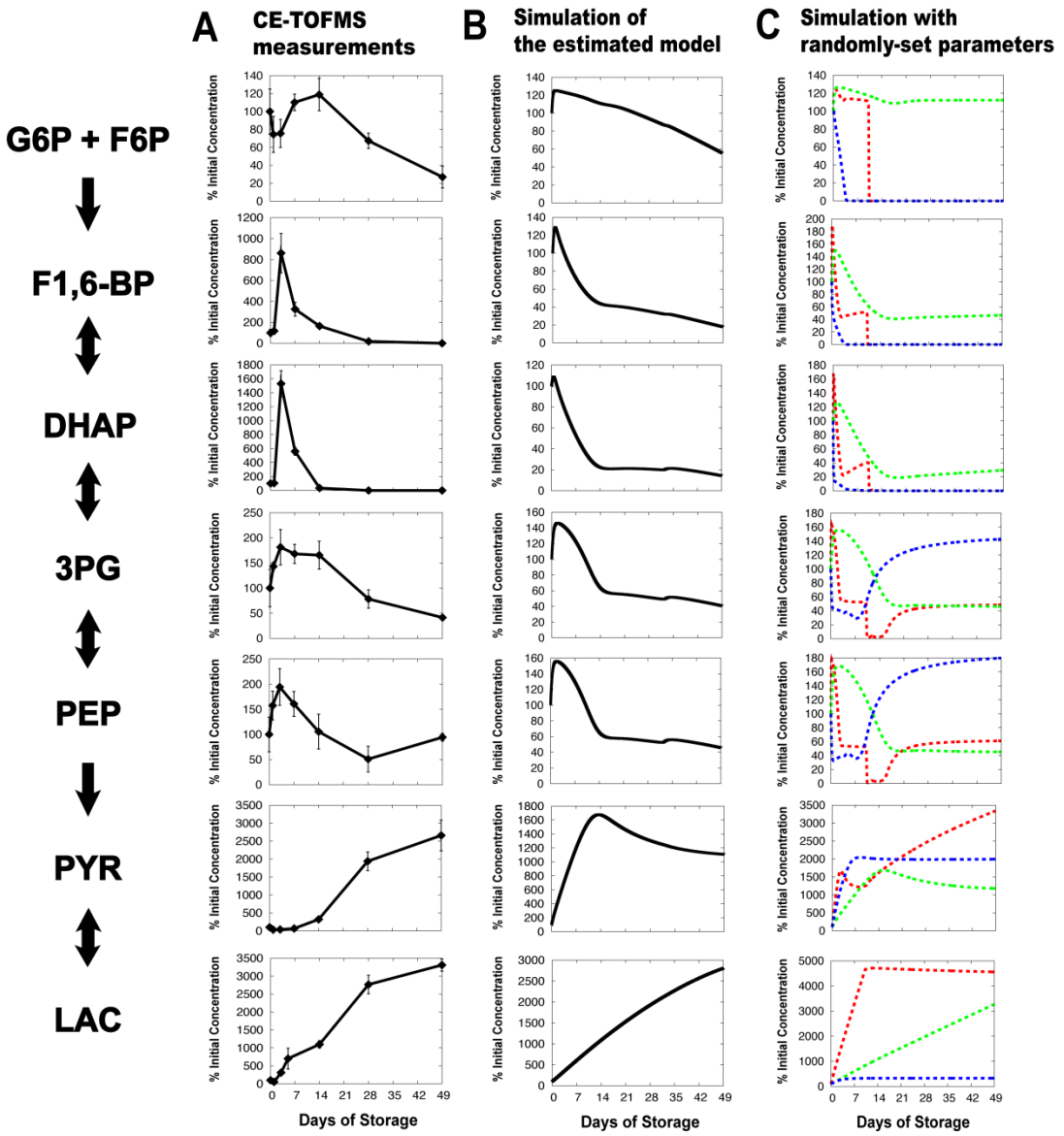

Figure 2.5 Comparison of the simulation results between the GA-based estimated model and the models with randomly-set parameters.

A and B, CE-TOFMS measurements and predictions from the GA-estimated model of glycolytic intermediates as shown in Figure 2.4. The estimated model implements 24% for purine metabolism enzyme activities, 0.6% for Na^+/K^+ pump activities, and 3.5% for all other reaction activities. C, Prediction of the models in which the three adjustable parameters used in GA analysis were randomly set. The models implements 24% for purine metabolism enzyme activities, 0.6% for Na^+/K^+ pump activity, and 24% for all other reaction activities (*broken red*); 0.6% for purine metabolism enzyme activities, 0.6% for Na^+/K^+ pump activity, and 3.5% for all other reaction activities (*broken green*); and 24% for purine metabolism enzyme activities, 24% for Na^+/K^+ pump activity, and 3.5 % for all other reaction activities (*broken blue*). Percentages are of the basal model levels for each parameter.

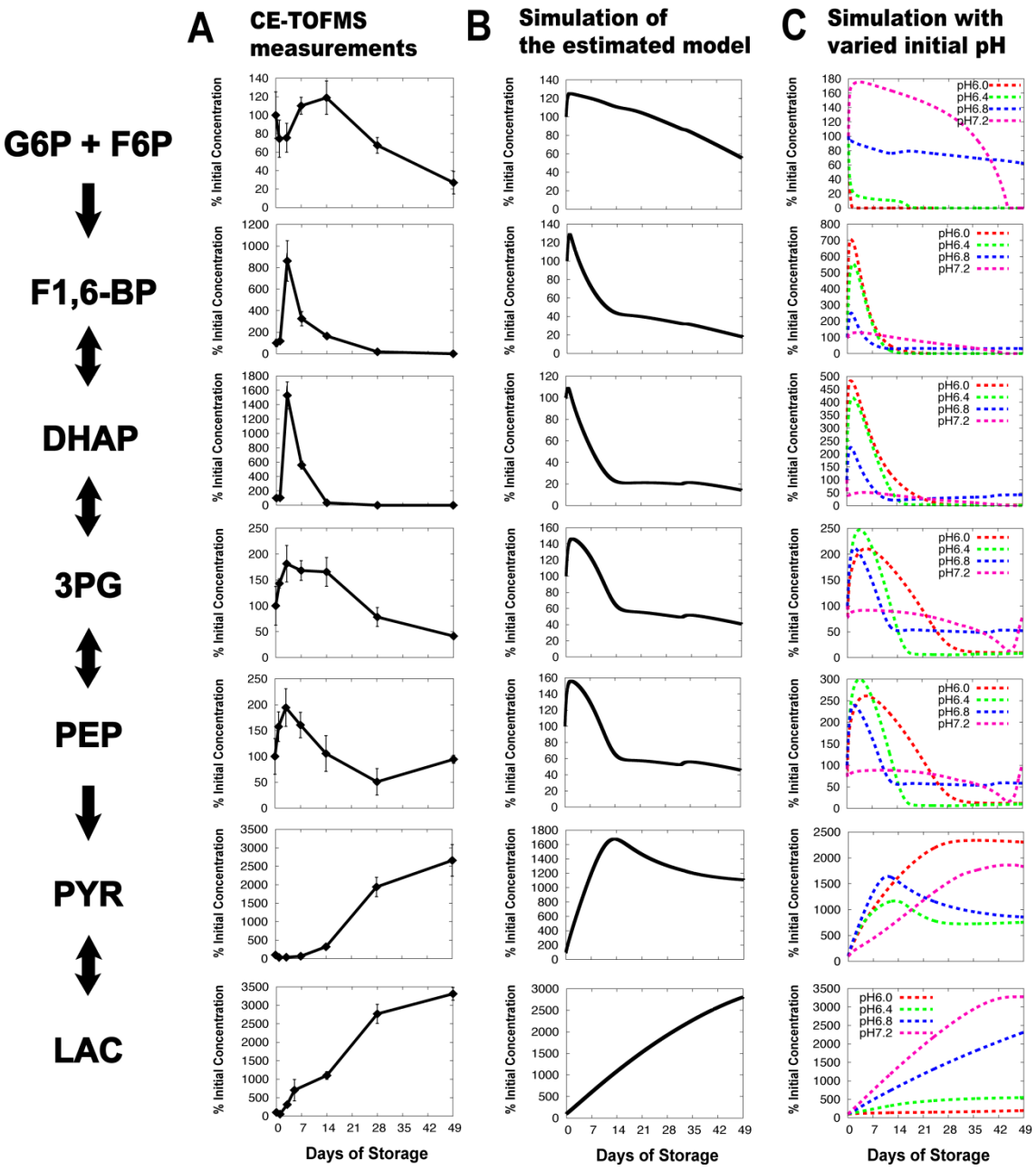

Figure 2.6 Prediction of the effects of initial pH on the concentrations of glycolytic intermediates.

A and B, CE-TOFMS measurements and predictions from the GA-estimated model of glycolytic intermediates as shown in Figure 2.4. The initial pH of the estimated model was set to 6.95, as reported in the literature [28]. C, Prediction of the models with various initial pHs, set at 6.0 (*broken red*), 6.4 (*broken green*), 6.8 (*broken blue*), or 7.2 (*broken pink*).

Chapter 3

Metabolic dynamics of PAGGGM-stored erythrocytes using a large-scale *in silico* model

In the previous chapter, we developed the first mathematical model of cold stored-RBCs and predicted possible enzymatic and biochemical reactions that can improve RBCs storage condition. In this chapter, we reproduced the metabolic dynamics of stored erythrocytes preserved in new additive solution that can maintain ATP and 2,3-BPG for 5 weeks of storage. Through simulations and analyses of the model, we clarified the mechanism of metabolic dynamics for effective production of ATP and 2,3-BPG and possible side-effects induced by the new additive solution.

3.1 Introduction

In Chapter 2, we developed a large-scale precise kinetic model for predicting the whole metabolic behavior of cold-stored RBCs with the commonly used additive solution in Japan [87]. From the *in silico* analysis, we suggested that the activation of PFK would lead to the maintenance of ATP and 2,3-BPG levels during RBC storage [87]. This prediction was confirmed by the experimental study of a novel additive solution named PAGGGM [88]. PAGGGM includes glucose, ADE, and GUO as energy substrates, and it is superior to conventional storage solutions for maintaining both ATP and 2,3-BPG levels over 5 weeks [33]. Burger and his colleagues observed the

time-related changes of glycolytic intermediates in PAGGGM-stored RBCs and first provided the experimental evidence that PFK activity is likely to be enhanced in PAGGGM relative to conventional additive solutions [88]. A comprehensive simulation model can trace the time-related changes not only in metabolites' levels, but also in enzymatic activities, which are difficult to observe in experimental procedures under blood storage condition, and helps us to understand the underlying regulatory mechanism of the associated maintenance of ATP and 2,3-BPG.

In addition, the fate of additives and the behavior of other metabolic intermediates in stored blood have received little attention, despite the excessive accumulation of metabolic byproducts like inosine (INO) and HX during cold-storage which are rapidly converted to toxic uric acid in the circulation [89]. A mechanism of increase of the metabolic byproducts should be considered by observing the metabolic dynamics in a comprehensive manner. For example, ADE is currently included in all commonly used RBC additive solutions due to its beneficial effect on ATP maintenance as a purine source; however, it is also known to break down into other metabolites like INO and HX, which can be toxic owing to the potential effect on uric acid generation or oxidative stress. An excess increase in plasma uric acid in blood transfusion causes liver function disorder, and can be a risk factor for hyperuricemia.

In this chapter, we predicted the metabolic dynamics of PAGGGM-stored RBCs with the large-scale *in silico* model in order to clarify the underlying mechanism of how 2 functional metabolites, namely, ATP and 2,3-BPG, can be maintained over a long storage period. We also determined the comprehensive roles of solution additives in the metabolic dynamics of cold-storage RBCs. Through the simulation analysis, we predicted the mechanism of PFK activation, as well as the fate of 2 major additives,

ADE and GUO, for RBCs in cold storage conditions in PAGGGM solution. A model of PAGGGM-stored RBCs was developed based on a curated RBC metabolic model developed by Kinoshita *et al.* [46] by changing environmental components and pH- or temperature-related enzymatic activities. The model prediction of overall metabolic changes during storage time was validated by experimental measurements of metabolic intermediates by CE-TOFMS analysis. The metabolic behavior of PAGGGM-stored RBCs predicted by the model was in qualitative agreement with that measured by CE-TOFMS analysis. From the simulation analysis, we concluded that ADE is useful for the maintenance of the adenylate pool, which can increase ATP levels, but causes an accumulation of metabolic waste like HX. Moreover, ADE induces the consumption of ribose phosphates, which leads to 2,3-BPG reduction. In contrast, GUO is used as a source of ribose phosphates in the non-oxidative pentose phosphate pathway (non-ox PPP) without increasing purine metabolites. Increasing concentrations of ribose phosphates result in an accumulation of upper glycolytic intermediates, leading to PFK activation and an associated increase in both ATP and 2,3-BPG. This indicates that GUO can compensate for the depletion of 2,3-BPG induced by ADE. Further analysis suggested that the fate of GUO itself is also controlled by ADE concentration. The trade-offs and coordinating mechanism between ADE and GUO, which provide metabolic benefits and disadvantages under RBC storage conditions, are discussed herein.

3.2 Materials and Methods

3.2.1 Blood collection and preservation

Whole blood samples were collected from healthy volunteers by using vacuum blood collection tubes with sodium heparin (Venoject II; Terumo Corp., Tokyo, Japan). Blood samples were washed and suspended in CPD solution (26.3 g/L sodium citrate hydrate, 3.27 g/L citric acid hydrate, 23.2 g/L glucose, and 14.57 g/L sodium dihydrogen phosphate). The blood suspended in CPD was centrifuged at 3300 ×*g* for 10 min, and the plasma and buffy coat were removed. The buffy coat free blood was suspended in PAGGGM solution (8.726 g/L sodium gluconate, 0.195 g/L ADE, 8.558 g/L glucose, 0.408 g/L GUO, 9.909 g/L mannitol, 1.248 g/L $NaH_2PO_4 \cdot H_2O$, and 0.2855 g/L $NaH_2PO_4 \cdot 12H_2O$), resulting in a hematocrit of 60%. Finally, RBCs suspended in PAGGGM solution were divided into 1-mL plastic tubes and stored at 4°C for 0–35 days.

3.2.2 Measurement of intracellular pH

Intracellular pH was measured as described previously [90]. Briefly, 900 µL of PAGGGM-stored RBCs was centrifuged at 3300 ×*g* for 5 min. The supernatant solution was removed and 100 µL erythrocytes hemolyzed by freezing in liquid nitrogen. Milli-Q water (100 µL) was added, and the pH of the lysate was measured by using a portable blood gas analyzer i-STAT 300F (Fuso Pharmaceutical Industries, Osaka, Japan) at days 0–14 and by using a compact pH meter (HORIBA B-211) at days 21–35.

3.2.3 Preparation of erythrocytes for CE-TOFMS analysis

To isolate erythrocytes, PAGGGM-stored RBCs were centrifuged at 3300 ×*g* and 4°C for 5 min, and the supernatant solution was removed. Next, 0.2 mL of the sample erythrocyte pellet was treated with 1.8 mL cold methanol containing 20 μM each of methionine sulfone and CSA as the internal standards. Chloroform (2 mL) and Milli-Q water (0.8 mL) were added, and the mixture was thoroughly mixed and then centrifuged at 5800 ×*g* for 5 min at 4°C. Next, the upper aqueous layer was filtered through a centrifugal filter (Millipore, 5-kDa cut-off filter) to remove proteins. The filtrate was concentrated centrifugally and then dissolved in 50 μL of Milli-Q water containing reference compounds (200 μM each of 3-aminopyrrolidine and trimesate) immediately prior to CE-TOFMS analysis [61].

3.2.4 Instrumentation

The instrumentation is described in 2.2.5.

3.2.5 CE-TOFMS conditions for cationic/anionic metabolites and nucleotides analysis

Separations of cationic metabolites were carried out in a fused-silica capillary (50 μm inner diameter × 103 cm total length) filled with 1 M formic acid as the reference electrolyte [74]. For anionic metabolites and nucleotides separations, a cationic polymer–coated COSMO(+) capillary (50 μm inner diameter × 106 cm total length; Nacalai Tesque, Kyoto, Japan) was used. Other analytical conditions for ionic metabolites and nucleotides are the same as described in 2.2.6 and 2.2.7.

3.2.6 CE-TOFMS data processing

The data processing is described in 2.2.9.

3.2.7 PAGGM-stored RBC model construction

We built a PAGGGM-stored RBC model based on a published model of human erythrocyte metabolism [46]. All simulation experiments were carried out on E-Cell 3. The basal model includes the major metabolic pathways such as glycolysis, pentose phosphate pathway, purine salvage pathway, membrane transport systems for intermediates, ion leak processes, ATP-dependent Na^+/K^+ pump process, and binding reactions between hemoglobin and metabolites. Figure 3.1 shows metabolic pathways included in the PAGGGM-stored RBC model. The PAGGGM solution comprised 47.5 mM glucose, 1.44 mM ADE and 1.44 mM GUO as the energy substrates, 8.00 mM Na_2HPO_4 and 8.00 mM NaH_2PO_4 as the source of phosphate and as the pH buffer, and 55.0 mM mannitol and 40.0 mM sodium gluconate as osmoregulatory substrates. The extracellular environments in the model were set as 47.5 mM glucose, 1.44 mM ADE and 1.44mM GUO, 64.0 mM of sodium ion, and 16.0 mM of inorganic phosphate, based on the components of the PAGGGM solution. In human erythrocytes, GUO is converted into guanine (GUA) and ribose 1-phosphate (R1P) by purine nucleoside phosphorylase [91]. Thus, in the present study, we modeled a process of GUO consumption as follows:

$$\mathrm{GUO} + \mathrm{Pi} \rightarrow \mathrm{GUA} + \mathrm{R1P} \tag{3.1}$$

$$v = k[\mathrm{GUO}][\mathrm{Pi}] \tag{3.2}$$

The phosphorylation rate constant (k = 1e+8 $s^{-1}\cdot M^{-2}$) was determined by manually

fitting the GUO depletion curve as measured by CE-TOFMS experiments (Figure 3.2).

We modeled the tense–relax state transition of hemoglobin and inactivation of all chemical reactions induced by low temperatures at 4°C and additive solution during blood storage as per our previous study in Chapter 2 [87]. Insomuch as hemoglobin is known to be stable in the R-state at low temperature, we set all hemoglobins as in R-state in the PAGGGM-stored RBC model. At low temperatures, all chemical reactions such as enzymatic reactions, chemical-binding reactions, and active transport processes are assumed to be significantly inactivated according to the Arrhenius equation. As mentioned in Chapter 2, all the chemical reactions can be divided into 3 groups on the basis of their sensitivity to temperature and pH, namely Na^+/K^+ pump activity, purine salvage activities, and all other reaction activities [87]. The reaction activities of each group were set as 0.1%, 25.0%, and 3.0% of the values in the basal model (37°C), respectively, by retuning the previous model of cold-stored RBCs preserved in the MAP solution in Chapter 2. Briefly, the parameter estimation was performed by a real-coded genetic algorithm to fit with 8 points time-series of ATP and 2,3-BPG in cold-stored RBCs preserved in commercially available MAP solution [28]. The parameters were searched within their feasible ranges which we provided in Chapter 2. CE-TOFMS measurements showed that the peak intracellular concentrations of F-1,6-BP, DHAP and LAC were significantly larger in PAGGGM-stored RBCs compared with RC-MAP (p-values < 0.001) (Figure 3.3). These differences in the peak concentrations could be reproduced with the computational models by changing the initial concentrations of extracellular additives and the decline curve in intracellular pH, and by adding the simple first-order process of GUO phosphorylation (Figure 3.3). The difference between the basal model (37°C), MAP-stored RBC model (4°C) and PAGGGM-stored RBC

model (4°C) was shown in Table 3.1.

We also modeled the pH-degradation profile of PAGGGM-stored RBCs. The time courses of intracellular pH in PAGGGM-stored RBCs were measured at 37°C (Figure 3.6A). However, the physiological pH in cold-stored erythrocytes is known to be much higher than that measured at 37°C [83]. Therefore, we estimated the actual intracellular pH in PAGGGM-stored RBCs at 4°C by using the relationship of temperature and intracellular pH, *i.e.*, Δ pH/°C = -0.0161, proposed by Guppy *et al*. [83] (Figure 3.6A). The pH degradation rate of intracellular pH during storage was approximated as eq.(3.3) from the estimated pH curve under 4°C. In eq.(3.3), a = 8.79e-14, b = -6.01e-7, and pH_0 = 7.62 were used as constants from the experimental data.

$$\frac{d\mathrm{pH}}{dt} = \sqrt{b^2 - 4a(\mathrm{pH}_0 - \mathrm{pH})} \tag{3.3}$$

3.2.8 Statistical analyses

Paired Student's *t*-test was employed to analyze CE-TOFMS time course data to show the differences from the value of day 0. A two-sided *p* value of < 0.01 was considered statistically significant. Differences in mean metabolic concentrations between MAP-stored RBCs and PAGGGM-stored RBCs were examined using two-sample *t*-test.

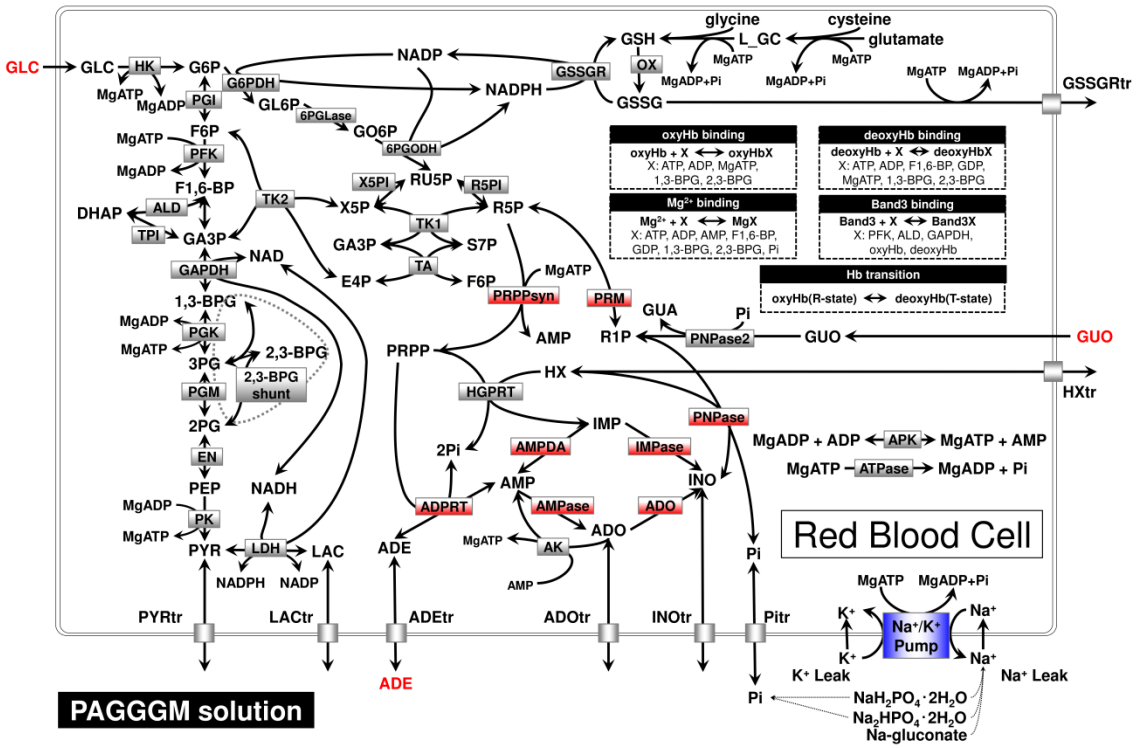

Figure 3.1 Metabolic pathway in the mathematical model of PAGGGM-stored RBCs.

In the map, nodes indicate metabolites or ions, and edges indicate enzymatic reactions or transport processes, which were divided into 3 groups (*red, blue, gray boxes*) by the difference in sensitivity of enzymatic or reaction activity to temperature or pH as described in Chapter 2 [87]. Abbreviations used in this figure are given in Table 2.1.

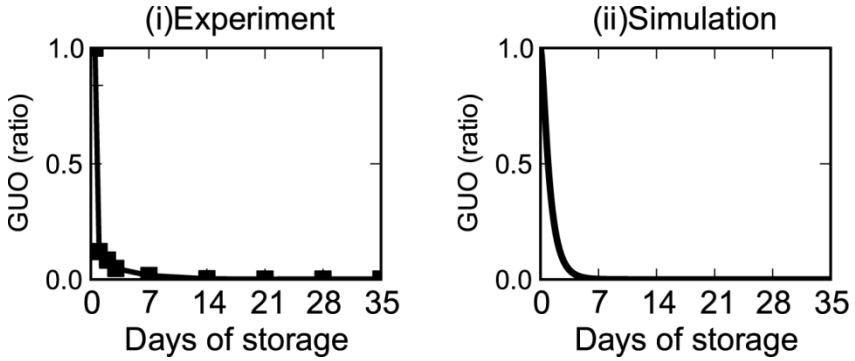

Figure 3.2 Measured and simulated time-series of GUO consumptions.

GUO consumptions in PAGGGM-stored RBCs measured by CE-TOFMS (i) and predicted by the PAGGGM-stored RBC model (ii) were displayed. The time-series of GUO levels was plotted as a normalized to the day 0 concentration in each dataset. CE-TOFMS data were expressed as means ± S.D. of 6 separate experiments.

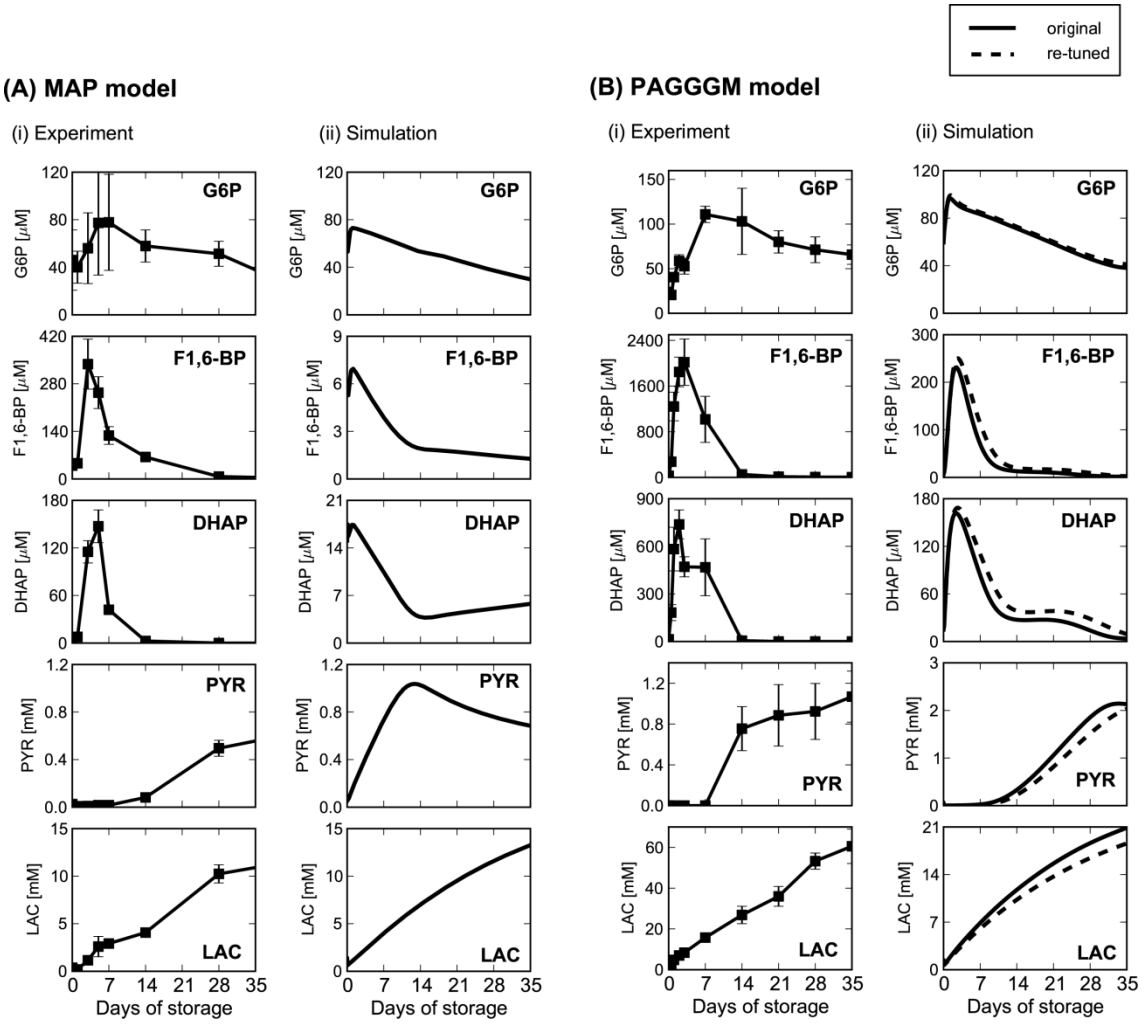

Figure 3.3 Time-series of glycolytic intermediates predicted by cold-stored RBC models with original and re-tuned parameters.

Measured and predicted time courses of intermediates in glycolysis in MAP-stored RBCs (A) and PAGGGM-stored RBCs (B) were illustrated. In simulation results of each panel, the time-series were predicted by original parameters in the Chapter 2 (*solid black line*), where three groups (Na^+/K^+ pump, purine salvage and other reactions) of reaction activities were set as 0.6%, 24%, 3.5% of the base model (37°C), and predicted by re-tuned parameters (*broken black line*), where those were set as 0.1%, 25%, 3.0%, respectively. Abbreviations used in this figure are given in Table 2.1 or Appendix B.

Table 3.1 Comparison between based and cold-stored RBC metabolic models.

	Base model (37℃)	MAP model (4℃)	PAGGGM model (4℃)
Enzymatic activities	100%	24%	25%
Purine metabolism activities	100%	35%	30%
Sodium/potassium pump activity	100%	6.0%	1.0%
Extracellular glucose	5 mM (fixed)	40 mM	47.5 mM
Extracellular adenine	0.015 mM (fixed)	1.04 mM	1.44 mM
Extracellular inorganic phosphate	1.1 mM (fixed)	6 mM	16 mM
Extracellular sodium ion	135 mM (fixed)	106 mM	64 mM
Extracellular guanosine	-	-	1.44 mM
Guanosine phosphorylation	-	-	First-order kinetics
pH setting	pH = 7.2 (fixed)	Initial pH = 6.95, $\mathrm{pH(t)} = at + 6.95$ $a = -8.66 \times 10^{-8}$	Initial pH = 7.62, $\mathrm{pH(t)} = at^2 + bt + 7.62$ $a = 8.79 \times 10^{-14}$ $b = -6.01 \times 10^{-7}$
State of hemoglobin	Transition between T- and R-state in response to various parameters; pO_2, pCO_2, pH, temperature and 2,3-BPG	R-state	R-state

3.3 Results and Discussion

3.3.1 Refinement of the RBC metabolic model to represent the dynamics of PAGGGM-stored RBC metabolism

The basal steady-state model assuming 37°C described in ref. [46] includes not only precise metabolic enzymatic reactions of comprehensive pathways but also other key chemical reactions associated with metabolic changes, such as allosteric transition in hemoglobin and subsequent binding or disassociation between a hemoglobin and ATP, 2,3-BPG / band3 membrane proteins / glycolytic enzymes. Each reaction in the basal model is described by detailed kinetic equations, where some enzymatic reactions in glycolysis, for instance, HK, PFK, GAPDH, PK, LDH, and reactions in 2,3-BPG shunt, are represented as pH-dependent kinetics. These features of the basal model are essential for the simulation of cold-stored RBCs, in which gradual but remarkable decline in pH, R-state stabilization of hemoglobin by low temperature, and non-uniform inactivation of chemical / enzymatic reactions occur at the same time. A PAGGGM-stored RBC model was developed by the refinement of our previous model of cold-stored RBC metabolism in MAP-solution [87] to meet the difference in environmental or intracellular conditions. Specifically, we changed initial concentrations of extracellular additives, added the simple first-order process of GUO phosphorylation, and refitted the parameters of enzymatic activities (Figure 3.3) and the decline curve in intracellular pH. The GUO phosphorylation rate constant (k = 1e+8 [$s^{-1} \cdot M^{-2}$]) was obtained from the manual adjustment to the GUO depletion curve measured by CE-TOFMS (Figure 3.2). This model showed good fit to the CE-TOFMS data. Moreover, we performed a simulation analysis to observe an influence of the rate

constant of GUO phosphorylation (k) on the dynamic behaviors of metabolic intermediates (Figure 3.4). In the analysis, k was varied from 1e+6 to 1e+9 and other conditions were same as the PAGGGM-stored RBC model. The dynamic behaviors of some metabolic indicators, ATP and total amount of HX, were not sensitive to the GUO phosphorylation rate. The peaks of 2,3-BPG and other metabolic intermediates, which were observed in the initial phase of storage period, were altered by the rate constant from 1e+6 to 1e+7, but not sensitive around 1e+8. Therefore, we considered that the rate constant used in our model is available to predict the effect of GUO supply, as well as the effect of the ratio of ADE and GUO on the metabolic dynamics of stored RBCs.

In our model, all kinetic parameters except for rate constants of pH-dependent reactions (*i.e.* k_{catf}, k_{catr}) were independent from changes in intracellular pH and temperature. pH-dependent reactions in our model were based on the erythrocyte metabolic model constructed by Mulquiney and Kuchel [41]. They validated the response of their model to a variety of pH levels ranging from 6.8 to 7.5 [41]. Therefore, we assumed that our model is also available to predict the metabolic dynamics in varying pH conditions. On the other hand, as for the assumptions related to cold temperature, such as lowering of enzymatic activities at 4℃, we used the genetic algorithm to estimate these activities because the reaction activities in cold-stored red cells could not be obtained from the literature. To confirm the effects of the lowering of enzymatic activities on dynamic behaviors of the model, we performed a parameter analysis and showed that the dynamics is not quite sensitive to the change of pH and temperature [87]. Moreover, sensitivity analysis of all kinetic parameters in the PAGGGM-stored RBC model against time-courses of ATP and 2,3-BPG indicated that the model dynamics is sufficiently robust to the parameter changes (Figure 3.5).

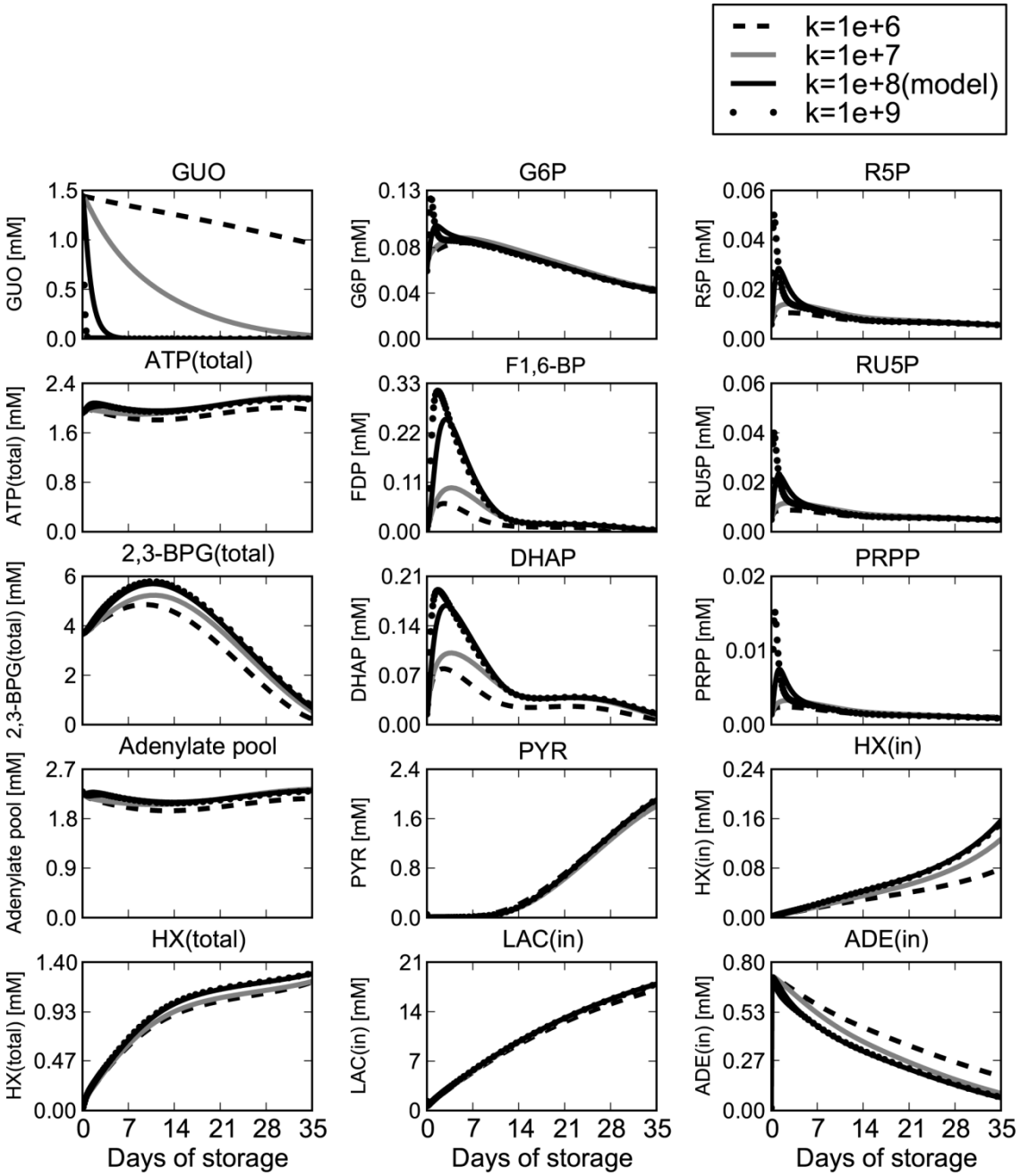

Figure 3.4 Sensitivities of metabolic intermediates dynamics to the rate constants of GUO phosphorylation.

The rate constant (*k*) of GUO phosphorylation process was varied from 1e+6 to 1e+9 in the model. *k* was changed to 1e+6 (*broken black*), 1e+7 (*solid gray*), 1e+8 (*solid black*; default value of the model), and 1e+9 (*dotted black*). Abbreviations used in this figure are given in Table 2.1 or Appendix B.

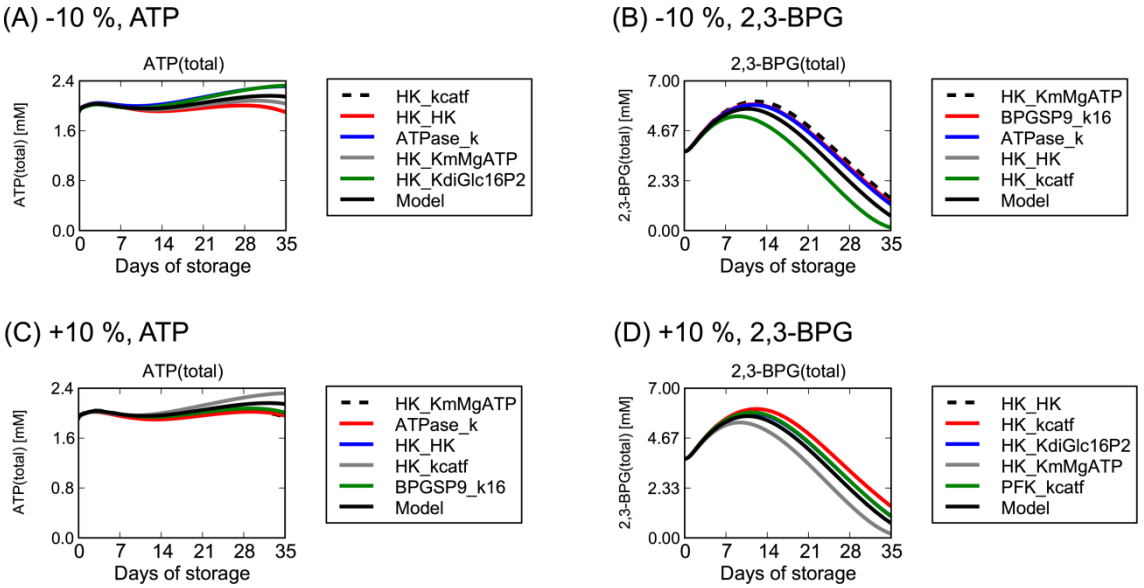

Figure 3.5 Robustness of the PAGGGM-stored RBC model against kinetic parameter changes.

The sensitivity analysis of all kinetic parameters against the dynamics of ATP and 2,3-BPG was carried out. Time courses of ATP and 2,3-BPG were plotted with 10% decrease (A and B) and with 10% increase (C and D) in each parameter. In the plots, black solid lines show the original behaviors with no change in parameters.
The sensitivities of ATP- and 2,3-BPG- time courses to the change of each kinetic parameter were not quite large (data not shown). This figure shows the change of dynamics of ATP and 2,3-BPG of the top five sensitive parameters for instance.

3.3.2 Measured and predicted time courses of metabolic intermediates in PAGGGM-stored RBCs

To validate the PAGGGM-stored RBC model, we measured time-courses of intermediates in PAGGGM-stored RBCs during 35 days of cold storage. Figure 3.6B-C shows the results of CE-TOFMS measurements and model predictions of PAGGGM-stored RBCs.

Metabolomic analysis provides us a comprehensive view of metabolic dynamics during blood storage. Intracellular metabolites of PAGGGM-stored RBCs were not in a steady state but largely changed with storage time, unlike those of flowing RBCs. The time-course changes of metabolite pools were clearly observed even in the cold temperature where enzymatic activities are assumed to be very low; some metabolites were significantly accumulated, but others were exhausted under storage conditions. Under these circumstances, the comprehensive kinetic model is useful to predict such non-linear dynamics of metabolic systems.

The predicted total amount of ATP was maintained at a high level during 35 days of storage, whereas the predicted total 2,3-BPG increased up to 1.5-fold during the first 1–2 weeks of storage and then gradually decreased (Figure 3.6B, *black broken curves*). These results agreed with those in the previous report by Burger *et al.* [88], in which ATP was kept at initial level throughout 35 days of storage, and 2,3-BPG was increased up to 1.3-fold of initial level during 21 days of storage and then rapidly decreased [88]. In contrast, our metabolomic analysis showed that ATP and 2,3-BPG were almost depleted at days 21 and 14, respectively (Figure 3.6B). We predicted free-form of ATP and 2,3-BPG for the sake of a comparison between predictions and

measurements, in accordance with the fact that large amounts of intracellular ATP and 2,3-BPG are known to bind to hemoglobin and band 3 membrane protein in order to modulate the oxygen absorbing capacity of hemoglobin, as well as to control glycolytic flux [46]. The time-series alterations measured by metabolomic analysis resembled those for free-form ATP and 2,3-BPG as predicted by the model (Figure 3.6B, *black solid curves*). This result is consistent with a report that only free-form ATP and 2,3-BPG would be quantified in CE-TOFMS measurements, because hemoglobin-binding ATP and 2,3-BPG were lost during the protein denaturation step in the preparation of CE-TOFMS analysis [46].

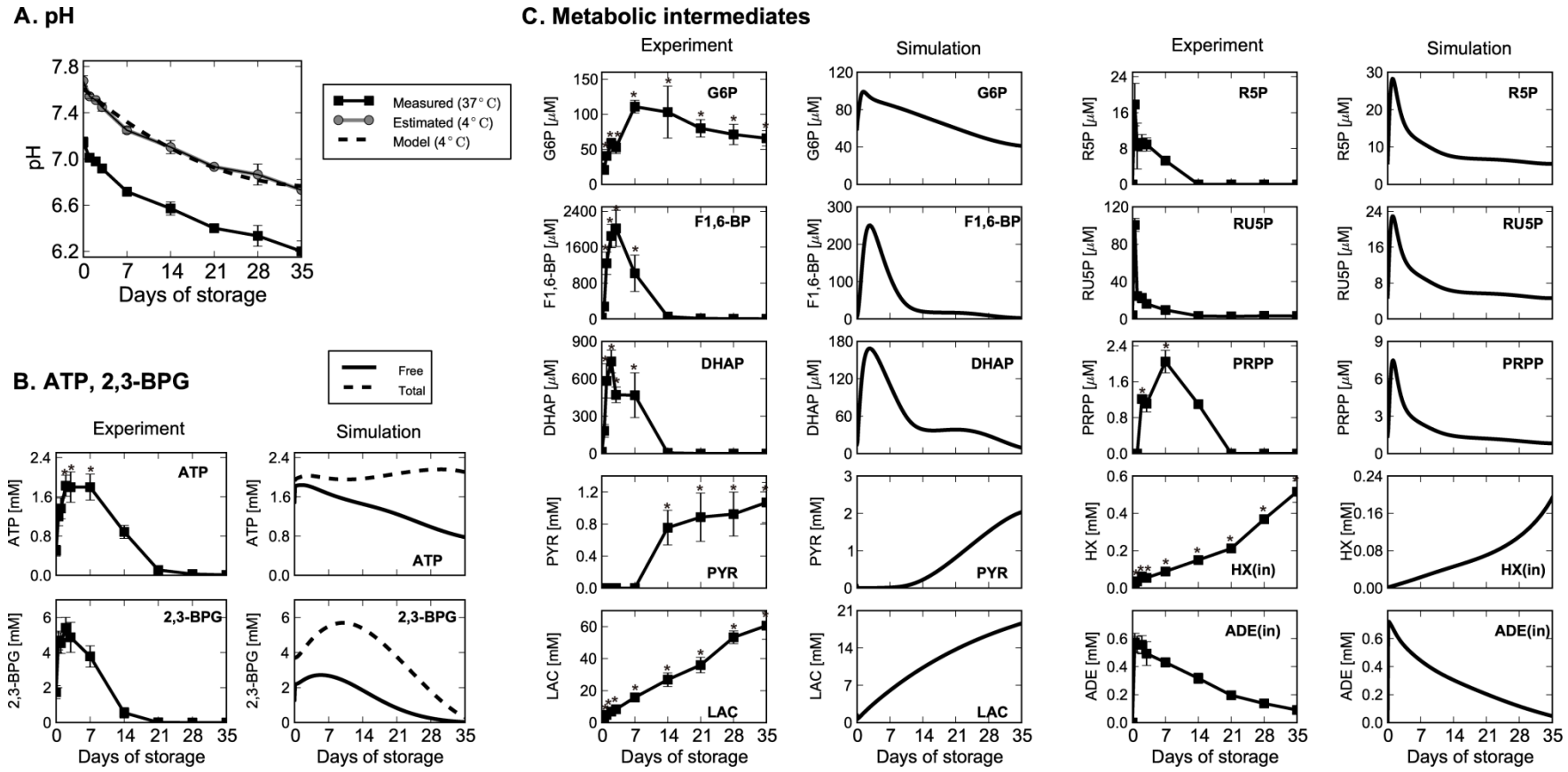

Figure 3.6 Measured and predicted time courses of pH and metabolic intermediates in PAGGGM-stored RBCs.

Panel A: Time courses of intracellular pH at 37°C (measured values; ■) and 4°C (estimated values; ●); fitted value used in the model (–). *Panel B*: ATP and 2,3-BPG were measured by CE-TOFMS (*left column*) and predicted by the mathematical model (*right column*) in which free-form (*solid black*) and total amount (*broken black*) of metabolites are shown separately. Since intracellular ATP and 2,3-bisphophoglycerate (2,3-BPG) are known to bind to hemoglobin and band 3 membrane protein [46], in our model,

free-form metabolite represents its amount in plasma, and total amount of metabolite represents the sum of metabolites (free-form) in plasma and their binding to the proteins. *Panel C*: Measured or predicted time courses of intermediates in glycolysis (G6P, F1,6-BP, DHAP, PYR, LAC), non-oxidative pentose phosphate pathway (R5P, RU5P), and purine salvage pathway (PRPP, intracellular HX, and ADE), respectively. pH and CE-TOFMS measurements data are expressed as means ± S.D. of 6 separate experiments. An asterisk indicates that a two-sided p-value is < 0.01 versus the day 0 values. Abbreviations used in this figure are given in Table 2.1 or Appendix B.

The results of the CE-TOFMS analysis and model prediction clearly indicated that metabolic intermediates can be decomposed into certain metabolic pools according to their dynamics. The glycolytic intermediates were classified into 3 groups based on their time-course patterns: upper (G6P and F6P), middle (F1,6-BP, and DHAP), and lower (PYR and LAC) stream of glycolysis (Figure 3.6C). According to both predictions and metabolome measurements, upper glycolytic intermediates increased within the first week of storage and then started to decrease moderately. Middle-glycolytic intermediates were significantly elevated during 2–3 days of storage (p-values < 0.001 versus day 0) but were not sustained after 14 days. The lower stream of glycolytic intermediates accumulated significantly throughout the storage period (p-values < 0.001 versus day 0). These results are consistent with the findings of Burger *et al*.; they found that F1,6-BP and DHAP accumulated in the first stage of RBC storage with PAGGGM solution, but the elevations in both metabolites were not sustained during storage period [88]. Intermediates of the non-ox PPP, such as ribose 5-phosphate (R5P) and ribulose 5-phosphate (RU5P), increased sharply within the first 2 days of storage along with a decline in the level of GUO, and then fell abruptly. These metabolites showed similar time series to middle-glycolytic intermediates. Intracellular HX, which is an intermediate of purine salvage pathway, increased progressively, while intracellular ADE was consumed throughout the storage period (Figure 3.6C).

3.3.3 Alteration of metabolic flux distributions and metabolic pools during cold storage

Using the simulation model, which successfully reproduced the dynamics of

metabolites, we showed the predicted alteration of enzymatic activities of glycolysis, non-ox PPP, and purine salvage pathway (Figure 3.7A), which facilitated the detection of the imbalance in metabolic pools to be found in PAGGGM-stored RBCs during the storage period. On the basis of the prediction of enzymatic activities and the related metabolite concentrations shown in Figure 3.7A and Figure 3.6, we predicted the flux distributions and the flows of the changes in metabolic pools in PAGGGM-stored RBCs (Figure 3.7B). Although all enzymatic activities seemed to be inactivated by low temperature during cold preservation, there were drastic changes in the patterns of enzymatic activities in our model (Figure 3.7A). Especially in 0-7 days of storage, both enzymatic activities and intermediates concentrations showed the significant changes compared with the later period. The following sections describe a predicted mechanism of the metabolic dynamics in each period.

3.3.4 Early response in the metabolic dynamics of PAGGGM-stored RBCs

Glycolytic enzymes except for HK, non-ox PPP enzymes, adenine phosphoribosyl transferase (ADPRT), and adenylate kinase (APK) were acutely activated during the first 7 days. In particular, non-ox PPP enzymes were significantly activated (~7.0 times higher than the initial condition) in the earliest stage. These activations seemed to be the result of a GUO-induced increase in non-ox PPP intermediates (Figure 3.6C). This increase in non-ox PPP through the conversion from GUO was reflected in the increase in the upper glycolytic pool (G6P and F6P) and 5-phosphoribosyl-1-pyrophosphate (PRPP), which are catalyzed by transketolase (TK)

and phosphoribosyl pyrophosphate synthetase (PRPPsyn), respectively. Furthermore, the increases in upper glycolysis and PRPP directly activated PFK and ADPRT, respectively. These results imply that the GUO supplement increased non-ox PPP intermediates and that this effect could be divided into 2 different fluxes, namely, boosting glycolysis and purine salvage pathway in the first 7 days of storage.

Firstly, in glycolysis, PFK activation is known to increase the pool of middle glycolytic intermediates, which results in maintaining 2,3-BPG [87,88]. Figure 3.6 shows that LAC was constantly increased throughout the storage period, although upper glycolysis was activated in first days of storage. This implies that the increased flux of upper and middle glycolysis flows into 2,3-BPG pool, but not into the latter half of glycolysis. On the other hand, from the model predictions, both glucose uptake and LAC production rates in the first week were twice as large as those during the rest of the period (Figure 3.8), indicating that the ratio of glucose uptake to LAC production was not changed in all over the storage period. The increase in the upper glycolytic pool repressed the activity of HK, which is one of the major ATP-consuming processes in RBCs, through the enzyme's strong product inhibition effect. Under these circumstances, the increase in the upper glycolytic pool serves as an efficient ATP production system with effective consumption of ATP at glycolysis.

Secondly, in the purine salvage pathway, the activation of ADPRT through the increase in PRPP promoted an efficient uptake of extracellular ADE. The large amount of ADE resulted in the activation of APK, which catalyzes the synthesis of ADP from AMP, as well as the regeneration of AMP and ATP from ADP. Intracellular ADE constantly decreased during storage from the initial impact of exposure to the ADE-added solution (Figure 3.6), while the total amount of HX (the sum of intracellular

and extracellular HX in the model) increased (Figure 3.7B, *top panel*). Although the addition of ADE as a source of ATP has been known to prevent the loss of ATP during blood storage [34], ADE might be involved in the accumulation of the end products of the purine salvage pathway, such as HX. In fact, purine nucleoside phosphorylase (PNPase), which catalyzes HX and R1P into INO, has been constantly reversed to produce HX during storage. These predictions and measured HX accumulations indicated that only a part of ADE uptake was supplied to the adenylate pool via AMP, whereas most ADE was eventually converted into HX, which was one of the most accumulated substrates in PAGGGM-stored RBCs.

In summary, flux from GUO through glycolysis contributes to 2,3-BPG accumulation and efficient ATP production in the early storage, also, GUO flux through purine salvage pathway accelerates ADE uptake and subsequently production of ATP and HX.

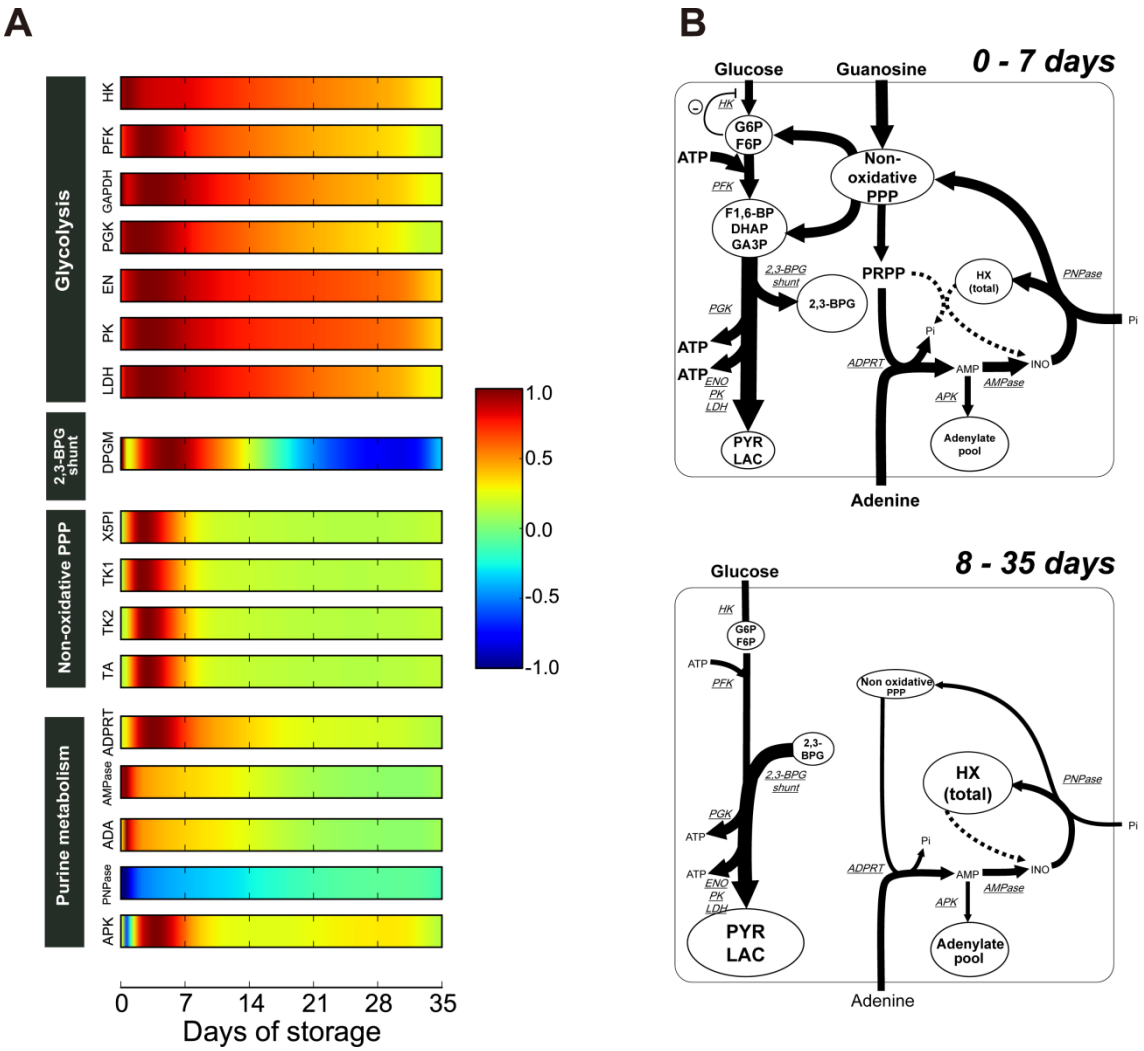

Figure 3.7 Predicted transition of enzymatic activities and the schematic representation of flux distributions in PAGGGM-stored RBCs.

Panel A: Transition of enzymatic activities. Each enzymatic activity was represented as a normalized value between -1.0 and 1.0. Each value was normalized by an absolute maximum value during 0–35 days of storage simulation. *Panel B*: Schematic representation of metabolic pools and flux distributions in PAGGGM-stored RBCs during 0–7 days of storage (early response; *top panel*) and 8–35 days of storage (long-term response; *bottom panel*). Total HX represents the sum of intracellular and extracellular HX. Circles and arrows indicate metabolic pools and fluxes, respectively. The width of arrows is proportional to fluxes of metabolic reactions predicted by the model. Abbreviations used in this figure are given in Table 2.1.

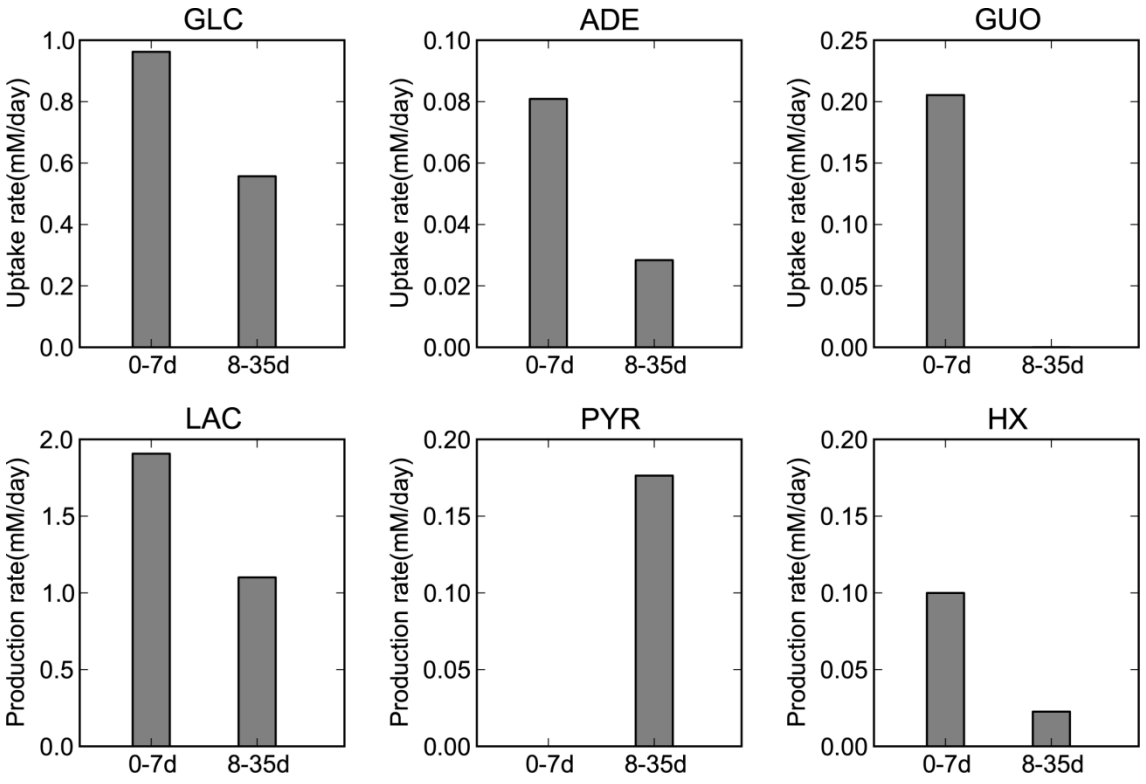

Figure 3.8 Prediction of the time-dependent changes in substrates uptake and production in PAGGGM-stored RBCs.

Glucose (GLC), ADE and GUO uptake rates and LAC, PYR and HX production rates were predicted. In each panel, the predicted uptake/production rates during 0-7 days and 8-35 days of storage were shown, respectively.

3.3.5 Long-term metabolic response in PAGGGM-stored RBC

In spite of the upper glycolytic activation in the beginning of storage, 2,3-BPG declined in the RBCs after 14 days. The decrease in 2,3-BPG was caused by the reversed flux of the 2,3-BPG shunt after 14 days of storage (Figure 3.7A). Owing to the co-operative inhibition effects of 2,3-BPG synthase activity by protons, the reversed flux was speculated to be due to the decline in pH [92]. This reversed flux of the 2,3-BPG shunt is crucial in maintaining the activities of the latter part of glycolysis and the production of ATP in the latter half of the storage period (Figure 3.7B, *bottom panel*). In fact, downstream enzymes of 2,3-BPG, such as enolase (ENO), PK, and LDH, kept higher activities, while the enzyme activities of other pathways were significantly repressed after 14 days of storage (Figure 3.7A). These activations in the latter part of glycolysis are essential for maintaining high ATP levels during the entire storage period, because re-phosphorylation of ADP to produce ATP mainly occurs via this pathway. Besides, the large increase in PYR production rate was predicted during 8-35 days of storage, indicating that ATP was continuously produced in the latter half period (Figure 3.8). As a result, ATP was maintained at a suitable level throughout the storage period.

3.3.6 Simulation analysis to identify the role of ADE and GUO in RBC preservation

Our predictions and metabolomic measurements indicated that the flux flow from GUO causes a global change in the RBC metabolism in the initial period of storage, which induces not only the accumulation of 2,3-BPG but also the maintenance of the ATP level in the entire storage period. Moreover, ADE contributes to enlarge the

adenylate pool size as well as leads to the accumulation of metabolic by-products like HX, which accumulate both intracellular and extracellular space.

Next, we performed simulation analysis to clarify the effect of ADE and GUO on the global metabolic change in PAGGGM-stored RBCs. Figure 3.9 and Figure 3.10 show the simulation results of the model with and without ADE and/or GUO. The level of the adenylate pool and total amount of ATP and HX were higher in ADE(+) conditions (*black solid line* and *black broken line*) than ADE(-) conditions (Figure 3.9). The largest pool sizes of these metabolites were shown in the ADE(+)GUO(+) model. At 35 days of storage, total concentrations of HX and ATP in the ADE(+)GUO(+) model were predicted to be 1.5 times and 1.6 times as much as those of the ADE(-)GUO(-) model, respectively. Whereas, intracellular HX was not significantly accumulated in ADE(+) rather than ADE(-) model owing to the acceleration of HX export by extracellular ADE (Figure 3.10). GUO can also contribute to the increase in ATP level, HX level, and the adenylate pool, but these boosting effects were observed only in the ADE(+) condition. These results showed that ADE is the most influential factor to determine the yields of the adenylate pool, ATP, and HX over the storage period. HX is known to react with xanthine oxidase to generate reactive oxygen species [93], and there is ample evidence that the reaction of xanthine oxidase in plasma induces sickle cell anemia [94]. Thus, a large amount of HX in the storage blood pack may therefore be harmful due to an increase in plasma reactive oxygen species after transfusion.

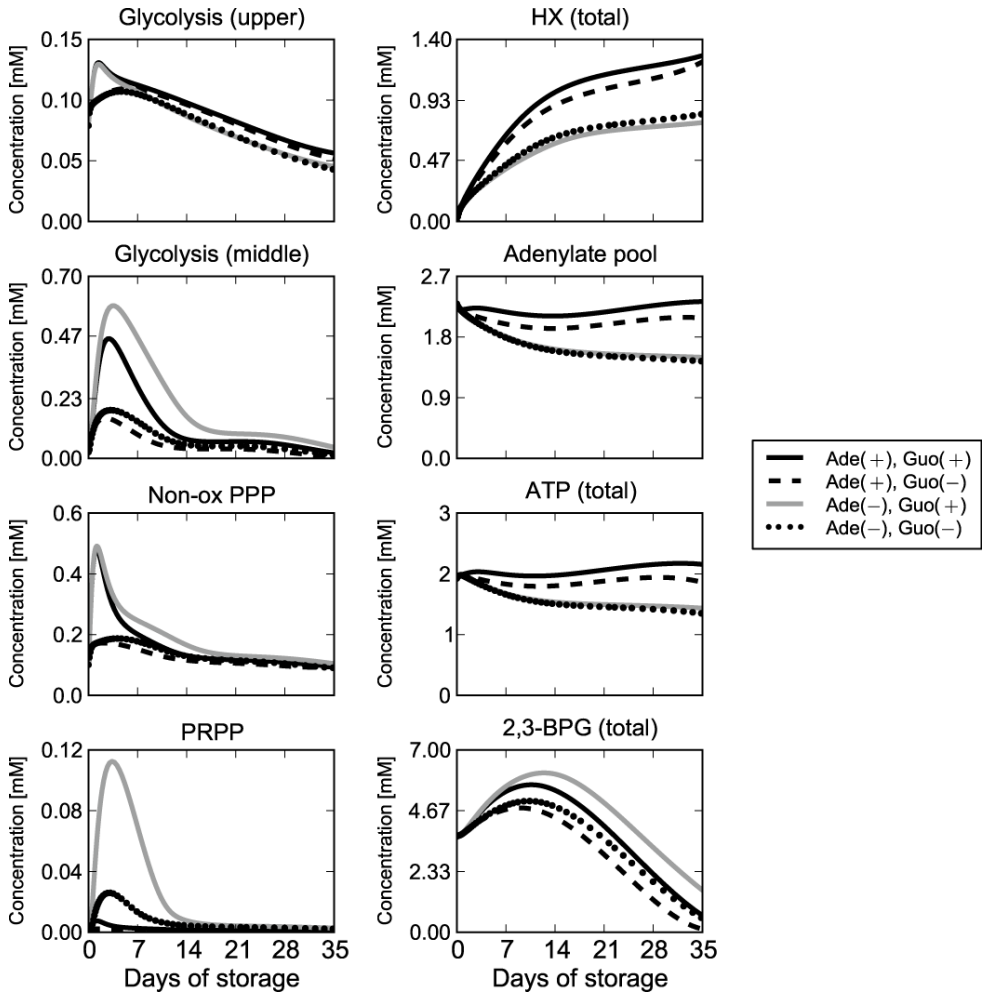

Figure 3.9 Prediction of ADE- and GUO-dependent metabolic alterations during cold storage.

Time-related changes of metabolic intermediates with or without ADE and GUO. Simulation with both ADE and GUO (*solid black*, PAGGGM solution), without GUO (*broken black*), without ADE (*solid gray*), and without neither ADE nor GUO (*dotted black*), respectively. Upper glycolysis represents the total concentrations of G6P and F6P; middle glycolysis represents the total of F1,6-BP, DHAP, and GA3P; and non-ox PPP represents the total of R5P, RU5P, X5P, and R1P. The adenylate pool represents the sum concentration of AMP, ADP, and ATP. Total HX represents the sum of intracellular and extracellular HX. Abbreviations are given in Table 2.1 or Appendix B.

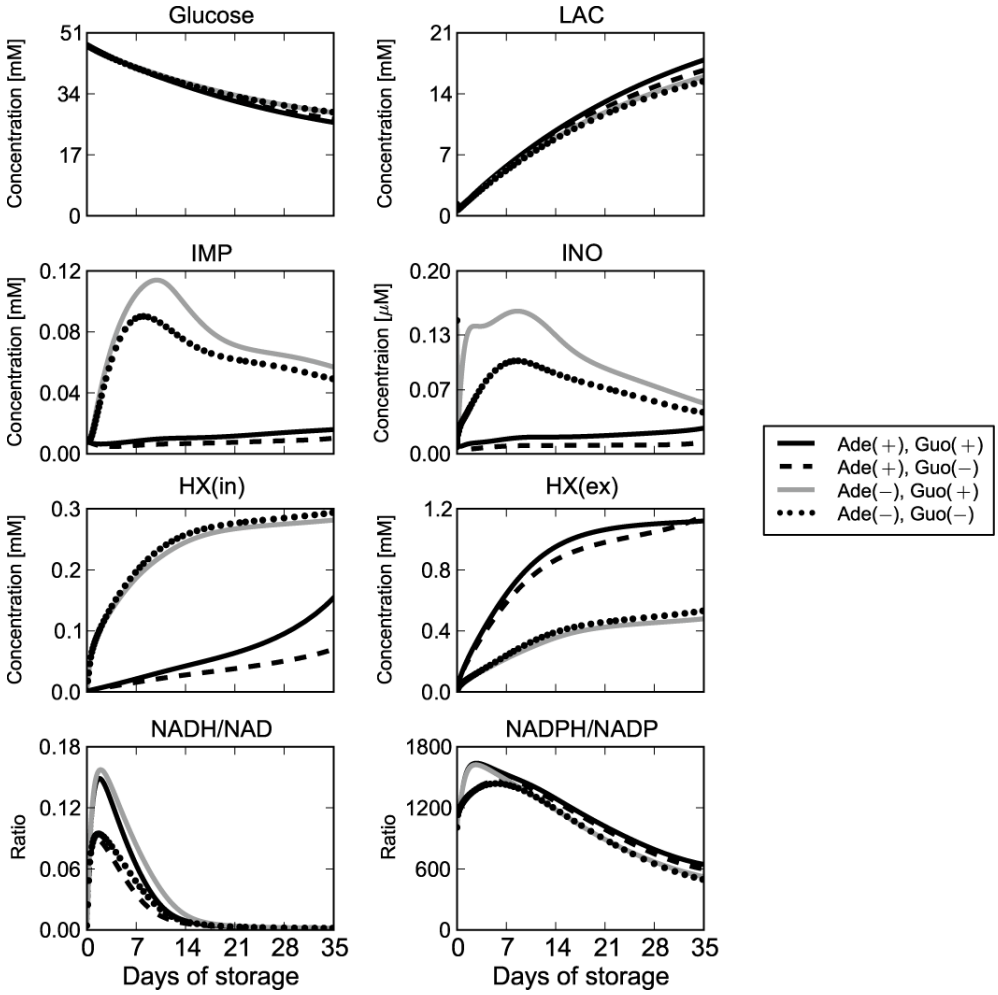

Figure 3.10 Predicted ADE- and GUO-dependent metabolic alterations during cold storage.

Time-related changes of metabolic intermediates with or without ADE and GUO. Abbreviations are given in Table 2.1. NADH/NAD and NADPH/NADP show the redox ratio of each co-enzyme, respectively.

To investigate the fate of ADE within RBCs during long-term storage, the ratio of flux distribution at an AMP branch point was calculated (Figure 3.11A). Because ADE is metabolized via this branch, one fate is into HX (J_{HX}), which is calculated as the sum of enzymatic activities of purine salvage pathway, including AMPDA, AMPase, and AK, and another fate is into the adenylate pool ($J_{ANPpool}$), which can be mimicked by APK activity. The ratio of flux through HX (%) is calculated as $J_{HX}/(J_{HX} + J_{ANPpool}) \times 100$. This result indicated that more than half of the flux from ADE was not fixed into the adenylate pool but directly passed through purine salvage pathway to supply HX from 2 to 12 days of storage (Figure 3.11A *1st panel*, (i)). In this period, the total flux from ADE through AMP was quite large (Figure 3.11A *bottom panel*) in the ADE(+)GUO(+) condition and resulted in the acceleration of HX accumulation during the initial period of storage. After 12 days of storage, flux flow from ADE into the adenylate pool was higher than that into HX (Figure 3.11A *1st panel*, (ii)). These results imply that the incorporation of ADE into the adenylate pool persisted throughout the storage period. These findings are consistent with the earlier observation of the continued gradual disappearance of ADE-^{14}C and the sustained rise in the adenine nucleotide with specific radioactivity in ACD-blood during storage [95].

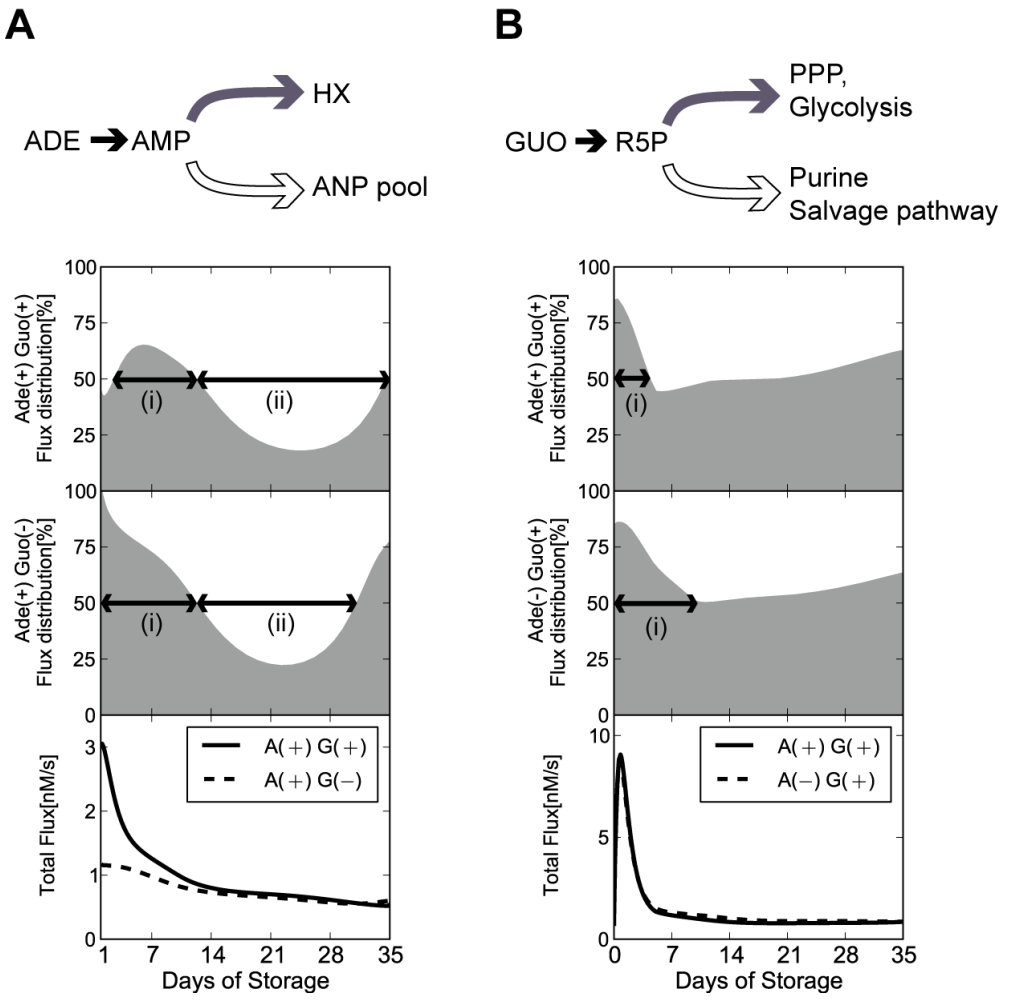

Figure 3.11 Utility of ADE and GUO in stored RBC metabolism.

Panel A: Time-related change of ADE flux distribution through AMP to HX or to the adenylate pool. The ratio of ADE flux distribution into HX (*gray filled curve)* is calculated as $J_{HX}/(J_{HX} + J_{ANPpool}) \times 100$, where J_{HX} is the sum of enzymatic activities of purine salvage pathway, including AMPDA, AMPase, and AK, and $J_{ANPpool}$ is the activity of APK. *1st* and *2nd panels* show the ratio of ADE flux distribution into HX in the ADE(+)GUO(+) model and ADE(+)GUO(-) model, respectively. *3rd panel* shows the time-related changes of total ADE flux ($J_{HX} + J_{ANPpool}$) in the ADE(+)GUO(+) (*solid black*) and ADE(+)GUO(-) *(broken black*) model. *Panel B*: Time-related change of GUO flux distribution through R5P to glycolysis or purine salvage pathway. The ratio of GUO flux distribution into glycolysis (*gray filled curves*) is calculated as $J_{glycolysis}/(J_{glycolysis} + J_{purine}) \times 100$, where $J_{glycolysis}$ is the sum of enzymatic activities of R5PI and TK1 and J_{purine} is the activity of PRPPsyn. *1st* and *2nd panels* show the ratio of GUO flux distribution into glycolysis in the ADE(+)GUO(+) model and ADE(-)GUO(+) model, respectively. *3rd panel* shows the total GUO flux ($J_{glycolysis} + J_{purine}$) in the ADE(+)GUO(+) (*solid black*) and ADE(-)GUO(+) (*broken black*) models.

The initial large peak of non-ox PPP appeared only in the GUO(+) condition (*black solid lin*e and *gray solid line*) (Figure 3.9). This acute increase in non-ox PPP implies that GUO is taken as a ribose source in non-ox PPP in RBCs. As mentioned above, the flux of the ribose source derived from GUO is partitioned into 2 directions, towards glycolysis and towards purine salvage pathway. The flux through glycolysis increases middle glycolytic intermediates and then results in 2,3-BPG production. In fact, in the models with GUO, glycolytic intermediates and 2,3-BPG accumulate more than in GUO(-) models (Figure 3.9). From these results, as well as the previous results, it can be concluded that GUO can boost the 2,3-BPG production via the accumulation of upper glycolytic intermediates, which can trigger PFK activation. The larger NADH/NAD ratio and unchanged LAC production rate in GUO(+) model also suggest that upper glycolytic flux was increased but retained in 2,3-BPG pool in the presence of GUO (Figure 3.10). Moreover, interestingly, these accumulations are enhanced in the ADE(-) condition (Figure 3.9). PRPP, which is located at the gate between purine salvage pathway and non-ox PPP, significantly accumulates under the ADE(-)GUO(+) condition, whereas purine metabolic intermediates such as HX and the adenylate pool do not increase under the same condition. Taken together with the fact that PRPP reacts with ADE catalyzed by ADPRT, these results suggest that the GUO flux fate is largely controlled by ADE.

To confirm the effect of ADE addition on GUO fate, we also calculated the ratio of flux distribution of GUO at the purine salvage pathway branch point (Figure 3.11B) with or without ADE. The ratio of GUO flux towards glycolysis (%) at the branch point is calculated as $J_{gly}/(J_{gly} + J_{purine}) \times 100$, where J_{gly} is the flux into glycolysis, which is the sum of enzymatic activities of TK and ribose 5-phosphate

isomerase (R5PI), and J_{purine} represents the flux into purine salvage pathway, which is considered an activity of PRPPsyn. Regardless of the presence or absence of ADE, flux distribution of GUO into glycolysis was more than 80% at the beginning of the storage period, after which the ratio gradually decreased. This unbalanced flux pattern lasted for only 4 days in the ADE(+) model (Figure 3.11B *1st panel* (i)), whereas it continued for as long as 11 days in the ADE(-) model (Figure 3.11B *2nd panel* (i)). These results reveal that ADE is capable of shifting the GUO flux into a purine salvage pathway other than glycolysis. The significant accumulation of inosine monophosphate (IMP) in ADE(-) also supports that the fate of GUO is strongly dependent on the presence of ADE (Figure 3.10). Besides, the ADE-induced shift of GUO flux to purine salvage pathway also results in reducing ribose phosphate in non-ox PPP and an accompanied reduction in 2,3-BPG in PAGGGM-stored RBCs. It is known that the addition of ADE promotes 2,3-BPG depletion [34]. The ADE-induced 2,3-BPG reduction is reported to be caused by favoring 1,3-BPG metabolism via phosphoglycerate kinase (PGK) due to the higher ADP level [95]. The present study also showed that PGK was activated in the ADE(+) model rather than in the ADE(-) model (data not shown). In addition, our simulation result showed that ADE-induced reduction of ribose phosphate also hastens 2,3-BPG depletion, but the addition of GUO can compensate for this depletion.

Our predicted results suggested the coordinating effects of ADE and GUO on RBC metabolism. Both GUO and ADE are necessary for the maintenance and improvement of ATP and 2,3-BPG levels in PAGGGM-stored RBCs. In addition, our results provided unique insights into the intricate regulatory network of energy metabolism by ADE and GUO during cold storage of RBCs. ADE acts as a source of ATP, but reduces 2,3-BPG. GUO is used as a source of ribose phosphate, and induces

PFK activation, which can result in compensating for the depletion of 2,3-BPG by ADE. The fate of GUO between the non-ox PPP and purine salvage pathway is largely controlled by ADE. These findings illustrated that the metabolic trade-offs between ATP and 2,3-BPG, which are commonly observed in conventional blood storage methods, can be offset by ADE and GUO in PAGGGM-stored RBCs.

Simulation approaches can unravel mechanisms of such a complicated system, networks, and regulations, including the coordinated effects of metabolites. Precise and large-scale kinetic modeling is also useful as a tool for predicting the ideal combination of solution additives for longer blood storage or for giving insights on the appropriate use of the different storage methods, depending on the patients' condition. For example, to determine the optimal amount of ADE and GUO as storage-solution additives, ATP, 2,3-BPG, and HX levels at various combinations of ADE and GUO concentrations after 7, 14, 28, and 35 days of storage were predicted (Figure 3.12). Higher ADE and GUO concentrations maintained higher ATP, unless ADE was below 1 mM, in which case ATP remarkably decreased with storage time, regardless of GUO concentration. As expected from the flux distribution analysis of GUO, the 2D plots in Figure 3.12 also shows the positive effect of the high concentration of GUO and the inhibitory effect of ADE on 2,3-BPG maintenance. HX level was predicted to be mainly determined by ADE and less affected by GUO, especially before 2 weeks of storage.

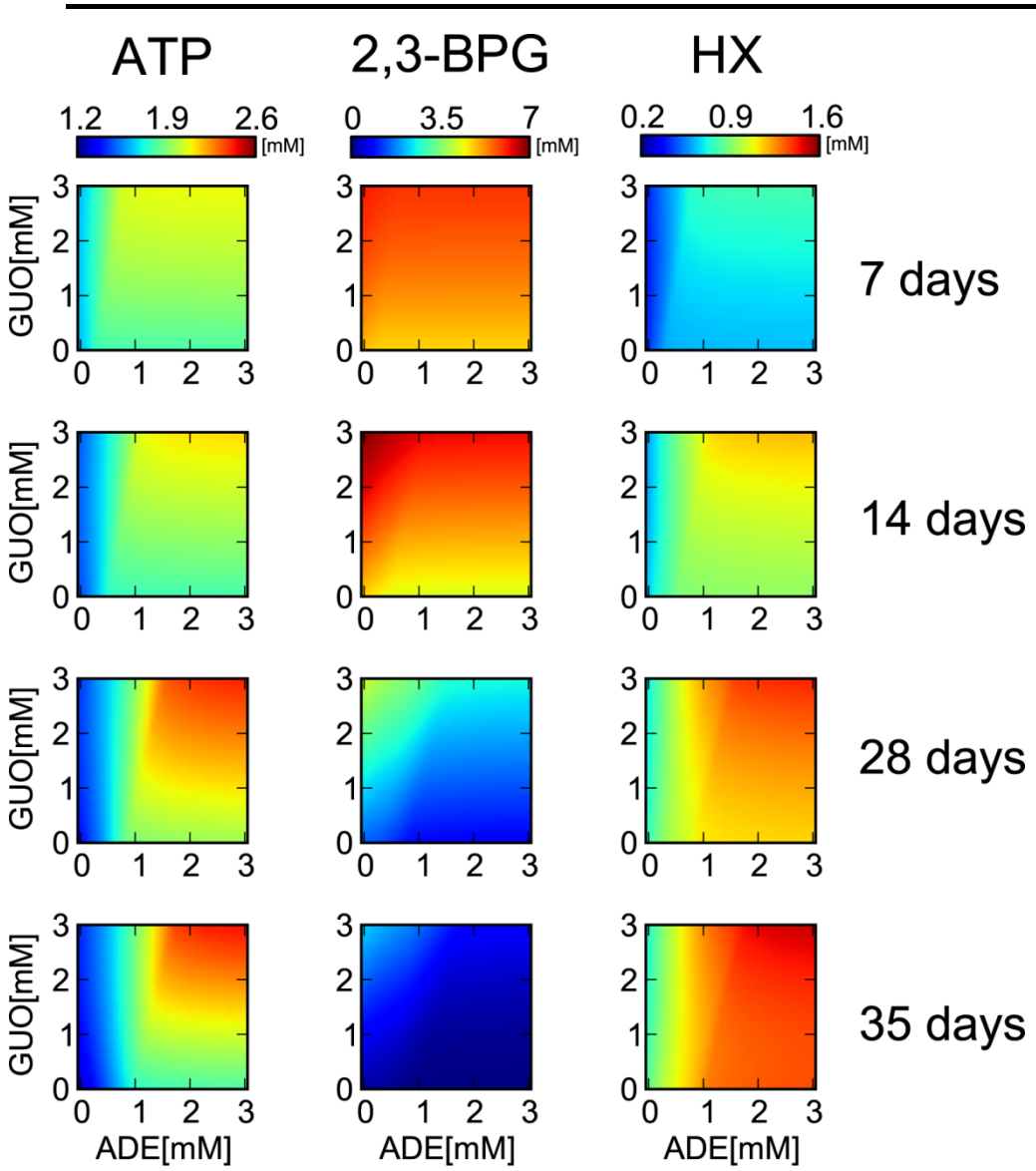

Figure 3.12 Prediction of intracellular metabolite levels depending on the combination of initial ADE and GUO concentrations.

Predicted concentrations of ATP (*left column*), 2,3-BPG (*center column*), and total HX (*right column*) at 7, 14, 28, and 35 days after storage in various combinations of ADE and GUO concentrations. In each panel, x and y axes represent initial concentration of ADE and GUO in the model, respectively. The initial setting of ADE and GUO varied between 0 to 3 mM.

Chapter 4

Concluding Remarks

4.1 Summary

This dissertation aims to investigate the metabolic dynamics of stored RBCs in relation to clarifying the mechanism of blood storage lesions using the *in silico* model and metabolomics data.

In Chapter 2, the first kinetic model of cold-stored RBC metabolism was constructed. Based on the steady-state erythrocyte metabolic model, we modeled the biochemical characteristics of MAP-stored erythrocytes, for example, MAP compositions, the pH-degradation profile, tense-relaxed transition of hemoglobin, and inactivation of enzymes by cold temperature. Metabolic dynamics of the new model showed good agreement with the metabolomics data of MAP-stored RBCs. From the simulation analysis, we suggested that the transition of hemoglobin from the R-state to the T-state and the activation of HK or PFK have a possibility to maintain ATP and 2,3-BPG during cold storage, which may serve as possible targets for improving blood storage methods. Furthermore, simulation results also indicated that higher pH is effective for maintaining 2,3-BPG level, but is lowering the level of ATP. Although pH-control has been one of the targets for creating novel storage solutions, our simulation results imply the difficulty in overcoming the trade-off between the maintenance of ATP and 2,3-BPG levels only with modulation of pH.

In Chapter 3, we discussed the effects of preservative additives on RBC storage

metabolism in respect to not only beneficial impacts but also possible side effects. The metabolic behavior of RBCs preserved with the PAGGGM solution including ADE and GUO was successfully reproduced by the cold-stored RBC model. Furthermore, the metabolic dynamics of stored RBCs were drastically changed in accordance with the supplementation levels of ADE and GUO. The simulation results of the stored RBC models with various combinations of these additives demonstrated that the coordinated action of ADE and GUO was required for dynamically maintaining of both ATP and 2,3-BPG under cold storage conditions. GUO is mainly used as a source of ribose phosphate in non-ox PPP and can boost the production of both ATP and 2,3-BPG depending on PFK activation. ADE can enlarge the adenylate pool, which results in keeping ATP levels high but directly causes HX accumulation. ADE also has an important role in the determination of the GUO fate in PAGGGM-stored RBCs. To our knowledge, this is the first *in silico* study to provide a detailed explanation of the underlying mechanism of metabolic lesions and compensations by solution additives in RBCs under long-term cold storage, as well as of the roles and fates of additives in the context of metabolic benefits and possible side effects.

In the current framework of the cell simulation study, to investigate a cellular function or a biochemical network, we have to measure an abundance of its kinetics data by *in vitro* experiments and reconstruct them into a mathematical representation. The reuse of an existing model as introduced in this study can reduce development time and costs for the new model to investigate other cellular functions. However, when we reuse or extend an existing model, it is important to improve the accuracy of the model to be consistent with prior research.

Lastly, in the reminder of this chapter, we describe possible future directions of

RBC storage studies in terms of the application of systems biology.

4.2 Future Directions

In recent years, proteomics and metabolomics approaches have been applied to investigate the RBC storage lesion [96,97,98,99]. However, it is difficult to interpret large sets of omics data for the extraction of essential information about biological systems. As we showed in this thesis, *in silico* simulation can help to extract novel information on metabolic dynamics in RBC storage from a massive amount of omics data. In this situation, a development of integrated systems biology platform for stored RBCs becomes important. This integrated platform including both computational and experimental sciences will provide novel insights into the molecular mechanism of RBC storage lesions.

Here, we identify several issues and problems of stored RBCs that should be dealt with in the field of systems biology.

4.2.1 Evaluation of post-transfusion red cell properties and estimation of physiological influences of stored red cells on circulation

Red cell viability and 2,3-BPG recovery after transfusion have been evaluated by ^{51}Cr-labeled experiments [18,32], and by transfusion of group O red cells into group A recipients [100]. However, these experiments, which are inconvenient and can only track limited molecular species, fail to meet our demands to estimate overall effects of preserved blood on recipients after transfusion. *In silico* simulation will be useful to assess the preserved RBC condition and function not only during storage but also

post-transfusion.

Figure 4.1 shows the 24-hour post-transfusion recovery of 2,3-BPG and ATP in RBCs stored with MAP or PAGGGM solution in various storage periods from 7 to 35 days. These results suggested that the recovery of metabolites is largely dependent on storage solutions and period of storage. Furthermore, the *in silico* model enables to estimate the response of transfused RBCs to their external environments like circulation or various tissues. Figure 4.2 shows the transition of the rate of HX efflux from transfused RBCs in various storage periods. This prediction indicated that an efflux of HX after transfusion is quite larger in RC-MAP than in PAGGGM-stored RBCs. Moreover, accumulation and elimination of HX are affected by not only a storage solution but also storage period. As mentioned in the previous chapter, an excessive accumulation of HX in the stored blood will be harmful due to increase in reactive oxygen species after transfusion. The same procedure is also applicable to post-transfusion dynamics of other RBC storage lesion indicators, such as LAC and potassium.

In this way, an *in silico* model is available for monitoring the metabolic dynamics of preserved blood after transfusion as well as during a period of storage. Thus, *in silico* analysis is useful to optimize the design of blood storage solutions with consideration for post-transfusion status.

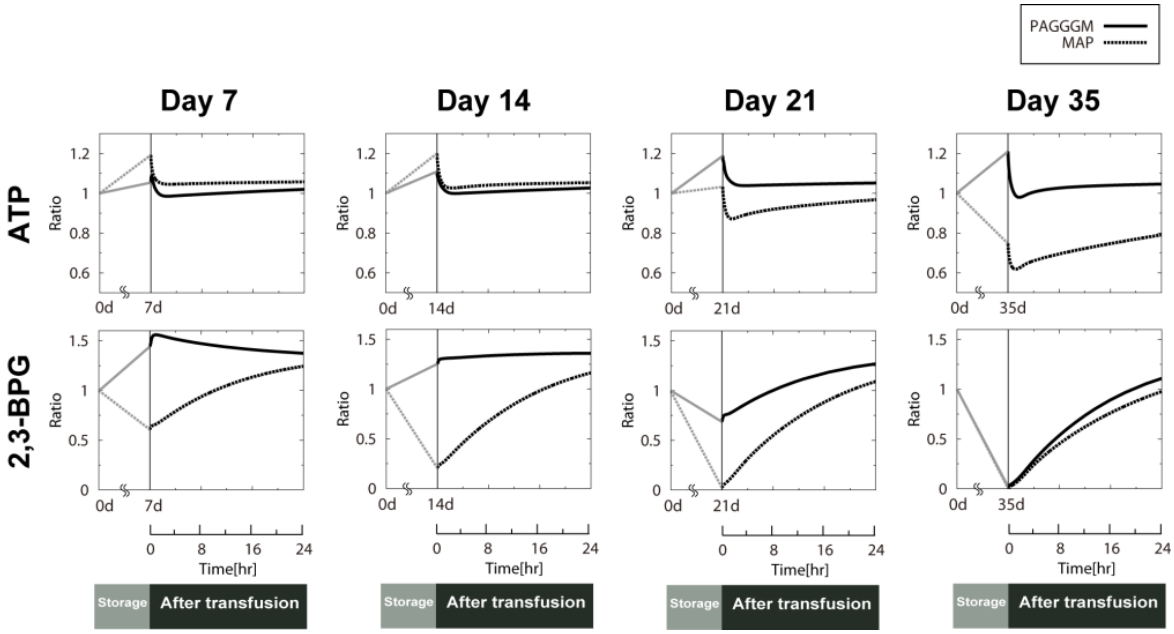

Figure 4.1 Prediction of 2,3-BPG and ATP recovery in stored RBCs after transfusion.

24-hour post-transfusion recovery of ATP (*upper panel*) and 2,3-BPG *(lower panel*) after 7, 14, 21 and 35 days of RBC storage was predicted by PAGGGM-stored RBC model (*solid black*; with GUO and high-pH condition) and by RC-MAP model (*broken black*; without GUO and low-pH condition). In each panel, 0 hr means the time when the simulation setting changes from the storage condition at 4 °C to physiological condition at 37 °C.

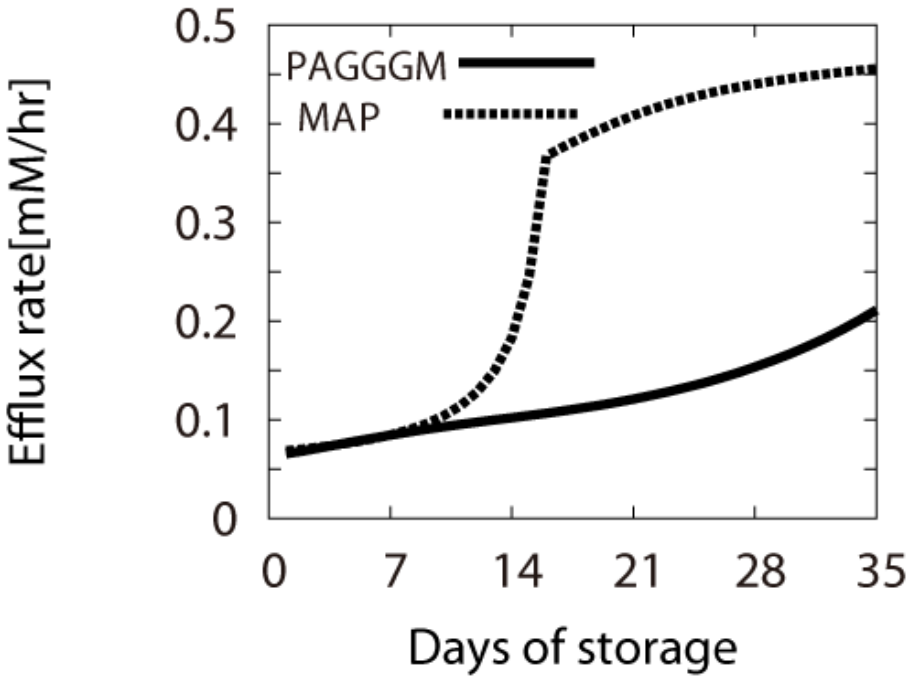

Figure 4.2 Prediction of an efflux rate of HX in stored RBCs after transfusion.

An efflux rate of HX from stored RBCs after transfusion were predicted by PAGGGM-stored RBC model (*solid black*; with GUO and high-pH condition) and by RC-MAP model (*broken black*; without GUO and low-pH condition). The efflux rate is calculated as an average of total emission concentration during 1 hour after transfusion.

4.2.2 Development of stored RBC rejuvenation method

Stored RBC rejuvenation is one of pre-transfusion treatments in order to improve post-transfusion RBC functions [101,102,103]. The rejuvenation is mainly used for stored blood at the end of its shelf-life and for thawing frozen blood. Although RBC rejuvenation is in practical use in the United States, optimization of additive solution for rejuvenation is in a developmental stage in the many other countries. As in the case in blood storage solutions, *in silico* simulation will enable to optimize rejuvenation solution and to evaluate not only post- but also pre- transfusion status of RBCs.

In general, stored blood is incubated with a rejuvenation solution that contains PYR, INO and phosphate at 37˚C for 3-4 hours. We have successfully reproduced a stored RBC rejuvenation experiment of Oski *et al*. [104] by using our simulation model (Figure 4.3). Simulation can be an effective and simple approach for developing a novel rejuvenation solution, and that leads to make an effective use of blood resources.

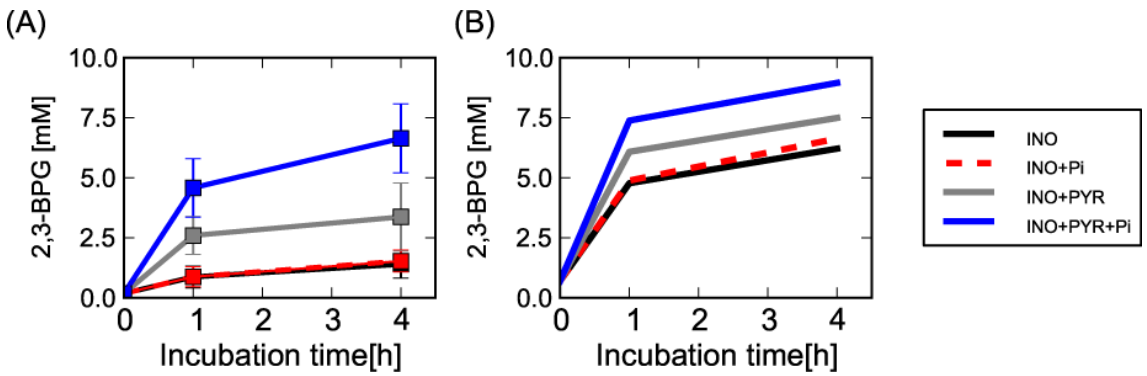

Figure 4.3 Recovery of 2,3-BPG in stored RBC rejuvenation treatment with INO, PYR and phosphate.

2,3-BPG recovery in stored RBCs incubated with various rejuvenation solutions; rejuvenation solution with INO (*black*), INO and phosphate (Pi) (*broken red*), INO and PYR (*gray*), and INO, Pi and PYR (*blue*) are displayed. *Panel A*; reported by Oski *et al.*[104], and *Panel B*; predicted by our *in silico* model.

4.2.3 Personalized blood storage system

The computational experiment using mathematical models allows us easily to examine thousands of different conditions for blood storage. The stored RBC model may serve as a useful tool to customize the blood storage system for individual patients, especially for patients of hereditary chronic anemia and donors of autologous blood donation. In autologous blood transfusion, blood collection takes weeks to months because it has to be performed in several times, and thus, autologous donation blood is required to maintain high viability of RBCs during long-term of storage. If personalized blood storage systems are realized, it would be expected that the time frame of scheduled blood collection would be prolonged, and as a result, patient stress would be reduced.

4.2.4 Extension and refinement of the stored RBC model

Although our model is helpful for predicting metabolic status of stored RBCs, some biochemical traits have yet to be integrated in the model, such as autonomic regulation of intracellular pH including acidotic shift caused by LAC accumulation, cell volume regulation and osmoregulation due to a change in ion balance. Metabolic dynamics is largely influenced by these traits. Above all, as mentioned in Chapter 3, pH has an effect on the enzymatic activities of 2,3-BPG synthesis pathway and glycolysis, and even causes the depletion of ATP and 2,3-BPG. Therefore, implementation of dynamics in pH response can be a critical aspect to propose a novel additive solution through *in silico* experiments.

In the future, we should reconstruct mechano-chemical features of erythrocyte

in order to allow for a quantitative evaluation of physiologic lesions, such as loss of membrane and its plasticity, and the associated alterations in cell shape and rheology [14], which are assessed in relation with metabolic injury like the depletion of ATP and anti-oxidative metabolites.

4.3 Conclusion

We provided a simulation model to predict the metabolic dynamics of stored RBCs and to clarify the mechanism for maintaining both ATP and 2,3-BPG during the long-term storage. We also demonstrated whole metabolic profile by using CE-TOFMS analysis. These are highly useful for understanding complicated metabolic behavior of stored RBCs. The simulation model and its findings in the principle of the stored RBC metabolism will help to develop novel blood preservation methods, which focus on not only RBC quality in blood storage period but also clinical outcomes in patients after transfusion.

We strongly believe that the strategy proposed in this thesis will be important for future system-level drug discovery efforts as well as for the improvement of blood storage methods.

.

Acknowledgements

I would like to express my gratitude to Dr. Masaru Tomita for giving me the helpful advice, support and good environment to pursue my postgraduate studies. I owe a great debt to my thesis committee members, Dr. Tomita, Dr. Yasuhiro Naito, Dr. Tomoyoshi Soga, and Dr. Hitomi Sano, for their constant help, encouragement and valuable advice throughout my PhD course.

I am deeply grateful to Dr. Ayako Yachie-Kinoshita for her role as a research advisor and mentor in the truest sense of the word. She has always provided me sound advice, inspiration and motivation. She has also been instrumental in helping me develop a scientific mind. Without her guidance and persistent help, this dissertation would not have materialized.

I am indebted to Mr. Akiyoshi Hirayama for professional advice and kind assistance especially in CE-TOFMS experiments. His guidance and support were essential for the experimental part of this research.

I received generous support from Dr. Makoto Suematsu and all members of the Suematsu laboratory who provided me technical assistance and use of facilities in blood storage experiments. Thanks are due to Dr. Takako Hishiki for her advice on preparing blood metabolomics samples.

Dr. Akio Kanai and Dr. Mitsuhiro Itaya always give me constructive comments and warm encouragement. I am grateful for their guidance.

I would like to thank Dr. Yukino Ogawa, Dr. Yoshihiro Toya, Dr. Kazuharu Arakawa and Dr. Nozomu Yachie for giving insightful comments, suggestions and

encouragement for my research. Discussions with them have been illuminating and exciting.

Special thanks are due to my junior colleagues, Ms. Hanae Shimo, Mr. Norikazu Saiki, Mr. Seiya Fujimoto, Ms. Seiko Nakatsuka, Ms. Noga Nakashima, Mr. Jun Yamakubo, Mr. Gembu Maryu, Mr. Kentaro Hayashi, Mr. Satoshi Tamaki and Dr. Nobuaki Kono. I am very happy to share the fun of research with them. The hours we have all spent together in and out of the laboratory are some of my favorite memories of my school life.

I would like to thank mt-rg secretaries, Ms. Ayumi Mikami, Ms. Ayami Mizukami, Ms. Miwa Hiramoto and Ms. Hinako Hayashi. They always helped and supported me throughout my student years.

I am indebted to my family, Michiko, Fumiyo, Hanako, Fusako and Kazuo, for their every support and tolerance during all of my student days as well as for their understanding in my pursuing academic research.

Finally, I would like to express my heartfelt appreciation to Dr. Kazunari Kaizu. He has been the best supporter I could hope for. I would never have completed my dissertation without his continuing support and sincere encouragement.

Bibliography

1. Kitano H (2002) Computational systems biology. *Nature* **420**: 206-210.

2. Kitano H (2002) Looking beyond the details: a rise in system-oriented approaches in genetics and molecular biology. *Current genetics* **41**: 1-10.

3. Kitano H (2002) Systems biology: a brief overview. *Science* **295**: 1662-1664.

4. Konig M, Bulik S, Holzhutter HG (2012) Quantifying the contribution of the liver to glucose homeostasis: a detailed kinetic model of human hepatic glucose metabolism. *PLoS computational biology* **8**: e1002577.

5. Duarte NC, Becker SA, Jamshidi N, Thiele I, Mo ML*, et al.* (2007) Global reconstruction of the human metabolic network based on genomic and bibliomic data. *Proc Natl Acad Sci U S A* **104**: 1777-1782.

6. Shlomi T, Cabili MN, Herrgard MJ, Palsson BO, Ruppin E (2008) Network-based prediction of human tissue-specific metabolism. *Nat Biotechnol* **26**: 1003-1010.

7. Jerby L, Shlomi T, Ruppin E (2010) Computational reconstruction of tissue-specific metabolic models: application to human liver metabolism. *Molecular systems biology* **6**: 401.

8. Shlomi T, Benyamini T, Gottlieb E, Sharan R, Ruppin E (2011) Genome-scale metabolic modeling elucidates the role of proliferative adaptation in causing the Warburg effect. *PLoS computational biology* **7**: e1002018.

9. Folger O, Jerby L, Frezza C, Gottlieb E, Ruppin E*, et al.* (2011) Predicting selective drug targets in cancer through metabolic networks. *Molecular systems biology* **7**: 501.

10. Shlomi T, Cabili MN, Ruppin E (2009) Predicting metabolic biomarkers of human inborn errors of metabolism. *Molecular systems biology* **5**: 263.

11. Paglia G, Palsson BO, Sigurjonsson OE (2012) Systems biology of stored blood cells: Can it help to extend the expiration date? *Journal of proteomics* **76**: 163-167.

12. Nakao K, Wada T, Kamiyama T, Nakao M, Nagano K (1962) A direct relationship between adenosine triphosphate-level and *in vivo* viability of erythrocytes. *Nature* **194**: 877-878.

13. Dern RJ, Brewer GJ, Wiorkowski JJ (1967) Studies on the preservation of human blood. II. The relationship of erythrocyte adenosine triphosphate levels and other *in vitro* measures to red cell storageability. *J Lab Clin Med* **69**: 968-978.

14. Hess JR (2010) Red cell changes during storage. *Transfusion and apheresis science : official journal of the World Apheresis Association : official journal of the European Society for Haemapheresis* **43**: 51-59.

15. Hogman CF, Lof H, Meryman HT (2006) Storage of red blood cells with improved maintenance of 2,3-bisphosphoglycerate. *Transfusion* **46**: 1543-1552.

16. Hogman CF, Meryman HT (2006) Red blood cells intended for transfusion: quality criteria revisited. *Transfusion* **46**: 137-142.

17. Loutit JF, Mollison PL (1943) Advantages of a disodium-citrate-glucose mixture as a blood preservative. *Br Med J* **2**: 744-745.

18. Orlina AR, Josephson AM (1969) Comparative viability of blood stored in ACD and CPD. *Transfusion* **9**: 62-69.

19. Gibson JG, 2nd, Rees SB, Mc MT, Scheitlin WA (1957) A cltrate-phosphatedextrose solution for the preservation of human blood. *Am J*

Clin Pathol **28**: 569-578.

20. Zuck TF, Bensinger TA, Peck CC, Chillar RK, Beutler E*, et al.* (1977) The *in vivo* survival of red blood cells stored in modified CPD with adenine: report of a multi-institutional cooperative effort. *Transfusion* **17**: 374-382.

21. Valeri CR, Valeri DA, Gray A, Melaragno A, Dennis RC*, et al.* (1982) Viability and function of red blood cell concentrates stored at 4 degrees C for 35 days in CPDA-1, CPDA-2, or CPDA-3. *Transfusion* **22**: 210-216.

22. Beutler E, West C (1983) Storage of red cell concentrates in CPD-A2 for 42 and 49 days. *J Lab Clin Med* **102**: 53-62.

23. Hogman CF, Akerblom O, Hedlund K, Rosen I, Wiklund L (1983) Red cell suspensions in SAGM medium. Further experience of *in vivo* survival of red cells, clinical usefulness and plasma-saving effects. *Vox Sang* **45**: 217-223.

24. Moore GL (1987) Additive solutions for better blood preservation. *Crit Rev Clin Lab Sci* **25**: 211-229.

25. Brecher ME, Zylstra-Halling VW, Pineda AA (1991) Rejuvenation of erythrocytes preserved with AS-1 and AS-3. *Am J Clin Pathol* **96**: 767-769.

26. Jeter EK, Gadsden RH, Cate Jt (1991) Effects of irradiation on red cells stored in CPDA-1 and CPD-ADSOL (AS-1). *Ann Clin Lab Sci* **21**: 177-186.

27. Valeri CR, Pivacek LE, Ragno G (2001) The quality of RBCs stored in CPD/ADSOL. *Transfusion* **41**: 1072-1073.

28. Shiba M, Mura T, Masuyama T, Nagahashi H, Tayama T*, et al.* (1991) Preperation and preservation of red blood cell concentrates in MAP solution by quadruple bag system. *Japanese Journal of Transfusion Medicine* **37**: 404-410.

29. Shimizu M, Fujii H, Mizoguchi H, Masuda M, Toyama K*, et al.* (1992) Multicenter clinical evaluation of red cell concentrates stored up to 6 weeks in MAP, a new additive solution. *The Japanese journal of clinical hematology [Rinsho ketsueki]* **33**: 148-156.

30. Walker WH, Netz M, Ganshirt KH (1990) 49 day storage of erythrocyte concentrates in blood bags with the PAGGS-mannitol. *Beitr Infusionsther* **26**: 55-59.

31. Yasutake M, Takahashi TA (1997) Current advance of blood preservation -- development and clinical application of additive solutions for preservation of red blood cells and platelets. *Nippon Rinsho* **55**: 2429-2433.

32. Beutler E, Wood L (1969) The *in vivo* regeneration of red cell 2,3 diphosphoglyceric acid (DPG) after transfusion of stored blood. *J Lab Clin Med* **74**: 300-304.

33. de Korte D, Kleine M, Korsten HG, Verhoeven AJ (2008) Prolonged maintenance of 2,3-diphosphoglycerate acid and adenosine triphosphate in red blood cells during storage. *Transfusion* **48**: 1081-1089.

34. Marshall Lichtman EB, Kenneth Kaushansky, Thomas Kipps, Uri Seligsohn, Josef Prchal, editor (2005) *Williams Hematology*. Seventh ed: McGraw-Hill Professional.

35. Rapoport TA, Heinrich R, Jacobasch G, Rapoport S (1974) A linear steady-state treatment of enzymatic chains. A mathematical model of glycolysis of human erythrocytes. *Eur J Biochem* **42**: 107-120.

36. Rapoport TA, Heinrich R, Rapoport SM (1976) The regulatory principles of glycolysis in erythrocytes *in vivo* and *in vitro*. A minimal comprehensive model describing steady states, quasi-steady states and time-dependent processes. *Biochem J* **154**: 449-469.

37. Joshi A, Palsson BO (1989) Metabolic dynamics in the human red cell. Part I--A comprehensive kinetic model. *J Theor Biol* **141**: 515-528.

38. Joshi A, Palsson BO (1989) Metabolic dynamics in the human red cell. Part II--Interactions with the environment. *J Theor Biol* **141**: 529-545.

39. Joshi A, Palsson BO (1990) Metabolic dynamics in the human red cell. Part III--Metabolic reaction rates. *J Theor Biol* **142**: 41-68.

40. Joshi A, Palsson BO (1990) Metabolic dynamics in the human red cell. Part IV--Data prediction and some model computations. *J Theor Biol* **142**: 69-85.

41. Mulquiney PJ, Kuchel PW (1999) Model of 2,3-bisphosphoglycerate metabolism in the human erythrocyte based on detailed enzyme kinetic equations: equations and parameter refinement. *Biochem J* **342**: 581-596.

42. Tomita M, Hashimoto K, Takahashi K, Shimizu TS, Matsuzaki Y*, et al.* (1999) E-CELL: software environment for whole-cell simulation. *Bioinformatics* **15**: 72-84.

43. Yachie-Kinoshita A, Nishino T, Shimo H, Suematsu M, Tomita M (2010) A metabolic model of human erythrocytes: practical application of the E-Cell Simulation Environment. *Journal of biomedicine & biotechnology* **2010**: 642420.

44. Nakayama Y, Kinoshita A, Tomita M (2005) Dynamic simulation of red blood cell metabolism and its application to the analysis of a pathological condition. *Theor Biol Med Model* **2**: 18.

45. Shimo H, Nishino T, Tomita M (2011) Predicting the Kinetic Properties Associated with Redox Imbalance after Oxidative Crisis in G6PD-Deficient Erythrocytes: A Simulation Study. *Advances in hematology* **2011**: 398945.

46. Kinoshita A, Tsukada K, Soga T, Hishiki T, Ueno Y*, et al.* (2007) Roles of hemoglobin Allostery in hypoxia-induced metabolic alterations in erythrocytes: simulation and its verification by metabolome analysis. *J Biol Chem* **282**: 10731-10741.

47. Monton MR, Soga T (2007) Metabolome analysis by capillary electrophoresis-mass spectrometry. *Journal of chromatography A* **1168**: 237-246; discussion 236.

48. Soga T, Ohashi Y, Ueno Y, Naraoka H, Tomita M*, et al.* (2003) Quantitative metabolome analysis using capillary electrophoresis mass spectrometry. *J Proteome Res* **2**: 488-494.

49. Sana TR, Waddell K, Fischer SM (2008) A sample extraction and chromatographic strategy for increasing LC/MS detection coverage of the erythrocyte metabolome. *Journal of chromatography B, Analytical technologies in the biomedical and life sciences* **871**: 314-321.

50. Darghouth D, Koehl B, Madalinski G, Heilier JF, Bovee P*, et al.* (2011) Pathophysiology of sickle cell disease is mirrored by the red blood cell metabolome. *Blood* **117**: e57-66.

51. Olszewski KL, Morrisey JM, Wilinski D, Burns JM, Vaidya AB*, et al.* (2009) Host-parasite interactions revealed by Plasmodium falciparum metabolomics. *Cell host & microbe* **5**: 191-199.

52. Chapman BE, Kuchel PW, Lovric VA, Raftos JE, Stewart IM (1985) Regeneration of phosphorylated metabolites in stored erythrocytes in an open perfusion system: studies using ^{31}P NMR spectroscopy. *British journal of haematology* **61**: 385-392.

53. Kuchel PW, Berthon HA, Bubb WA, McIntyre LM, Nygh NK*, et al.* (1990) ^{13}C and ^{31}P NMR studies of the pentose phosphate pathway in human erythrocytes. *Biomed Biochim Acta* **49**: S105-110.

54. McIntyre LM, Thorburn DR, Bubb WA, Kuchel PW (1989) Comparison of computer simulations of the F-type and L-type non-oxidative hexose monophosphate shunts with ^{31}P-NMR experimental data from human erythrocytes. *Eur J Biochem* **180**: 399-420.

55. Petersen A, Kristensen SR, Jacobsen JP, Horder M (1990) ^{31}P-NMR measurements of ATP, ADP, 2,3-diphosphoglycerate and Mg^{2+} in human erythrocytes. *Biochim Biophys Acta* **1035**: 169-174.

56. Markuszewski MJ, Szczykowska M, Siluk D, Kaliszan R (2005) Human red blood cells targeted metabolome analysis of glycolysis cycle metabolites by capillary electrophoresis using an indirect photometric detection method. *Journal of pharmaceutical and biomedical analysis* **39**: 636-642.

57. Kuchel PW, Berthon HA, Bubb WA, Bulliman BT, Collins JG (1990) Computer simulation of the pentose-phosphate pathway and associated metabolism used in conjunction with NMR experimental data from human erythrocytes. *Biomed Biochim Acta* **49**: 757-770.

58. Hess JR (2006) An update on solutions for red cell storage. *Vox Sang* **91**: 13-19.

59. Hess JR, Greenwalt TG (2002) Storage of red blood cells: new approaches. *Transfus Med Rev* **16**: 283-295.

60. Hogman CF (1998) Preparation and preservation of red cells. *Vox Sang* **74 Suppl 2**: 177-187.

61. Soga T, Baran R, Suematsu M, Ueno Y, Ikeda S*, et al.* (2006) Differential metabolomics reveals ophthalmic acid as an oxidative stress biomarker indicating hepatic glutathione consumption. *J Biol Chem* **281**: 16768-16776.

62. Hogman CF, Knutson F, Loof H (1999) Storage of whole blood before separation: the effect of temperature on red cell 2,3 DPG and the accumulation of lactate.

Transfusion **39**: 492-497.

63. Imai K, Yonetani T (1975) Thermodynamical studies of oxygen equilibrium of hemoglobin. Nonuniform heats and entropy changes for the individual oxygenation steps and enthalpy-entropy compensation. *J Biol Chem* **250**: 7093-7098.

64. Messana I, Orlando M, Cassiano L, Pennacchietti L, Zuppi C*, et al.* (1996) Human erythrocyte metabolism is modulated by the O_2-linked transition of hemoglobin. *FEBS Lett* **390**: 25-28.

65. Ellory JC, Willis JS (1982) Kinetics of the sodium pump in red cells of different temperature sensitivity. *J Gen Physiol* **79**: 1115-1130.

66. Daddona PE, Wiesmann WP, Lambros C, Kelley WN, Webster HK (1984) Human malaria parasite adenosine deaminase. Characterization in host enzyme-deficient erythrocyte culture. *J Biol Chem* **259**: 1472-1475.

67. Agarwal RP, Parks RE (1978) Adenosine deaminase from human erythrocytes. *Methods Enzymol* **67**: 502-507.

68. Lee RS, Ford HC (1988) 5'-Nucleotidase of human placental trophoblastic microvilli possesses cobalt-stimulated FAD pyrophosphatase activity. *J Biol Chem* **263**: 14878-14883.

69. Nowak G, Kaletha K (1992) Purification and properties of AMP-deaminase from human kidney. *Biochem Med Metab Biol* **47**: 232-241.

70. Dutka P, Szydlowska M, Chodorowski Z, Rybakowska I, Nagel-Starczynowska G*, et al.* (2004) AMP-deaminase from normal and cirrhotic human liver: a comparative study. *Mol Cell Biochem* **262**: 119-126.

71. Olsen AS, Milman G (1978) Hypoxanthine phosphoribosyltransferase from Chinese

hamster brain and human erythrocytes. *Methods Enzymol* **51**: 543-549.

72. Yamada Y, Goto H, Ogasawara N (1981) Adenosine kinase from human liver. *Biochim Biophys Acta* **660**: 36-43.

73. Kikuchi S, Tominaga D, Arita M, Takahashi K, Tomita M (2003) Dynamic modeling of genetic networks using genetic algorithm and S-system. *Bioinformatics* **19**: 643-650.

74. Soga T, Heiger DN (2000) Amino acid analysis by capillary electrophoresis electrospray ionization mass spectrometry. *Anal Chem* **72**: 1236-1241.

75. Soga T, Ueno Y, Naraoka H, Ohashi Y, Tomita M*, et al.* (2002) Simultaneous determination of anionic intermediates for Bacillus subtilis metabolic pathways by capillary electrophoresis electrospray ionization mass spectrometry. *Anal Chem* **74**: 2233-2239.

76. Soga T, Ishikawa T, Igarashi S, Sugawara K, Kakazu Y*, et al.* (2007) Analysis of nucleotides by pressure-assisted capillary electrophoresis-mass spectrometry using silanol mask technique. *J Chromatogr A* **1159**: 125-133.

77. MacDonald JA, Storey KB (2002) Purification and characterization of fructose bisphosphate aldolase from the ground squirrel, Spermophilus lateralis: enzyme role in mammalian hibernation. *Arch Biochem Biophys* **408**: 279-285.

78. Macdonald JA, Storey KB (2005) Temperature and phosphate effects on allosteric phenomena of phosphofructokinase from a hibernating ground squirrel (Spermophilus lateralis). *Febs J* **272**: 120-128.

79. Hess JR, Hill HR, Oliver CK, Lippert LE, Greenwalt TJ (2002) Alkaline CPD and the preservation of RBC 2,3-DPG. *Transfusion* **42**: 747-752.

80. Yoshida T, AuBuchon JP, Dumont LJ, Gorham JD, Gifford SC*, et al.* (2008) The

effects of additive solution pH and metabolic rejuvenation on anaerobic storage of red cells. *Transfusion* **48**: 2096-2105.

81. Suganuma K, Tsukada K, Kashiba M, Tsuneshige A, Furukawa T*, et al.* (2006) Erythrocytes with T-state-stabilized hemoglobin as a therapeutic tool for postischemic liver dysfunction. *Antioxid Redox Signal* **8**: 1847-1855.

82. Bloxham DP, Lardy HA (1973) Phosphofructokinase. In: Boyer, P.D. , editor. The Enzymes, 3rd Ed.; Boyer PD, editor, editor. New York: Academic Press. 239-278.

83. Guppy M, Attwood PV, Hansen IA, Sabaratnam R, Frisina J*, et al.* (1992) pH, temperature and lactate production in human red blood cells: implications for blood storage and glycolytic control. *Vox Sang* **62**: 70-75.

84. Stocchi V, Magnani M, Canestrari F, Dacha M, Fornaini G (1982) Multiple forms of human red blood cell hexokinase. Preparation, characterization, and age dependence. *J Biol Chem* **257**: 2357-2364.

85. Ishii N, Nakahigashi K, Baba T, Robert M, Soga T*, et al.* (2007) Multiple high-throughput analyses monitor the response of E. coli to perturbations. *Science* **316**: 593-597.

86. Ohashi Y, Hirayama A, Ishikawa T, Nakamura S, Shimizu K*, et al.* (2008) Depiction of metabolome changes in histidine-starved Escherichia coli by CE-TOFMS. *Mol Biosyst* **4**: 135-147.

87. Nishino T, Yachie-Kinoshita A, Hirayama A, Soga T, Suematsu M*, et al.* (2009) *In silico* modeling and metabolome analysis of long-stored erythrocytes to improve blood storage methods. *J Biotechnol* **144**: 212-223.

88. Burger P, Korsten H, De Korte D, Rombout E, Van Bruggen R*, et al.* (2010) An improved red blood cell additive solution maintains 2,3-diphosphoglycerate and

adenosine triphosphate levels by an enhancing effect on phosphofructokinase activity during cold storage. *Transfusion* **50**: 2386-2392.

89. Simon T, Snyder E, Stowell C, Strauss R, Solheim B*, et al.*, editors (2009) *Rossi's Principles of Transfusion Medicine*. 4th ed: Wiley.

90. Meryman HT, Hornblower M (1991) Manipulating red cell intra- and extracellular pH by washing. *Vox Sang* **60**: 99-104.

91. Stoychev G, Kierdaszuk B, Shugar D (2002) Xanthosine and xanthine. Substrate properties with purine nucleoside phosphorylases, and relevance to other enzyme systems. *Eur J Biochem* **269**: 4048-4057.

92. Mulquiney PJ, Bubb WA, Kuchel PW (1999) Model of 2,3-bisphosphoglycerate metabolism in the human erythrocyte based on detailed enzyme kinetic equations: *in vivo* kinetic characterization of 2,3-bisphosphoglycerate synthase/phosphatase using ^{13}C and ^{31}P NMR. *Biochem J* **342**: 567-580.

93. Suematsu M, Suzuki H, Delano FA, Schmid-Schonbein GW (2002) The inflammatory aspect of the microcirculation in hypertension: oxidative stress, leukocytes/endothelial interaction, apoptosis. *Microcirculation* **9**: 259-276.

94. Akinsheye I, Klings ES (2010) Sickle cell anemia and vascular dysfunction: the nitric oxide connection. *Journal of cellular physiology* **224**: 620-625.

95. Sugita Y, Simon ER (1965) The Mechanism of Action of Adenine in Red Cell Preservation. *The Journal of clinical investigation* **44**: 629-642.

96. D'Amici GM, Rinalducci S, Zolla L (2007) Proteomic analysis of RBC membrane protein degradation during blood storage. *J Proteome Res* **6**: 3242-3255.

97. Lion N, Crettaz D, Rubin O, Tissot JD (2010) Stored red blood cells: a changing universe waiting for its map(s). *Journal of proteomics* **73**: 374-385.

98. Gevi F, D'Alessandro A, Rinalducci S, Zolla L (2012) Alterations of red blood cell metabolome during cold liquid storage of erythrocyte concentrates in CPD-SAGM. *Journal of proteomics* **76**: 168-180.

99. D'Amici G M, Mirasole C, D'Alessandro A, Yoshida T, Dumont LJ*, et al.* (2012) Red blood cell storage in SAGM and AS3: a comparison through the membrane two-dimensional electrophoresis proteome. *Blood transfusion* **10 Suppl 2**: 46-54.

100. Heaton A, Keegan T, Holme S (1989) *In vivo* regeneration of red cell 2,3-diphosphoglycerate following transfusion of DPG-depleted AS-1, AS-3 and CPDA-1 red cells. *British journal of haematology* **71**: 131-136.

101. Messana I, Ferroni L, Misiti F, Girelli G, Pupella S*, et al.* (2000) Blood bank conditions and RBCs: the progressive loss of metabolic modulation. *Transfusion* **40**: 353-360.

102. Lockwood WB, Hudgens RW, Szymanski IO, Teno RA, Gray AD (2003) Effects of rejuvenation and frozen storage on 42-day-old AS-3 RBCs. *Transfusion* **43**: 1527-1532.

103. Koshkaryev A, Zelig O, Manny N, Yedgar S, Barshtein G (2009) Rejuvenation treatment of stored red blood cells reverses storage-induced adhesion to vascular endothelial cells. *Transfusion* **49**: 2136-2143.

104. Oski FA, Travis SF, Miller LD, Delivoria-Papadopoulos M, Cannon E (1971) The *in vitro* restoration of red cell 2,3-diphosphoglycerate levels in banked blood. *Blood* **37**: 52-58.

105. Hawkins CF, Bagnara AS (1987) Adenosine kinase from human erythrocytes: kinetic studies and characterization of adenosine binding sites. *Biochemistry* **26**: 1982-1987.

106. Mimouni M, Bontemps F, Van den Berghe G (1994) Kinetic studies of rat liver adenosine kinase. Explanation of exchange reaction between adenosine and AMP. *J Biol Chem* **269**: 17820-17825.

107. Buckwitz D, Jacobasch G, Kuckelkorn U, Plonka A, Gerth C (1990) Glucose-6-phosphate dehydrogenase from Plasmodium berghei: kinetic and electrophoretic characterization. *Exp Parasitol* **70**: 264-275.

108. Domin BA, Mahony WB, Zimmerman TP (1988) Purine nucleobase transport in human erythrocytes. Reinvestigation with a novel "inhibitor-stop" assay. *J Biol Chem* **263**: 9276-9284.

109. Dash RK, Bassingthwaighte JB (2004) Blood HbO_2 and $HbCO_2$ dissociation curves at varied O_2, CO_2, pH, 2,3-DPG and temperature levels. *Ann Biomed Eng* **32**: 1676-1693.

110. Mulquiney PJ, Kuchel PW (2003) Modelling metabolism with Mathematica. Boca Raton, FL: CRC Press.

111. von Ruckmann B, Schubert D (2002) The complex of band 3 protein of the human erythrocyte membrane and glyceraldehyde-3-phosphate dehydrogenase: stoichiometry and competition by aldolase. *Biochim Biophys Acta* **1559**: 43-55.

112. Jenkins JD, Madden DP, Steck TL (1984) Association of phosphofructokinase and aldolase with the membrane of the intact erythrocyte. *J Biol Chem* **259**: 9374-9378.

113. Walder JA, Chatterjee R, Steck TL, Low PS, Musso GF*, et al.* (1984) The interaction of hemoglobin with the cytoplasmic domain of band 3 of the human erythrocyte membrane. *J Biol Chem* **259**: 10238-10246.

Appendix A

Detailed description of the mathematical model of the human erythrocyte metabolism

In this thesis, we used the published model of comprehensive metabolism in circulating human erythrocytes including binding processes between metabolites and magnesium ion/hemoglobins and hemoglobin transition [46]. All reactions expressed in the model are shown below. Parameters represented as unitless numbers mean dimensionless coefficients.

A.1 Kinetic equations and parameters used in the model

Abbreviation of enzymes and metabolites are corresponding to those shown in Table 2.1 in the main text. e_t denotes enzyme concentration.

Hexokinase

$$v = \frac{e_t\left(\frac{theK_{catf}\,\mathrm{AB}}{K_{i,\mathrm{B}}K_{m,\mathrm{A}}} - \frac{theK_{catr}\,\mathrm{PQ}}{K_{i,\mathrm{Q}}K_{m,\mathrm{P}}}\right)}{1 + \frac{\mathrm{A}}{K_{i,\mathrm{A}}} + \frac{\mathrm{B}}{K_{i,\mathrm{B}}} + \frac{\mathrm{AB}}{K_{i,\mathrm{B}}K_{m,\mathrm{A}}} + \frac{\mathrm{P}}{K_{i,\mathrm{P}}} + \frac{\mathrm{Q}}{K_{i,\mathrm{Q}}} + \frac{\mathrm{PQ}}{K_{i,\mathrm{Q}}K_{m,\mathrm{Q}}} + \sum_{j=1}^{4}\frac{\mathrm{I}_j\mathrm{B}}{K'_{i,\mathrm{I}j}K_{i,\mathrm{B}}}} \tag{S1}$$

$$theK_{catf} = \frac{1.662\,k_{catf}}{\left(1 + \frac{10^{-\mathrm{pH}}}{10^{-7.02}} + \frac{10^{-9.55}}{10^{-\mathrm{pH}}}\right)} \tag{S2}$$

$$theK_{catr} = \frac{1.662\, k_{catr}}{\left(1 + \frac{10^{-\mathrm{pH}}}{10^{-7.02}} + \frac{10^{-9.55}}{10^{-\mathrm{pH}}}\right)} \tag{S3}$$

Symbols: A, MgATP; B, GLC; P, G6P; Q, MgADP; I, Pi, 2,3-BPG and GDP

Parameter	Value
e_t (M)	2.50E–08
$K_{m,\mathrm{MgADP}}$, $K_{i,\mathrm{MgADP}}$ (M)	1.00E–03
$K_{m,\mathrm{MgATP}}$, $K_{i,\mathrm{MgATP}}$ (M)	1.00E–03
$K'_{i,2,3\mathrm{BPG}}$ (M)	2.70E–03
$K'_{i,\mathrm{GSH}}$ (M)	3.00E–03
$K'_{i,\mathrm{GDP}}$ (M)	1.00E–05
$K'_{i,\mathrm{G6P}}$ (M)	1.00E–05
$K_{i,\mathrm{GLC}}$ (M)	4.70E–05
$K_{m,\mathrm{G6P}}$, $K_{i,\mathrm{G6P}}$ (M)	4.70E–05
k_{catf} (s^{-1})	180
k_{catr} (s^{-1})	1.16

Parameter values were taken from [41] or adjusted
by reference to observed data corrected by the literature.

Phosphoglucoisomerase (PGI), Triose phosphate isomerase (TPI), Phosphoglyceromutase (PGM)

$$v = \frac{e_t\left(\frac{k_{catf}\,\mathrm{A}}{K_{m,\mathrm{A}}} - \frac{k_{catr}\,\mathrm{P}}{K_{m,\mathrm{P}}}\right)}{1 + \frac{\mathrm{A}}{K_{m,\mathrm{A}}} + \frac{\mathrm{P}}{K_{m,\mathrm{P}}}} \tag{S4}$$

Symbols: (PGI) A,G6P; P, F6P (TPI) A, DHAP; P, GA3P (PGM) A, 3PG; P, 2PG

Parameter	Value
PGI	
e_t (M)	2.18E–07
$K_{m,\mathrm{G6P}}$ (M)	1.81E–04
$K_{m,\mathrm{F6P}}$ (M)	7.10E–05
k_{catf} (s^{-1})	1470
k_{catr} (s^{-1})	1760
PGM	
e_t (M)	4.10E–07
$K_{m,\mathrm{2PG}}$ (M)	4.60E–05
$K_{m,\mathrm{3PG}}$ (M)	1.68E–04
k_{catf} (s^{-1})	795
k_{catr} (s^{-1})	714
TPI	
e_t (M)	1.14E–06
$K_{m,\mathrm{DHAP}}$ (M)	1.62E–04
$K_{m,\mathrm{GA3P}}$ (M)	4.46E–04
k_{catf} (s^{-1})	1280
k_{catr} (s^{-1})	14560

Parameter values were taken from [41] or adjusted by reference to observed data corrected by the literature.

Phosphofructokinase

$$v = \frac{e_t\left(\frac{k_{catf}\,\mathrm{AB}}{K_{mR,\mathrm{A}}K_{mR,\mathrm{B}}} - \frac{k_{catr}\,\mathrm{PQ}}{K_{mR,\mathrm{P}}K_{mR,\mathrm{Q}}}\right)}{1+\frac{\mathrm{A}}{K_{mR,\mathrm{A}}}+\frac{\mathrm{B}}{K_{mR,\mathrm{B}}}+\frac{\mathrm{AB}}{K_{mR,\mathrm{A}}K_{mR,\mathrm{B}}}+\frac{\mathrm{P}}{K_{mR,\mathrm{P}}}+\frac{\mathrm{Q}}{K_{mR,\mathrm{Q}}}+\frac{\mathrm{PQ}}{K_{mR,\mathrm{P}}K_{mR,\mathrm{Q}}}}\times\rho \tag{S5}$$

$$\rho = \frac{1}{1+L_{PFK}} \tag{S6}$$

$$L_{PFK} = \frac{\left(\frac{10^{-\mathrm{pH}}}{K_a}\right)^n\left(1+\frac{\mathrm{ATP}}{K_{T,\mathrm{ATP}}}\right)^4\left(1+\frac{\mathrm{Mg}^{2+}}{K_{T,\mathrm{Mg}^{2+}}}\right)^4\left(1+\frac{\mathrm{2,3BPG}}{K_{T,\mathrm{2,3BPG}}}\right)^4}{\left(1+\frac{\mathrm{F6P}}{K_{mR,\mathrm{F6P}}}+\frac{\mathrm{F16BP}}{K_{mR,\mathrm{F16BP}}}\right)^4\left(1+\frac{\mathrm{AMP}}{K_{R,\mathrm{AMP}}}\right)^4\left(1+\frac{\mathrm{Pi}}{K_{R,\mathrm{Pi}}}\right)^4\left(1+\frac{\mathrm{GDP}}{K_{R,\mathrm{GDP}}}\right)^4} \tag{S7}$$

Symbols: A, MgATP; B, F6P; P, F1,6BP; Q, MgADP

Parameter	Value
e_t (M)	1.10E–07
$K_{R,\mathrm{AMP}}$ (M)	3.50E–05
$K_{R,\mathrm{GDP}}$ (M)	1.51E–05
$K_{R,\mathrm{Pi}}$ (M)	4.31E–04
$K_{T,\mathrm{ATP}}$ (M)	9.80E–06
$K_{T,2,3\mathrm{BPG}}$ (M)	1.44E–03
$K_{T,\mathrm{Mg}^{2+}}$ (M)	4.40E–04
$K_{mR,\mathrm{F1,6BP}}$ (M)	4.20E–04
$K_{mR,\mathrm{F6P}}$ (M)	2.70E–04
$K_{mR,\mathrm{MgADP}}$ (M)	5.40E–04
$K_{mR,\mathrm{MgATP}}$ (M)	6.80E–05
n	2
K_a	8.91E–08
k_{catf} (s^{-1})	822
k_{catr} (s^{-1})	36

Parameter values were taken from [41] or adjusted by reference to observed data corrected by the literature.

Aldolase

$$v = \frac{e_t\left(\frac{k_{catf}\,\mathrm{A}}{K_{m,\mathrm{A}}} - \frac{k_{catr}\,\mathrm{PQ}}{K_{i,\mathrm{Q}}K_{m,\mathrm{P}}}\right)}{1 + \frac{\mathrm{I}}{K_{i,\mathrm{I}}} + \frac{\mathrm{A}}{K_{m,\mathrm{A}}} + \frac{K_{m,\mathrm{A}}\mathrm{P}}{K_{m,\mathrm{P}}K_{i,\mathrm{Q}}} + \left(1 + \frac{\mathrm{I}}{K_{i,\mathrm{I}}}\right) + \frac{\mathrm{Q}}{K_{i,\mathrm{Q}}} + \frac{K_{m,\mathrm{Q}}\mathrm{AP}}{K_{i,\mathrm{A}}K_{m,\mathrm{P}}K_{i,\mathrm{Q}}} + \frac{\mathrm{PQ}}{K_{i,\mathrm{Q}}K_{m,\mathrm{P}}}} \qquad \text{(S8)}$$

Symbols: A, F1,6BP; P, GA3P; Q, DHAP;I, 2,3BPG

Parameter	Value
e_t (M)	3.70E–07
$K_{m,\mathrm{F1,6BP}}$ (M)	1.65E–05
$K_{i,\mathrm{F1,6BP}}$ (M)	1.98E–05
$K_{m,\mathrm{DHAP}}$ (M)	3.50E–05
$K_{i,\mathrm{DHAP}}$ (M)	1.10E–05
$K_{m,\mathrm{GA3P}}$ (M)	1.90E–04
$K_{i,2,3\mathrm{BPG}}$ (M)	1.50E–03
k_{catf} (s^{-1})	68
k_{catr} (s^{-1})	234

Parameter values were taken from [41] or adjusted by reference to observed data corrected by the literature.

Glyceraldehyde phosphate dehydrogenase

$$v = \frac{e_t\left(\frac{k_{catf}\,\mathrm{ABC}}{K_{m,\mathrm{A}}K_{i,\mathrm{B}}K_{i,\mathrm{C}}} - \frac{10^{-\mathrm{pH}}k_{catr}\,\mathrm{PQH}}{10^{-7.2}K_{i,\mathrm{P}}K_{m,\mathrm{Q}}}\right)}{GAPDH_{rd}} \tag{S9}$$

$$\begin{aligned} GAPDH_{rd} = {} & \frac{\mathrm{C}}{K_{i,\mathrm{C}}}\left(1+\frac{\mathrm{C}}{K'_{i,\mathrm{C}}}\right)+\frac{\mathrm{P}}{K_{i,\mathrm{P}}}\left(1+\frac{\mathrm{C}}{K'_{i,\mathrm{C}}}\right)+\frac{10^{-\mathrm{pH}}K_{m,\mathrm{P}}\mathrm{Q}}{10^{-7.2}K_{i,\mathrm{P}}K_{m,\mathrm{Q}}}+ \\ & \frac{K_{m,\mathrm{C}}\mathrm{AB}}{K_{m,\mathrm{A}}K_{i,\mathrm{B}}K_{i,\mathrm{C}}}+\frac{\mathrm{AC}}{K_{i,\mathrm{A}}K_{i,\mathrm{C}}}+\frac{\mathrm{BC}}{K_{i,\mathrm{B}}K_{i,\mathrm{C}}}\left(1+\frac{\mathrm{C}}{K'_{i,\mathrm{C}}}\right)+\frac{\mathrm{AP}}{K_{i,\mathrm{A}}K_{i,\mathrm{P}}}+\frac{10^{-\mathrm{pH}}K_{m,\mathrm{P}}\mathrm{BQ}}{10^{-7.2}K_{i,\mathrm{B}}K_{i,\mathrm{P}}K_{m,\mathrm{Q}}}+ \\ & \frac{10^{-\mathrm{pH}}\mathrm{CQ}}{10^{-7.2}K_{i,\mathrm{C}}K_{i,\mathrm{Q}}}+\frac{10^{-\mathrm{pH}}\mathrm{PQ}}{10^{-7.2}K_{i,\mathrm{P}}K_{m,\mathrm{Q}}}+\frac{\mathrm{ABC}}{K_{m,\mathrm{A}}K_{i,\mathrm{B}}K_{i,\mathrm{C}}}+\frac{K_{m,\mathrm{C}}\mathrm{ABP}}{K_{i,\mathrm{C}}K_{m,\mathrm{A}}K_{i,\mathrm{B}}K'_{i,\mathrm{P}}}+ \\ & \frac{10^{-\mathrm{pH}}\mathrm{BCQ}}{10^{-7.2}K_{i,\mathrm{B}}K_{i,\mathrm{C}}K_{i,\mathrm{Q}}}+\frac{10^{-\mathrm{pH}}K_{m,\mathrm{P}}\mathrm{BPQ}}{10^{-7.2}K_{i,\mathrm{P}}K_{m,\mathrm{Q}}K_{i,\mathrm{B}}K'_{i,\mathrm{P}}} \end{aligned} \tag{S10}$$

Symbols: A, NAD^+; B, Pi; C, GA3P; P, 1,3BPG; Q, NADH

Parameter	Value
e_t (M)	7.66E–06
K_{m,NAD^+} (M)	4.50E–05
K_{i,NAD^+} (M)	4.50E–05
$K_{m,1,3\mathrm{BPG}}$ (M)	3.30E–06
$K_{i,\mathrm{GA3P}}$ (M)	6.50E–02
$K_{i,1,3\mathrm{BPG}}$ (M)	1.00E–02
$K_{m,\mathrm{Pi}}$ (M)	3.16E–03
$K_{i,\mathrm{Pi}}$ (M)	3.16E–03
$K_{m,\mathrm{GA3P}}$ (M)	9.50E–05
$K'_{i,\mathrm{GA3P}}$ (M)	3.10E–05
$K_{i,\mathrm{NADH}}$ (M)	1.00E–05
$K'_{i,1,3\mathrm{BPG}}$ (M)	1.00E–06
$K_{m,\mathrm{NADH}}$ (M)	3.30E–06
k_{catf} (s^{-1})	232
k_{catr} (s^{-1})	2765

Parameter values were taken from [41] or adjusted by reference to observed data corrected by the literature.

Phosphoglycerate kinase

$$v = \frac{e_t\left(\frac{k_{catf}\,\mathrm{AB}}{K_{m,\mathrm{A}}K_{i,\mathrm{B}}} - \frac{k_{catr}\,\mathrm{PQ}}{K_{i,\mathrm{Q}}K_{m,\mathrm{P}}}\right)}{1 + \frac{\mathrm{A}}{K_{i,\mathrm{A}}} + \frac{\mathrm{B}}{K_{i,\mathrm{B}}} + \frac{\mathrm{AB}}{K_{i,\mathrm{B}}K_{m,\mathrm{A}}} + \frac{\mathrm{P}}{K_{i,\mathrm{P}}} + \frac{\mathrm{Q}}{K_{i,\mathrm{Q}}} + \frac{\mathrm{PQ}}{K_{i,\mathrm{Q}}K_{m,\mathrm{P}}}} \qquad \text{(S11)}$$

Symbols: A, 1,3BPG; B, MgADP; P, 3PG; Q, MgATP

Parameter	Value
e_t (M)	2.74E–06
$K_{i,\text{1,3-BPG}}$ (M)	1.60E–06
$K_{i,\text{MgADP}}$ (M)	8.00E–05
$K_{i,\text{MgATP}}$ (M)	1.30E–04
$K_{i,\text{3PG}}$ (M)	2.05E–04
$K_{m,\text{1,3-BPG}}$ (M)	2.00E–06
$K_{m,\text{3PG}}$ (M)	1.1E–03
k_{catf} (s^{-1})	2290
k_{catr} (s^{-1})	917

Parameter values were taken from [41] or adjusted by reference to observed data corrected by the literature.

Enolase

$$v = \frac{e_t\left(\frac{k_{catf}\,\mathrm{AB}}{K_{m,\mathrm{A}}K_{i,\mathrm{B}}} - \frac{k_{catr}\,\mathrm{PQ}}{K_{i,\mathrm{Q}}K_{m,\mathrm{P}}}\right)}{1 + \frac{\mathrm{A}}{K_{i,\mathrm{A}}} + \frac{\mathrm{B}}{K_{i,\mathrm{B}}} + \frac{\mathrm{AB}}{K_{i,\mathrm{B}}K_{m,\mathrm{A}}} + \frac{\mathrm{Q}}{K_{i,\mathrm{Q}}} + \frac{\mathrm{PQ}}{K_{i,\mathrm{Q}}K_{m,\mathrm{P}}}} \qquad \text{(S12)}$$

Symbols: A, 2PG; B, Mg^{2+}; P, Mg^{2+}; Q, PEP

Parameter	Value
e_t (M)	2.20E–07
$K_{i,\mathrm{Mg}^{2+}}$ (M)	4.60E–04
$K_{i,\text{PEP}}$ (M)	3.10E–04
$K_{i,\text{2PG}}$ (M)	1.40E–04
$K_{m,\mathrm{Mg}^{2+}}$ (M)	4.60E–05
$K_{m,\text{2PG}}$ (M)	1.40E–04
k_{catf} (s^{-1})	190
k_{catr} (s^{-1})	50

Parameter values were taken from [41] or adjusted by reference to observed data corrected by the literature.

Pyruvate kinase

$$v = \frac{e_t\left(\frac{k_{catf}\,\mathrm{AB}}{K_{mR,\mathrm{A}}K_{mR,\mathrm{B}}} - \frac{k_{catr}\,\mathrm{PQ}}{K_{mR,\mathrm{P}}K_{mR,\mathrm{Q}}}\right)}{1+\frac{\mathrm{A}}{K_{mR,\mathrm{A}}}+\frac{\mathrm{B}}{K_{mR,\mathrm{B}}}+\frac{\mathrm{AB}}{K_{mR,\mathrm{A}}K_{mR,\mathrm{B}}}+\frac{\mathrm{P}}{K_{mR,\mathrm{P}}}+\frac{\mathrm{Q}}{K_{mR,\mathrm{Q}}}+\frac{\mathrm{PQ}}{K_{mR,\mathrm{P}}K_{mR,\mathrm{Q}}}} \times \rho \tag{S13}$$

$$\rho = \frac{1}{1+L_{PK}} \tag{S14}$$

$$L_{PK} = \frac{\left(\frac{10^{-6.8}}{10^{-\mathrm{pH}}}\right)\left(1+\frac{\mathrm{ATP}}{K_{T,\mathrm{ATP}}}\right)^4}{\left(1+\frac{\mathrm{PEP}}{K_{mR,\mathrm{PEP}}}+\frac{\mathrm{PYR}}{K_{mR,\mathrm{PYR}}}\right)^4\left(1+\frac{\mathrm{F1,6BP}}{K_{R,\mathrm{F1,6BP}}}+\frac{\mathrm{GDP}}{K_{R,\mathrm{GDP}}}\right)^4} \tag{S15}$$

Symbols: A, MgADP; B, PEP; P, PYR; Q, MgATP.

Parameter	Value
e_t (M)	8.70E–08
$K_{R,\mathrm{F1,6BP}}$ (M)	5.00E–06
$K_{R,\mathrm{GDP}}$ (M)	1.00E–04
$K_{R,\mathrm{MgADP}}$ (M)	4.74E–04
$K_{R,\mathrm{MgATP}}$ (M)	3.00E–03
$K_{mR,\mathrm{PEP}}$ (M)	2.25E–04
$K_{mR,\mathrm{PYR}}$ (M)	2.00E–03
$K_{T,\mathrm{ATP}}$ (M)	3.39E–03
k_{catf} (s^{-1})	1386
k_{catr} (s^{-1})	3.26

Parameter values were taken from [41] or adjusted by reference to observed data corrected by the literature.

Lactate dehydrogenase

$$v = \frac{e_t\left(\frac{k_{catf}\,\mathrm{AB}}{K_{i,\mathrm{A}}K_{m,\mathrm{B}}} - \frac{k_{catr}\,\mathrm{PQ}}{K_{i,\mathrm{Q}}K_{m,\mathrm{P}}}\right)}{LDH_{rd}} \tag{S16}$$

$$LDH_{rd} = \left(1 + \frac{K_{m,\mathrm{A}}\mathrm{B}}{K_{i,\mathrm{A}}K_{m,\mathrm{B}}} + \frac{K_{mQ}\mathrm{P}}{K_{mP}K_{iQ}}\right)\left(1 + \frac{\mathrm{B}}{K'_{i,\mathrm{B}}}\right) + \frac{\mathrm{A}}{K_{i,\mathrm{A}}} + \frac{\mathrm{Q}}{K_{iQ}} + \frac{\mathrm{AB}}{K_{i,\mathrm{A}}K_{m,\mathrm{B}}} + \frac{K_{m,\mathrm{Q}}\mathrm{AP}}{K_{i,\mathrm{A}}K_{m,\mathrm{P}}K_{i,\mathrm{Q}}} + \frac{K_{m,\mathrm{A}}\mathrm{BQ}}{K_{i,\mathrm{A}}K_{m,\mathrm{B}}K_{i,\mathrm{Q}}} + \frac{\mathrm{PQ}}{K_{i,\mathrm{Q}}K_{m,\mathrm{P}}} + \frac{\mathrm{ABP}}{K_{i,\mathrm{A}}K_{m,\mathrm{B}}K_{i,\mathrm{P}}} + \frac{\mathrm{BPQ}}{K_{i,\mathrm{B}}K_{m,\mathrm{P}}K_{i,\mathrm{Q}}} \tag{S17}$$

Symbols: A, NADH; B, PYR; P, NAD^+; Q, LAC

Parameter	Value
e_t (M)	3.43E–06
$K_{m,\mathrm{NADH}}$ (M)	8.44E–06
$K_{i,\mathrm{NADH}}$ (M)	2.45E–06
K_{m,NAD^+} (M)	1.07E–04
K_{i,NAD^+} (M)	5.03E–04
$K_{m,\mathrm{PYR}}$ (M)	1.37E–04
$K_{i,\mathrm{PYR}}$ (M)	2.28E–04
$K'_{i,\mathrm{PYR}}$ (M)	1.01E–04
$K_{m,\mathrm{LAC}}$ (M)	1.07E–03
$K_{i,\mathrm{LAC}}$ (M)	7.33E–03
k_{catf} (s^{-1})	458
k_{catr} (s^{-1})	115

Parameter values were taken from [41] or adjusted by reference to observed data corrected by the literature.

Lactate dehydrogenase (NADPH dependent)

$$v = \frac{e_t\left(\frac{k_{catf}\,\mathrm{AB}}{K_{m,\mathrm{A}}K_{m,\mathrm{B}}} - \frac{k_{catr}\,\mathrm{PQ}}{K_{m,\mathrm{P}}K_{m,\mathrm{Q}}}\right)}{1 + \frac{\mathrm{B}}{K_{m,\mathrm{B}}} + \frac{\mathrm{Q}}{K_{m,\mathrm{Q}}}} \tag{S18}$$

Symbols: A, NADPH; B, PYR; P, $NADP^+$; Q, LAC

Parameter	Value
$e_t\,k_{catf}/K_{m,\mathrm{NADPH}}$ (s^{-1})	3.46E–03
$e_t\,k_{catr}/K_{m,\mathrm{NADP}}$ (s^{-1})	5.43E–07
$K_{m,\mathrm{PYR}}$ (M)	4.14E–04
$K_{m,\mathrm{LAC}}$ (M)	4.14E–04

Parameter values were taken from [41] or adjusted by reference to observed data corrected by the literature.

2,3-BPG shunt reactions

(2,3-BPG mutase, DPGM; 2,3-BPG phosphatase, DPGase)

DPGM:

$$v = \frac{e_t\left(N_1\mathrm{AB} + N_2\mathrm{AC} + N_3\mathrm{AH}\right)}{D_1\mathrm{A} + D_2\mathrm{B} + D_3\mathrm{C} + D_4\mathrm{D} + D_5\mathrm{H} + D_6\mathrm{AB} + D_7\mathrm{AC} + D_8\mathrm{AH} + D_9\mathrm{BD} + D_{10}\mathrm{CD} + D_{11}\mathrm{DH}} \tag{S19}$$

DPGase:

$$v = \frac{e_t\left(N_3\mathrm{AH} + N_7\mathrm{DH} + N_{11}\mathrm{DH}\right)}{D_1\mathrm{A} + D_2\mathrm{B} + D_3\mathrm{C} + D_4\mathrm{D} + D_5\mathrm{H} + D_6\mathrm{AB} + D_7\mathrm{AC} + D_8\mathrm{AH} + D_9\mathrm{BD} + D_{10}\mathrm{CD} + D_{11}\mathrm{DH}} \tag{S20}$$

$$N_1 = k_1k_{12}(k_{15} + k_{16})k_3k_4(k_{10} + k_7)k_8$$
$$N_2 = k_1k_{10}k_{12}(k_{15} + k_{16})k_3k_6(k_5 + k_8)$$
$$N_3 = k_1k_{14}k_{16}k_3(k_{10}(k_{12}(k_5 + k_8) + k_5k_9) + k_7(k_{11}(k_5 + k_8) + k_{12}(k_5 + k_8) + k_5k_9))$$
$$N_4 = k_{13}k_{14}k_{16}(k_2 + k_3)(k_{11}k_7(k_5 + k_8) + k_5(k_{10} + k_7)k_9)$$
$$N_5 = k_1k_{11}(k_{15} + k_{16})k_3k_4k_7k_8$$
$$N_6 = k_1k_{10}(k_{15} + k_{16})k_3k_6(k_{12}(k_5 + k_8) + k_5k_9)$$
$$N_7 = k_{11}k_{13}k_{14}k_{16}(k_2 + k_3)k_7(k_5 + k_8)$$
$$N_8 = k_{11}k_{13}(k_{15} + k_{16})(k_2 + k_3)k_4k_7k_8$$
$$N_9 = k_{10}k_{13}(k_{15} + k_{16})(k_2 + k_3)k_5k_6k_9$$
$$N_{11} = k_{13}k_{14}k_{16}(k_2 + k_3)k_5(k_{10} + k_7)k_9$$
$$D_1 = k_1(k_{15} + k_{16})k_3(k_{10}(k_{12}(k_5 + k_8) + k_5k_9) + k_7(k_{11}(k_5 + k_8) + k_{12}(k_5 + k_8) + k_5k_9))$$
$$D_2 = k_{12}(k_{15} + k_{16})(k_2 + k_3)k_4(k_{10}k_7)k_8$$
$$D_3 = k_{10}k_{12}(k_{15} + k_{16})(k_2k_3)k_6(k_5 + k_8)$$
$$D_4 = k_{13}(k_{15} + k_{16})(k_2 + k_3)(k_{11}k_7(k_5 + k_8) + k_5(k_{10} + k_7)k_9)$$
$$D_5 = k_{14}k_{16}(k_2 + k_3)(k_{10}(k_{12}(k_5 + k_8) + k_5k_9) + k_7(k_{11}(k_5 + k_8) + k_{12}(k_5 + k_8) + k_5k_9))$$
$$D_6 = k_1(k_{15} + k_{16})k_4(k_{11}k_3(k_7k_8) + k_{10}(k_{12}(k_3 + k_8) + k_3(k_8 + k_9)) + k_7(k_{12}(k_3 + k_8) + k_3(k_8 + k_9)))$$
$$D_7 = k_1(k_{15} + k_{16})k_6(k_3(k_{12}k_5 + k_{12}k_8 + k_{11}(k_5 + k_8) + k_5k_9) + k_{10}(k_{12}(k_5 + k_8) + k_3(k_5 + k_8 + k_9)))$$
$$D_8 = k_1k_{14}(k_{16} + k_3)(k_{10}(k_{12}(k_5 + k_8) + k_5k_9) + k_7(k_{11}(k_5 + k_8) + k_{12}(k_5 + k_8) + k_5k_9))$$
$$D_9 = k_{13}(k_{15} + k_{16})(k_2 + k_3)k_4(k_{11}k_3(k_7k_8) + (k_{10} + k_7)(k_8 + k_9))$$
$$D_{10} = k_{13}(k_{15} + k_{16})(k_2 + k_3)k_6(k_{11}(k_5 + k_8) + k_5k_9 + k_{10}(k_5 + k_8 + k_9))$$
$$D_{11} = k_{13}k_{14}(k_2 + k_3)(k_{11}(k_{16} + k_7)(k_5 + k_8) + k_{10}(k_5k_9 + k_{16}(k_5 + k_8 + k_9)) + k_7(k_5k_9 + k_{16}(k_5 + k_8 + k_9)))$$

(S21-S42)

Symbols: A, 1,3-BPG; B, 3PG; C, 2PG; D,2,3-BPG; H, 2PG or Pi

Parameter	Value
e_t (M)	4.1E–07
k_2 (s^{-1})	400
k_3 (s^{-1})	9.9
k_4 ($M^{-1} s^{-1}$)	1.85E+08
k_5 ($M^{-1} s^{-1}$)	1.00E+08
k_6 (s^{-1})	1000
k_7 (s^{-1})	1000
k_8 (s^{-1})	10000
k_9 (s^{-1})	0.55
k_{10} (s^{-1})	1979
k_{11} (s^{-1})	0.01
k_{12} (s^{-1})	1000
k_{13} ($M^{-1} s^{-1}$)	1800000
k_{14} ($M^{-1} s^{-1}$)	1.00E+09
k_{15} (s^{-1})	610000
k_{16} (s^{-1})	0.19

Parameter values were taken from [92].

Phosphoribosyl pyrophosphate synthetase

$$v = \frac{V_m \left(\mathrm{AB} - \dfrac{\mathrm{PQ}}{K_{eq}} \right)}{K_{m,\mathrm{A}} \mathrm{B} + K_{m,\mathrm{B}} \mathrm{A} + \dfrac{K_v K_{m,\mathrm{Q}} \mathrm{P}}{K_{eq}} + \dfrac{K_v K_{m,\mathrm{P}} \mathrm{Q}}{K_{eq}} + \mathrm{AB} + K_v \mathrm{P}} \qquad \text{(S43)}$$

Symbols: A, R5P; B, MgATP; P, PRPP; Q, AMP

Parameter	Value
$K_{m,\mathrm{AMP}}$ (M)	2.75E–04
$K_{m,\mathrm{ATP}}$ (M)	1.70E–04
K_{eq}	28.6
$K_{m,\mathrm{PRPP}}$ (M)	9.00E–05
$K_{m,\mathrm{R5P}}$ (M)	6.50E–04
K_v (M)	7.50E–04
V_m ($M\ h^{-1}$)	5.54E–04

Parameter values were taken from [54].

Adenosine kinase

$$v = \frac{V_m \, \mathrm{AB}}{K_{i,\mathrm{A}} K_{m,\mathrm{B}} + K_{m,\mathrm{A}} \, \mathrm{B} + K_{m,\mathrm{B}} \, \mathrm{A} + \mathrm{AB}} \tag{S44}$$

Symbols: A, ADO; B, MgATP

Parameter	Value
$K_{i,\ \mathrm{ADO}}$ (M)	5.40E–07
$K_{m,\ \mathrm{ADO}}$ (M)	1.75E–06
$K_{m,\ \mathrm{MgATP}}$ (M)	2.70E–05
V_m (M s^{-1})	5.50E–07

Parameter values were taken from [105] and [106].

Adenylate kinase

$$v = \frac{e_t \left(k_{catf} \ \frac{\mathrm{AB}}{K_{m,\mathrm{A}} K_{m,\mathrm{B}}} - k_{catr} \ \frac{\mathrm{PQ}}{K_{m,\mathrm{P}} K_{m,\mathrm{Q}}} \right)}{1 + \frac{\mathrm{A}}{K_{m,\mathrm{A}}} + \frac{\mathrm{B}}{K_{m,\mathrm{B}}} + \frac{\mathrm{AB}}{K_{m,\mathrm{A}} K_{m,\mathrm{B}}} + \frac{\mathrm{P}}{K_{m,\mathrm{P}}} + \frac{\mathrm{Q}}{K_{m,\mathrm{Q}}} + \frac{\mathrm{PQ}}{K_{m,\mathrm{P}} K_{m,\mathrm{Q}}}} \tag{S45}$$

Symbols: A, ADP; B, MgADP; P, AMP; Q, MgATP

Parameter	Value
e_t (M)	9.70E–07
$K_{m,\mathrm{ADP}}$ (M)	1.00E–05
$K_{m,\mathrm{MgADP}}$ (M)	1.00E–04
$K_{m,\mathrm{MgATP}}$ (M)	1.10E–04
$K_{m,\mathrm{AMP}}$ (M)	6.70E–05
k_{catf} (s^{-1})	2080
k_{catr} (s^{-1})	3800

Parameter values were taken from [41].

Adenosine triphosphate phosphohydrolase (ATPase), Adenosine monophosphate phosphohydrolase (AMPase), Inosine monophosphatase (IMPase), Glutathione turnover (GSHox), non-glycolytic NADH consumption process (NADHox)

$$v = k\,\mathrm{S} \tag{S46}$$

S: substrate of the reaction

Parameter	Value
AMPase [a]	
k (h^{-1})	1.58
ATPase [c]	
k (h^{-1})	7.12E–01
IMPase [a]	
k (h^{-1})	9.00E–02
GSHox [c]	
k (s^{-1})	2.38E–05
NADHox [b]	
k (s^{-1})	1.63E–02

Parameter values were taken from [a][37], [b][41] or [c]adjusted to achieve the appropriate steady-state concentration of metabolites.

Adenine phosphoribosyl transferase (ADPRT), Hypoxanthine-guanine phosphoryl transferase (HGPRT)

$$v = V_m \left(\frac{\mathrm{A}}{1 + K_{m,\mathrm{A}}} \right) \left(\frac{\mathrm{B}}{1 + K_{m,\mathrm{B}}} \right) \tag{S47}$$

Symbols: (ADPRT) A, ADE; B, PRPP (HGPRT) A, PRPP; B, HX

Parameter	Value
ADPRT	
$K_{m,\mathrm{ADE}}$ (M)	2.30E–06
$K_{m,\mathrm{PRPP}}$ (M)	1.95E–05
V_m (M h^{-1})	7.80E–05
HGPRT	
$K_{m,\mathrm{PRPP}}$ (M)	5.00E–06
$K_{m,\mathrm{HX}}$ (M)	2.20E–04
V_m (M h^{-1})	2.01E–04

Parameter values were taken from [37].

Purine nucleoside phophorylase (PNPase), Phosphoribomutase (PRM)

$$v = ka\ \mathrm{A} - kd\ \mathrm{P} \tag{S48}$$

Symbols: (PNPase) A, INO; P, HX. (PRM) A, R1P; P, R5P.

Parameter	Value
PNPase	
ka (s^{-1})	1.11E+03
kd (s^{-1})	1.00E+02
PRM	
ka (s^{-1})	7.25
kd (s^{-1})	1.00E+02

Parameter values were taken from [64].

6-phosphogluconolactonase (6PGLase), Adenosine deaminase (ADA), Adenosine monophosphate deaminase (AMPDA)

$$v = \frac{V_m\ \mathrm{S}}{K_m + \mathrm{S}} \tag{S49}$$

S: substrate of the reaction

Parameter	Value
6PGLase [a]	
K_m (M)	7.99E–05
V_m (M h^{-1})	2.2518
ADA [b]	
K_m (M)	5.20E–05
V_m (M h^{-1})	2.00E–02
AMPDA [b]	
K_m (M)	8.00E–04
V_m (M h^{-1})	1.00E–05

Parameter values were taken from [a][54], [b][37].

Glucose 6-phosphate dehydrogenase

$$v = \frac{V_m \dfrac{\mathrm{AB}}{K_{m,\mathrm{A}} K_{m,\mathrm{B}}}}{1 + \dfrac{\mathrm{B}}{K_{m,\mathrm{B}}}\left(1 + \dfrac{\mathrm{A}}{K_{m,\mathrm{A}}}\right) + \dfrac{\mathrm{P}}{K_{m,\mathrm{P}}} + \dfrac{\mathrm{ATP}}{K_{\mathrm{ATP}}} + \dfrac{2{,}3\text{ - BPG}}{K_{2,3\text{-BPG}}}} \tag{S50}$$

Symbols: A, G6P; B, NADP; P, NAPDH

Parameter	Value
K_{ATP} (M)	7.49E–04
$K_{2,3\mathrm{BPG}}$ (M)	2.29E–03
$K_{m,\mathrm{G6P}}$ (M)	6.67E–05
$K_{m,\mathrm{NADP}}$ (M)	3.67E–06
$K_{m,\mathrm{NADPH}}$ (M)	3.12E–06
V_m (M s^{-1})	6.40E-05

Parameter values were taken from [107].

6-phosphogluconate dehydrogenase

$$v = \frac{e_t(N_1\mathrm{AB} - N_2\mathrm{PQ})}{D_1 + D_2\mathrm{A} + D_3\mathrm{B} + D_4\mathrm{P} + D_5\mathrm{Q} + D_6\mathrm{AB} + D_7\mathrm{AP} + D_8\mathrm{BQ} + D_9\mathrm{PQ} + D_{10}\mathrm{ABP} + D_{11}\mathrm{BPQ}} \tag{S51}$$

$$N_1 = k_1k_3k_5k_7k_9$$
$$N_2 = k_2k_4k_6k_8k_{10}$$
$$D_1 = k_2k_9(k_4k_6 + k_5k_6 + k_5k_7)$$
$$D_2 = k_1k_9(k_4k_6 + k_5k_6 + k_5k_7)$$
$$D_3 = k_3k_5k_7k_9$$
$$D_4 = k_2k_4k_6k_8$$
$$D_5 = k_2k_{10}(k_4k_6 + k_5k_6 + k_5k_7)$$
$$D_6 = k_1k_3(k_5k_7 + k_5k_9 + k_6k_9 + k_7k_9)$$
$$D_7 = k_1k_4k_6k_8$$
$$D_8 = k_3k_5k_7k_{10}$$
$$D_9 = k_8k_{10}(k_2k_4 + k_2k_5 + k_2k_6 + k_4k_6)$$
$$D_{10} = k_1k_3k_8(k_5 + k_6)$$
$$D_{11} = k_3k_8k_{10}(k_5 + k_6)$$

(S52-S64)

Symbols: A, NADP; B, GO6P; P, RU5P; Q, NADPH

Parameter	Value
e_t (M)	2.10E–06
k_1 ($M^{-1} s^{-1}$)	2.40E+06
k_2 (s^{-1})	4.10E+02
k_3 ($M^{-1} s^{-1}$)	2.00E+09
k_4 ($M^{-1} s^{-1}$)	2.60E+04
k_5 (s^{-1})	48.0
k_6 (s^{-1})	30.0
k_7 (s^{-1})	6.30E+02
k_8 ($M^{-1} s^{-1}$)	3.60E+04
k_9 (s^{-1})	8.00E+02
k_{10} ($M^{-1} s^{-1}$)	2.25E+05
k_{11} (s^{-1})	3.00E+02
k_{12} ($M^{-1} s^{-1}$)	4.95E+06

Parameter values were taken from [54].

Glutathione reductase

$$v = \frac{e_t(N_1 \mathrm{AB} - N_2 \mathrm{P}^2 \mathrm{Q})}{GSSGRrd} \tag{S65}$$

$$GSSGR_{rd} = D_1 + D_2 \mathrm{A} + D_3 \mathrm{B} + D_4 \mathrm{P} + D_5 \mathrm{Q} + D_6 \mathrm{AB} + D_7 \mathrm{AP} + D_8 \mathrm{BQ} + D_9 \mathrm{P}^2 + (D_{10} + D_{11})\mathrm{PQ} + (D_{12} + D_{13})\mathrm{ABP} + D_{14} \mathrm{AP}^2 + D_{15} \mathrm{BPQ} + D_{16} \mathrm{P}^2 \mathrm{Q} + D_{17} \mathrm{ABP}^2 + D_{18} \mathrm{BP}^2 \mathrm{Q} \tag{S66}$$

$$
\begin{aligned}
N_1 &= k_1k_3k_5k_7k_9k_{11}\\
N_2 &= k_2k_4k_6k_8k_{10}k_{12}\\
D_1 &= k_2k_9k_{11}(k_4k_6 + k_4k_7 + k_5k_7)\\
D_2 &= k_1k_9k_{11}(k_4k_6 + k_4k_7 + k_5k_7)\\
D_3 &= k_3k_5k_7k_9k_{11}\\
D_4 &= k_2k_4k_6k_8k_{11}\\
D_5 &= k_2k_9k_{12}(k_4k_6 + k_4k_7 + k_5k_7)\\
D_6 &= k_1k_3(k_5k_9k_{11} + k_6k_9k_{11} + k_7k_9k_{11} + k_5k_7k_9 + k_5k_7k_{11})\\
D_7 &= k_1k_4k_6k_8k_{11}\\
D_8 &= k_3k_5k_7k_9k_{12}\\
D_9 &= k_2k_4k_6k_8k_{10}\\
D_{10} &= k_2k_4k_6k_8k_{12}\\
D_{11} &= k_2k_{10}k_{12}(k_4k_6 + k_4k_7 + k_5k_7)\\
D_{12} &= k_1k_3k_8k_{11}(k_5 + k_6)\\
D_{13} &= k_1k_3k_5k_7k_9k_{10}\\
D_{14} &= k_1k_4k_6k_8k_{10}\\
D_{15} &= k_3k_5k_7k_{10}k_{12}\\
D_{16} &= k_8k_{10}k_{12}(k_2k_4 + k_2k_5 + k_2k_6 + k_4k_6)\\
D_{17} &= k_1k_3k_8k_{10}(k_5 + k_6)\\
D_{18} &= k_3k_8k_{10}k_{12}(k_5 + k_6)
\end{aligned}
\qquad \text{(S67-S87)}
$$

Symbols: A, NADPH; B, GSSG;P, GSH; Q, NADP

Parameter	Value
e_t (M)	1.25E–07
k_1 ($M^{-1} s^{-1}$)	8.50E+07
k_2 (s^{-1})	5.10E+02
k_3 ($M^{-1} s^{-1}$)	1.00E+08
k_4 ($M^{-1} s^{-1}$)	5.60E+05
k_5 (s^{-1})	8.10E+02
k_6 (s^{-1})	1.00E+03
k_7 (s^{-1})	1.00E+06
k_8 ($M^{-1} s^{-1}$)	5.00E+07
k_9 (s^{-1})	1.00E+06
k_{10} ($M^{-1} s^{-1}$)	5.00E+07
k_{11} (s^{-1})	7.00E+03
k_{12} ($M^{-1} s^{-1}$)	1.00E+08

Parameter values were taken from [54].

Ribose 5-phosphate isomerase (R5PI), Xylulose 5-phosphate isomerase (X5PI)

$$v = \frac{e_t\left(\frac{k_3\mathrm{A}}{K_{m,\mathrm{A}}} - \frac{k_2\mathrm{P}}{K_{m,\mathrm{P}}}\right)}{1 + \frac{\mathrm{A}}{K_{m,\mathrm{A}}} + \frac{\mathrm{P}}{K_{m,\mathrm{P}}}} \tag{S88}$$

$$K_{m,\mathrm{A}} = \frac{k_2 + k_3}{k_1},\ K_{m,\mathrm{P}} = \frac{k_2 + k_3}{k_4} \tag{S89}$$

Symbols: (R5PI) A, RU5P; P, R5P. (X5PI) A, RU5P; P, X5P.

Parameter	Value
R5PI	
e_t (M)	1.42E–05
k_1 ($M^{-1} s^{-1}$)	6.09E+04
k_2 (s^{-1})	33.3
k_3 (s^{-1})	14.2
k_4 ($M^{-1} s^{-1}$)	2.16E+04
X5PI	
e_t (M)	4.22E–06
k_1 ($M^{-1} s^{-1}$)	3.91E+06
k_2 (s^{-1})	4.38E+02
k_3 (s^{-1})	3.05E+02
k_4 ($M^{-1} s^{-1}$)	1.49E+06

Parameter values were taken from [54].

Transaldolase (TA), Transketolase 1 (TK1), Transketolase 2 (TK2)

$$v = \frac{e_t\,(N_1\mathrm{AB} - N_2\mathrm{PQ})}{D_1\mathrm{A} + D_2\mathrm{B} + D_3\mathrm{P} + D_4\mathrm{Q} + D_5\mathrm{AB} + D_6\mathrm{PQ} + D_7\mathrm{BQ} + D_8\mathrm{AP}} \tag{S90}$$

$$\begin{aligned}
N_1 &= k_1k_3k_5k_7 \\
N_2 &= k_2k_4k_6k_8 \\
D_1 &= k_1k_3(k_6 + k_7) \\
D_2 &= k_5k_7(k_2 + k_3) \\
D_3 &= k_2k_4(k_6 + k_7) \\
D_4 &= k_6k_8(k_2 + k_3) \\
D_5 &= k_1k_5(k_3 + k_7) \\
D_6 &= k_4k_8(k_2 + k_6) \\
D_7 &= k_5k_8(k_2 + k_3) \\
D_8 &= k_1k_4(k_6 + k_7)
\end{aligned} \tag{S91-S101}$$

Symbols: (TA) A, S7P; B, GA3P; P, E4P; Q, F6P (TK1) A, X5P; B, R5P; P, GA3P; Q, S7P (TK2) A, X5P; B, E4P; P, GA3P; Q, F6P

Parameter	Value
TA	
e_t (M)	6.90E–07
k_1 ($M^{-1} s^{-1}$)	2.16E+04
k_2 (s^{-1})	45.3
k_3 (s^{-1})	16.3
k_4 ($M^{-1} s^{-1}$)	3.00E+04
k_5 ($M^{-1} s^{-1}$)	4.90E+05
k_6 (s^{-1})	60.0
k_7 (s^{-1})	17.0
k_8 ($M^{-1} s^{-1}$)	7.90E+04
TK1	
e_t (M)	3.30E–07
k_1 ($M^{-1} s^{-1}$)	2.16E+05
k_2 (s^{-1})	38.0
k_3 (s^{-1})	34.0
k_4 ($M^{-1} s^{-1}$)	1.56E+05
k_5 ($M^{-1} s^{-1}$)	3.29E+05
k_6 (s^{-1})	1.75E+02
k_7 (s^{-1})	40.0
k_8 ($M^{-1} s^{-1}$)	4.48E+04
TK2	
e_t (M)	3.30E–07
k_1 ($M^{-1} s^{-1}$)	2.16E+05
k_2 (s^{-1})	38.0
k_3 (s^{-1})	34.0
k_4 ($M^{-1} s^{-1}$)	1.56 E+05
k_5 ($M^{-1} s^{-1}$)	2.24E+06
k_6 (s^{-1})	1.75E+02
k_7 (s^{-1})	40.0
k_8 ($M^{-1} s^{-1}$)	2.13E+04

Parameter values were taken from [54].

Gamma-glutamyl cysteine synthetase

$$v = \frac{\dfrac{V_m\ \mathrm{ABC}}{\alpha K_{m,\mathrm{A}} K^{app}_{m,\mathrm{Glu}} K_{m,\mathrm{C}}}}{1 + \dfrac{\mathrm{B}}{K^{app}_{m,\mathrm{Glu}}} + \dfrac{\mathrm{BC}}{K^{app}_{m,\mathrm{Glu}} K_{m,\mathrm{C}}} + \dfrac{\mathrm{AB}}{K_{m,\mathrm{A}} K^{app}_{m,\mathrm{Glu}}} + \dfrac{\mathrm{ABC}}{\alpha K_{m,\mathrm{A}} K^{app}_{m,\mathrm{Glu}} K_{m,\mathrm{C}}}} \tag{S102}$$

$$K^{app}_{m,\mathrm{Glu}} = \frac{K_{m,\mathrm{Glu}} (1 + \mathrm{GSH}\ )}{K_{i,\mathrm{GSH}}} \tag{S103}$$

Symbols: A, MgATP; B, glutamate; C, cysteine

Parameter	Value
$K_{i,\mathrm{GSH}}$ (M)	3.40E–03
$K_{m,\mathrm{MgATP}}$ (M)	4.00E–04
$K_{m,\mathrm{Glu}}$ (M)	1.80E–03
$K_{m,\mathrm{C}}$ (M)	1.00E–04
V_m (M h^{-1})	5.00E–02
α	0.20

Parameter values were taken from [44].

Glutathione synthetase

$$v = \frac{\dfrac{V_m\ \mathrm{ABC}}{\alpha K_{m,\mathrm{A}} K_{m,\mathrm{B}} K_{m,\mathrm{C}}}}{1 + \dfrac{\mathrm{A}}{K_{m,\mathrm{A}}} + \dfrac{\mathrm{AB}}{K_{m,\mathrm{A}} K_{m,\mathrm{B}}} + \dfrac{\mathrm{AC}}{K_{m,\mathrm{A}} K_{m,\mathrm{C}}} + \dfrac{\mathrm{ABC}}{\alpha K_{m,\mathrm{A}} K_{m,\mathrm{B}} K_{m,\mathrm{C}}}} \tag{S104}$$

Symbols: A, L_GC; B, glycine; C, MgATP

Parameter	Value
$K_{m,\mathrm{L\_GC}}$ (M)	9.90E–03
$K_{m,\mathrm{glycine}}$ (M)	1.37E–03
$K_{m,\mathrm{MgATP}}$ (M)	2.30E–03
V_m (M h^{-1})	8.84E–02
α	2.60

Parameter values were taken from [54].

Glutathione transport process

$$v = V_m \left(\frac{\text{GSSG}}{\text{GSSG} + K_{m,\text{GSSG}}} \right) \left(\frac{\text{MgATP}}{\text{MgATP} + K_{m,\text{MgATP}}} \right) \quad \text{(S105)}$$

Parameter	Value
$K_{m,\text{GSSG}}$ (M)	1.00E–04
$K_{m,\text{MgATP}}$ (M)	6.30E–04
V_m (M h^{-1})	1.90E–04

Parameter values were taken from [54].

Hypoxanthine transport process

$$v = P_m \text{HX}_{in} + \frac{V_m \text{HX}_{in}}{\text{HX}_{in} + K_m} - \frac{V_{min} \text{HX}_{ex}}{K_{min}\left(1 + \frac{\text{ADE}_{ex}}{K_i}\right) + \text{HX}_{ex}} \quad \text{(S106)}$$

Parameter	Value
K_i (M)[a]	1.20E–05
K_m (M)	4.00E–04
K_{min} (M)	1.80E–04
P_m (h^{-1})	37.8
V_m (M h^{-1})	0.1516
V_{min} (M h^{-1})	0.1008

Parameter values were taken from [37] and [108].

Lactate/Pyruvate/Inorganic phosphate transport process (LACtr, PYRtr, Pitr)

$$v = k_0 \text{X}_{in} - k_1 \text{X}_{ex} \quad \text{where} \quad k_0 = k_1 / K_{eq} \quad \text{(S107)}$$

$$K_{eq} = 1 + \frac{10^{pHi - pKa}}{1 + 10^{pHi - pKa} r^{-1}} \quad \text{(S108)}$$

Calculated using Donnan ratio (r) = 0.69, *pKa* (PYR) = 2.39, *pKa* (LAC) = 0.00506, *pKa* (Pi) = 6.75 where Hct = 0.5.

X: LAC, PYR, Pi

Parameter	Value
LACtr	
k_0 (s^{-1})	7.33E–03
k_1 (s^{-1})	5.06E–03
PYRtr	
k_0 (s^{-1})	2.61E–02
k_1 (s^{-1})	1.80E–02
Pitr	
k_0 (s^{-1})	6.06E–04
k_1 (s^{-1})	5.60E–04

Parameter values were taken from [41].

Inosine/Adenosine/Adenine transport process (INOtr, ADOtr, ADEtr)

$$v = V_m \left(\frac{X_{in}}{K_m + X_{in}} - \frac{X_{ex}}{K_m + X_{ex}} \right) \quad \text{(S109)}$$

X: INO, ADO, ADE

Parameter	Value
ADEtr	
K_m (M)	2.60E–03
V_m (M h^{-1})	90.0E–02
ADOtr	
K_m (M)	1.20E–04
V_m (M h^{-1})	6.12E–02
INOtr	
K_m (M)	1.20E–04
V_m (M h^{-1})	6.12E–02

Parameter values were taken from [37].

Sodium/potassium pump

$$v = \frac{\left(\frac{\mathrm{ATP}}{\mathrm{ATP} + K_m}\right)\left(\frac{V_m}{2}\right)\left((\mathrm{K}^+_{ex})^2 + \frac{B_2\,\mathrm{K}^+_{ex} z}{2}\right)}{Pump_{rd}} \tag{S110}$$

$$Pump_{rd} = B_1 B_2 + 2B_2\,\mathrm{K}^+_{ex} + (\mathrm{K}^+_{ex})^2 + \left(\frac{B_3}{\mathrm{Na}^+_{in}} + 1\right)^3 \left(B_1 B_2 k_2 k_1 + k_3 k_1 (\mathrm{K}^+_{ex})^2 + B_2\,\mathrm{K}^+_{ex} z\right) \tag{S111}$$

Parameter	Value
B_1 (M)	6.17E–05
B_2 (M)	1.33E–04
B_3 (M)	6.27E–03
K_m (M)	7.64E–04
V_m (M h^{-1})	2.32E–03
$k_2\,k_1$	8.20E–03
$k_3\,k_1$	5.01E–02
z	0.711

Parameter values were taken from [37].

Leak of potassium (K^+ leak), Leak of sodium (Na^+ leak)

$$v = \frac{K_x z \log(r)\left(\mathrm{X}_{ex} - r\,\mathrm{X}_{in}\right)}{r-1} + \frac{V_m \mathrm{X}_{ex}}{\left(K_m + \mathrm{X}_{ex}\right) - r\frac{\mathrm{X}_{in}}{\left(K_m + r\,\mathrm{X}_{in}\right)}} \tag{S112}$$

X : Na^+, K^+

Parameter	Value
K^+ leak	
K_m (M)	4.00E–03
K_x (M)	6.35E–06
V_m (M h^{-1})	3.12E–03
r	0.620
z	1.00
Na^+ leak	
K_m (M)	2.10E–02
K_x (M)	7.06E–06
V_m (M h^{-1})	2.82E–03
r	0.620
z	1.00

Parameter values were taken from [37].

A.2 Calculation of oxygen saturation of hemoglobin

The following model for oxygen saturation of hemoglobin was incorporated into the metabolic model [109]. The value of pO_2 is converted into the absolute concentration of oxygen in the cell volume and then substituted into the following equation to calculate the distribution ratio between oxyHb and deoxyHb (oxygen saturation = $SHbO_2$).

$$S_{HbO\,2} = \frac{[\mathrm{HbO}_2]}{[\mathrm{Hb}]} = \frac{K_{HbO\,2}[\mathrm{O}_2]^n}{1 + K_{HbO\,2}}[\mathrm{O}_2]^n \tag{S113}$$

$$K_{HbO\,2} = \frac{K_4'\left(K_3'[\mathrm{CO}_2]\left(1 + \frac{K_3''}{[10^{-\mathrm{pH}}]}\right) + \left(1 + \frac{[10^{-\mathrm{pH}}]}{K_6''}\right)\right)}{\left(K_2'[\mathrm{CO}_2]\left(1 + \frac{K_2''}{[10^{-\mathrm{pH}}]}\right) + \left(1 + \frac{[10^{-\mathrm{pH}}]}{K_5''}\right)\right)} \tag{S114}$$

$$K_4' = K_4''\left(\frac{[10^{-\mathrm{pH}}]_s}{[10^{-\mathrm{pH}}]}\right)^{n1}\left(\frac{[\mathrm{CO}_2]_s}{[\mathrm{CO}_2]}\right)^{n2}\left(\frac{[2{,}3\text{ - BPG}]_s}{[2{,}3\text{ - BPG}]}\right)^{n3}\left(\frac{T_s}{T}\right)^{n4} \tag{S115}$$

$$[\mathrm{O}_2] = \frac{10^{-6}\left\{1.37 - 0.0137\,(T-37) + 0.00058\,\times(T-37)^2\right\}\times 0.65 \times P_{O_2}}{0.94} \tag{S116}$$

$$[\mathrm{CO}_2] = \frac{10^{-5}\left\{3.07 - 0.057\,(T-37) + 0.002\,\times(T-37)^2\right\}\times 0.65 \times P_{CO_2}}{0.94} \tag{S117}$$

$$n1 = -6.775 + 2.0372\ pH - 0.1235\ pH^2 \tag{S118}$$

$$n2 = -0.008765 + 0.00086\ P_{CO_2} + 6.3\times 10^{-7}(P_{CO_2})^2 \tag{S119}$$

$$n3 = 0.2583 + 28.6978\,[2{,}3\text{ - BPG}] - 917.69\,[2{,}3\text{ - BPG}]^2 \tag{S120}$$

$$n4 = 1.6914 + 0.0618\ T + 0.00048\ T^2 \tag{S121}$$

Parameter	Value
K_2'	2.40E–05
K_2''	1.00E–06
K_3'	2.40E–05
K_3''	5.00E–06
K_4''	6.77E+11
K_5''	7.20E–08
K_6''	8.40E–09
n	2.7
T	37
P_{O2}	100
P_{CO2}	40

Parameter values were taken from [109].

A.3 Descriptions of binding processes of metabolites to Mg^{2+}, oxyHb and deoxyHb.

The binding processes between metabolites to Mg^{2+} and hemoglobin are also considered in the model. Kinetics and association constants for calculation of these bindings were shown below:

Binding of metabolites to hemoglobin

Binding substrates		Complex
deoxyHb + 1,3-BPG	↔	deoxyHb1,3-BPG
deoxyHb + 2,3-BPG	↔	deoxyHb2,3-BPG
deoxyHb + fADP	↔	deoxyHbADP
deoxyHb + fATP	↔	deoxyHbATP
deoxyHb + F-1,6BP	↔	deoxyHbF-1,6BP
deoxyHb + GDP	↔	deoxyHbGDP
deoxyHb + MgATP	↔	deoxyHbMgATP
oxyHb + 1,3-BPG	↔	oxyHb1,3-BPG
oxyHb + 2,3-BPG	↔	oxyHb2,3-BPG
oxyHb + ADP	↔	oxyHbADP
oxyHb + ATP	↔	oxyHbATP
oxyHb +	↔	oxyHbMgATP

$$v = K'_a \mathrm{AB} - K_d \mathrm{P} \tag{S122}$$

$$K'_a = \frac{1 + \frac{2n}{10^{-7.2}} + \left(\frac{n}{10^{-7.2}}\right)^2}{1 + \frac{2n}{10^{-\mathrm{pH}}} + \left(\frac{n}{10^{-\mathrm{pH}}}\right)^2} \times K_a \tag{S123}$$

Symbols: A and B, binding substrates; P, complex

Parameter	Value
deoxyHb1,3-BPG	
K_a	1860000
K_d	1200
n	1.00E–06
deoxyHb1,3-BPG	
K_a	6000000
K_d	1200
n	1.00E–06
deoxyHbADP	
K_a	1440000
K_d	1200
n	1.00E–06
deoxyHbATP	
K_a	3120000
K_d	1200
n	1.00E–06
deoxyHbF-1,6BP	
K_a	1212000
K_d	1200
n	1.00E–06
deoxyHbGDP	
K_a	1212000
K_d	1200
n	1.00E–06
deoxyHbMgATP	
K_a	168000
K_d	1200
n	1.00E–06
oxyHb1,3-BPG	
K_a	380000
K_d	1200
n	1.00E–06

Continued from the preceding page

oxyHb2,3-BPG	
K_a	300000
K_d	1200
n	1.00E–06
oxyHbADP	
K_a	300000
K_d	1200
n	1.00E–06
oxyHbATP	
K_a	432000
K_d	1200
n	1.00E–06
oxyHbMgATP	
K_a	46800
K_d	1200
n	1.00E–06

Parameter values were taken from [110].

Binding of 1,3-BPG to Mg^{2+} (Mg1,3-BPG), Binding of 2,3-BPG to Mg^{2+} (Mg2,3-BPG)

Binding substrates		Complex
Mg^{2+} + 1,3-BPG	↔	Mg1,3-BPG
Mg^{2+} + 2,3-BPG	↔	Mg2,3-BPG

$$v = K'_a \mathrm{AB} - K_d \mathrm{P} \tag{S124}$$

$$K'_a = \frac{0.0032\ K_a \left(Kmgbpg + 10^{-\mathrm{pH}} \times Khbpg \times Kmghbpg\right)}{1 + \left(10^{-\mathrm{pH}} \times Khbpg\right) + \left(10^{-2\mathrm{pH}} \times Khbpg \times Kh2bpg\right) + \left(\mathrm{K}^{+} \times Kkbpg\right) + \left(\mathrm{K}^{+} \times 10^{-\mathrm{pH}} \times Khbpg \times Kkhbpg\right)} \tag{S125}$$

Symbols: A and B, binding substrates; P, complex

Parameter	Value
Mg1,3-BPG	
K_a	228000
K_d	1200
Kh2bpg	4270000
Khbpg	162000000
Kkbpg	85.1
Kkhbpg	8.9
Kmgbpg	7410
Kmghbpg	513
Mg2,3-BPG	
K_a	804000
K_d	1200
Kh2bpg	4270000
Khbpg	162000000
Kkbpg	85.1
Kkhbpg	8.9
Kmgbpg	7410
Kmghbpg	513

Parameter values were taken from [110].

Binding of AMP to Mg^{2+} (MgAMP)

Binding substrates		Complex
$Mg^{2+} + AMP$	$\leftrightarrow$	MgAMP

$$v = K_a AB - K_d P \tag{S126}$$

Symbols: A and B, binding substrates; P, complex

Parameter	Value
K_a	54054
K_d	1200

Parameter values were taken from [110].

Binding of ADP to Mg^{2+} (MgADP)

Binding substrates		Complex
$Mg^{2+} + ADP$	$\leftrightarrow$	MgADP

$$v = K'_a AB - K_d P \tag{S127}$$

$$K'_a = \frac{Kmgadp + \left(10^{-pH} \times Khadp \times Kmgadp\right)}{1 + \left(10^{-pH} \times Khadp\right) + \left(K^{+} \times Kkadp\right)} \times K_a \tag{S128}$$

Symbols: A and B, binding substrates; P, complex

Parameter	Value
K_a	1711.2
K_d	1200
Khadp	5420000
Kkadp	4.8
Kmgadp	3290
Kmghadp	107

Parameter values were taken from [110].

Binding of ATP to Mg^{2+} (MgATP)

Binding substrates		Complex
$Mg^{2+} + ATP$	$\leftrightarrow$	MgATP

$$v = K'_a AB - K_d P \tag{S129}$$

$$K'_a = \frac{Kmgadp + \left(10^{-pH} \times Khadp \times Kmgadp\right)}{1 + \left(10^{-pH} \times Khadp\right) + \left(K^{+} \times Kkadp\right)} \times K_a \tag{S130}$$

Symbols: A and B, binding substrates; P, complex

Parameter	Value
K_a	2620.8
K_d	1200
Khatp	9070000
Kkatp	14.0
Kmgatp	43200
Kmghatp	748.0

Parameter values were taken from [110].

Binding of F1,6-BP to Mg^{2+} (MgF1,6-BP), Binding of GDP to Mg^{2+} (MgGDP)

Binding substrates		Complex
Mg^{2+} + F1,6-BP	$\leftrightarrow$	MgF1,6-BP
Mg^{2+} + GDP	$\leftrightarrow$	MgGDP

$$v = K'_{a,A} AB - K_{d,A} P \tag{S131}$$

$$K'_{a,A} = \frac{0.0083\ K_{a,A}\left(Kmg,A + 10^{-pH} \times Kh,A \times Kmgh,A\right)}{1 + \left(10^{-pH} \times Kh,A\right) + \left(10^{-2pH} \times Kh,A \times Kh2,A\right) + \left(K^{+} \times Kh,A\right) + \left(K^{+} \times 10^{-pH} \times Kh,A \times Kkh,A\right)} \tag{S132}$$

Symbols: A, B, binding substrates; P, complex, *A*, *f16bp* or *gdp*.

Parameter	Value
MgF-1,6-BP	
$K_{a,f16bp}$	480000
$K_{d,f16bp}$	1200
Kh2,f16bp	1120000
Kh,f16bp	7560000
Kk,f16bp	10.7
Kkh,f16bp	3.3
Kmg,f16bp	363.0
Kmgh,f16bp	89.0
MgGDP	
$K_{a,gdp}$	480000
$K_{d,gdp}$	1200
Kh2,gdp	1120000
Kh,gdp	7560000
Kk,gdp	10.7
Kkh,gdp	3.3
Kmg,gdp	363.0
Kmgh,dgp	89.0

Parameter values were taken from [110].

Binding of inorganic phosphate to Mg^{2+} (MgPi)

Binding substrates		Complex
Mg^{2+} + Pi	↔	MgPi

$$v = K'_a \mathrm{AB} - K_d \mathrm{P} \tag{S133}$$

$$K'_a = \frac{10^{-7.2} \times Khpi + 0.15\, Kkpi}{1 + \left(10^{-\mathrm{pH}} \times Khpi\right) + \left(\mathrm{K}^{+} \times Kkpi\right)} \times K_a \tag{S134}$$

Symbols: A, B, binding substrates; P, complex

Parameter	Value
K_a	40800
K_d	1200
Khpi	5680000
Kkpi	3.0

Parameter values were taken from [110].

A.4 Descriptions of band3 protein mediated interactions between hemoglobin and glycolytic enzymes.

Reversible binding of some glycolytic enzymes and two allosteric form of hemoglobin to band3 protein, Kinetics and association constants for calculation of these bindings were shown below:

Binding proteins		Complex
Band3 + ALD	↔	Band3-ALD
Band3 + GAPDH	↔	Band3-GAPDH
Band3 + PFK	↔	Band3-PFK
Band3 + deoxyHb	↔	Band3-deoxyHb
Band3 + oxyHb	↔	Band3-oxyHb

$$v = K_a \mathrm{AB} - K_d \mathrm{P} \tag{S135}$$

Symbols: A, B, binding proteins; P, complex

Parameter	Value
Band3-ALD[a]	
K_a	1200000000
K_d	1200
Band3-GAPDH[a]	
K_a	2400000000
K_d	1200
Band3-PFK[b]	
K_a	6000000000
K_d	1200
Band3-deoxyHb[c]	
K_a	12000000
K_d	1200
Band3-oxyHb[c]	
K_a	120000
K_d	1200

Parameter values were taken from [a][111], [b][112], [c][113].

A.5 Initial and steady-state concentrations of all substrates in the model

Abbreviation of metabolites and enzymes are corresponding to those shown in Table 2.1 in the main text.

Substrate	Concentration(M)
ADE	1.53E–05
ADO	4.62E–08
DHAP	1.51E–05
E4P	4.57E–07
F6P	1.94E–05
F1,6-BP	5.35E–06
G6P	5.96E–05
GA3P	3.69E–06
GDP	8.77E–05
GL6P	5.33E–09
GLC	5.00E–03
GO6P	4.47E–05
GSH	3.27E–03
GSSG	4.65E–06
HX	1.61E–06
IMP	8.06E–06
INO	1.45E–07
LAC	1.33E–03
L_GC	4.22E–07
NAD	6.51E–05
NADH	2.40E–07
NADP	6.47E–08
NADPH	6.53E–05
Na^+	3.39E–02
K^+	1.33E–01
PEP	8.19E–06
PRPP	1.41E–06
PYR	5.16E–05
Pi	1.01E–03
R1P	8.08E–05
R5P	5.86E–06
RU5P	4.93E–06
S7P	2.10E–05
X5P	8.99E–06

Continued from the preceding page

Substrate	Concentration(M)
1,3-BPG	2.15E–07
2PG	1.45E–05
3PG	4.77E–05
2,3-BPG (free)	8.09E–04
2,3-BPG (total)	3.68E–03
AMP	2.48E–05
ADP	6.28E–05
ATP (free)	5.51E–05
ATP (total)	1.91E–03
glutamate	2.00E–04
glycine	1.80E–04
cycteine	2.00E–07
ADE (extracellular)	1.50E–05
ADO (extracellular)	7.00E–08
HX (extracellular)	2.70E–06
INO (extracellular)	1.20E–07
K^+ (extracellular)	9.50E–03
Na^+ (extracellular)	1.40E–05
LAC (extracellular)	1.80E–03
PYR (extracellular)	7.50E–05
Pi (extracellular)	1.10E–03
Band3 binding region (free)	2.71E–06
Band3-ALD complex	2.70E–07
Band3-GAPDH complex	6.47E–06
Band3-PFK complex	1.02E–07
ALD (free)	9.95E–05
GAPDH (free)	1.19E–03
PFK (free)	7.54E–06
Band3-deoxyHb complex	1.05E–06
Band3-deoxyHb1,3-BPG complex	3.83E–10
Band3-deoxyHb2,3-BPG complex	6.81E–06
Band3-deoxyHbADP complex	1.13E–07
Band3-deoxyHbATP complex	2.30E–07
Band3-deoxyHbF1,6-BP complex	6.07E–09
Band3-deoxyHbGDP complex	9.95E–08
Band3-deoxyHbMgATP complex	2.07E–07
Band3-oxyHb complex	1.30E–06
Band3-oxyHb1,3-BPG complex	9.67E–11
Band3-oxyHb2,3-BPG complex	4.21E–07
Band3-oxyHbADP complex	2.93E–08
Band3-oxyHbATP complex	3.94E–08

Continued from the preceding page

Substrate	Concentration(M)
Band3-oxyHbF1,6-BP complex	0.00
Band3-oxyHbGDP complex	0.00
Band3-oxyHbMgATP complex	7.15E–08
deoxyHb (free)	3.86E–05
deoxyHb-1,3-BPG complex	1.41E–08
deoxyHb-2,3-BPG complex	2.51E–04
deoxyHb-ADP complex	4.18E–06
deoxyHb-ATP complex	8.48E–06
deoxyHb-F1,6-BP complex	2.24E–06
deoxyHb-GDP complex	3.67E–07
deoxyHb-MgATP complex	7.65E–06
oxyHb (free)	4.78E–03
oxyHb-1,3-BPG complex	3.57E–07
oxyHb-1,3-BPG complex	1.55E–03
oxyHb-ADP complex	1.08E–04
oxyHb-ATP complex	1.45E–04
oxyHb-MgATP complex	2.64E–04
Mg^{2+} (free)	6.03E–04
Mg^{2+}-1,3-BPG complex	2.92E–08
Mg^{2+}-2,3-BPG complex	5.69E–04
Mg^{2+}-ADP complex	1.30E–04
Mg^{2+}-AMP complex	9.11E–07
Mg^{2+}-ATP complex	1.41E–03
Mg^{2+}-F1,6-BP complex	1.48E–06
Mg^{2+}-GDP complex	2.43E–05
Mg^{2+}-Pi complex	2.14E–05

Appendix B

Lists of Abbreviations

B.1 Abbreviations of metabolites

Abbreviation	Metabolite
1,3-BPG	1,3-bisphosphoglycerate
2,3-BPG	2,3-bisphosphoglycerate
3PG	3-phosphoglycerate
ADE	adenine
DHAP	dihydroxyacetone phosphate
F-1,6BP	fructose 1,6-bisphosphate
F6P	fructose 6-phosphate
F-1,6BP	fructose 1,6-bisphosphate
G6P	glucose 6-phosphate
GUO	guanosine
HX	hypoxanthine
INO	inosine
LAC	lactate
PEP	phosphoenolpyruvate
PRPP	5-phosphoribosyl-1-pyrophosphate
PYR	pyruvate
R1P	ribose 1-phosphate
R5P	ribose 5-phosphate
RU5P	ribulose 5-phosphate
S7P	sedoheptulose 7-phosphate

B.2 Abbreviations of enzymes

Abbreviation	Enzyme
ADPRT	adenine phosphoribosyl transferase
AK	adenosine kinase
AMPDA	adenosine monophosphate deaminase
AMPase	adenosine monophosphate phosphohydrolase
APK	adenylate kinase
GAPDH	glyceraldehyde phosphate dehydrogenase
HK	hexokinase
LDH	lactate dehydrogenase
PFK	phosphofructokinase
PGK	phosphoglycerate kinase
PK	pyruvate kinase
PRPPsyn	phosphoribosyl pyrophosphate synthetase
TK	transketolase

B.3 Abbreviations of storage solutions and preserved blood

Abbreviation	Solution
ACD	Acid-Citrate-Dextrose
CPD	Citrate-Phosphate-Dextrose
MAP	Mannitol-Adenine-Phosphate
PAGGGM	Phosphate-Adenine-Glucose-Guanosine-Gluconate-Mannitol
RC-MAP	red blood cells stored in MAP
PAGGGM-stored RBCs	red blood cells stored in PAGGGM

Appendix C

List of Publications

Journal Papers

[1] Nishino, T., Yachie-Kinoshita, A., Hirayama, A., Soga, T., Suematsu, M. and Tomita, M. "*In silico* modeling and metabolome analysis of long-stored erythrocytes to improve blood storage methods" *Journal of Biotechnology*, **144**(3):212-223, 2009

(The research described in Chapter 2 was reported in this paper.)

[2] Nishino, T., Yachie-Kinoshita, A., Hirayama, A., Soga, T., Suematsu, M. and Tomita, M. "Dynamic simulation and metabolome analysis of long-term erythrocyte storage in adenine–guanosine solution" *PLOS ONE*, in press (accepted on Jun 27, 2013)

(The research described in Chapter 3 was reported in this paper.)

[3] Yachie-Kinoshita, A., Nishino, T., Shimo, H., Suematsu, M. and Tomita, M. "A metabolic Model of Human Erythrocytes: Practical Application of the E-Cell Simulation Environment" *Journal of Biomedicine and Biotechnology*, 2010, doi: 10.1155/2010/642420

[4] Shimo, H., Nishino, T., Tomita, M. "Predicting the kinetic properties associated with redox imbalance after oxidative crisis in G6PD-deficient erythrocytes: a simulation study" *Advances in Hematology*, 2011, doi: 10.1155/2011/398945

International Conferences (Poster Presentations)

[1] Nishino, T., Yachie-Kinoshita, A., Hirayama, A., Soga, T., Suematsu, M. and Tomita, M., "*In Silico* Modeling and Metabolome Analysis of Preserved Red Blood Cells towards Improvement of Blood Storage", The 10th International Conference on Systems Biology, (Stanford, California, 2009.9.2)

[2] Nishino, T., Yachie-Kinoshita, A., Hirayama, A., Soga, T., Suematsu, M. and Tomita, M., "Mathematical modeling of preserved red blood cells towards improvement of blood storage" The 18th Annual International Conference on Intelligent Systems for Molecular Biology, (Boston, Massachusetts, 2010.7.11)

[3] Nishino, T., Yachie-Kinoshita, A., Hirayama, A., Soga, T., Suematsu, M. and Tomita, M., "Mathematical modeling and metabolome analysis of preserved red blood cells towards improvement of blood storage method" The 11th International Conference on Systems Biology, (Edinburgh, UK, 2010.10.11)

[4] Nishino, T., Yachie-Kinoshita, A., Hirayama, A., Soga, T., Suematsu, M., Tomita, M., "Prediction of the metabolic alterations in cold-storage erythrocytes by using large-scale and detailed simulation model" The 12th International Conference on Systems Biology, (Mannheim, Germany, 2011.8.30)